Hepatic Steatosis and TNF-α Signaling

by

Nita Modi

A thesis
presented to the University of Waterloo
in fulfillment of the
thesis requirement for the degree of
Master of Science
in
Biology

Waterloo, Ontario, Canada, 2007

I hereby declare that I am the sole author of this thesis. This is a true copy of the thesis, including any required final revisions, as accepted by my examiners.

I understand that my thesis may be made electronically available to the public.

Abstract

The overall objective of this research was to investigate the status of tumor necrosis factor-α (TNF-α), and molecules associated with its signaling, in the pathological state of hepatic steatosis. The effect of NSAID piroxicam, a cancer preventive agent also known to affect TNF-α signaling on hepatic steatosis, was also investigated. The biological state of the tissue was assessed by examining the expression of TNF-α signaling molecule in whole tissue, as well as in hepatic lipid raft. Lipid rafts are dynamic assemblies of cholesterol and sphingolipids, microdomains that form in the exoplasmic leaflet of the biological membranes shown to play a role in compartmentalization, modulation and integration of the cell signaling.

In the present research, Zucker obese rats were used as a model of human obesity and insulin resistant state. These rats exhibit hepatic steatosis in adulthood similar to those noted in obese individuals. Female Zucker obese and lean rats (5 weeks old) were fed a semisynthetic diet with or without piroxicam (150 ppm). Zucker lean counterparts served as control. After 8 weeks of feeding, rats were euthanized and liver from each animal was collected. Liver tissue from each animal was processed for histology and biochemical analysis which included lipids and proteins (COX-1 and 2, TNF-α, TNF-RI and RII, IKK-β, IκB-α and NF-κB). Liver histology and the level of total lipids confirmed that Zucker obese rats had hepatic steatosis, which was further augmented by piroxicam treatment. Whole tissue protein expression, using western blot, showed that the steatotic liver differed from non-steatotic livers by having lower levels of TNF-RII. TNF-RII showed a trend which was inversely proportional to the pathological state of the tissue. The obese-piroxicam liver had the lowest level of TNF-RII and lean livers had the highest ($p<0.05$). The total NF-κB level was higher in the obese and obese-piroxicam groups compared to the lean or lean-piroxicam groups ($p<0.05$). Piroxicam treatment lowered the level of NF-κB in obese and lean livers. IκB-α was higher in obese livers than in lean livers. The nuclear level of NF-κB by western blot analysis showed the same pattern as noted in the whole tissue homogenate. However, the difference in the level between obese and lean was marked. The obese nuclei contained two to three fold higher levels of NF-κB protein than the lean liver nuclei. IκB-α level was significantly higher in the obese liver tissues and nuclei than their lean counterparts. While transcriptionally active NF-κB was higher ($p<0.05$) in the obese livers than in the lean livers, the difference between obese and lean groups was not as significant as that noted for the level of NF-κB assessed by western blot. This suggests that the proportion of active NF-κB present in the nuclear fraction is much higher in the lean than in the obese nuclei.

Lipid raft was extracted and identified successfully from obese and lean livers. The total caveolin and flotillin levels were significantly higher in the liver lipid rafts of the obese-piroxicam than that of the other groups. This is the group that also exhibited higher steatosis. Piroxicam treatment significantly decreased the level of caveolin in the lean liver and significantly increased the level of flotillin in the obese liver. While COX-1 was not detectable, however, the level of COX-2 and TNF-RII in lipid raft was opposite to the level noted in the whole tissue homogenate. TNFRII was highest in the obese-piroxicam lipid raft and lowest in the lean-piroxicam lipid raft. TNF-RII, COX-2, IκB-α and NF-κB proteins were the molecules profoundly affected by the pathological state of the tissue and piroxicam treatment. This research is the first to report the presence of IκB-α in the nuclear compartment with a higher level in the nuclei and whole tissue in the obese liver than in the lean liver. This research demonstrates that TNF-α to NF-κB axis is altered in steatotic liver, and analysis of lipid rafts in steatotic and non-steatotic liver demonstrates that lipid rafts play a distinct role in modifying the biological availability of key proteins in the pathological state of liver steatosis.

Acknowledgements

This thesis acknowledges the conclusion of my Master of Science in Biology. There have been many people who helped me throughout my studies and I thank you all. Your support and positive attitude helped me complete this project successfully, and in a timely manner.

A sincere 'thank you' to my advisor, Dr. Ranjana P. Bird, for all her guidance towards my research project, and always motivating me to be a persistent student. Thank you for your critical and valuable suggestions and always being there for me. The fact that you have assisted me during weekends was much appreciated, as was your trust in my capabilities for teaching the lab techniques to fellow students.

I would also like to gratefully acknowledge my committee members, Dr. Niels Bols and Dr. Ken Stark, for their valuable critiques, time, and analysis towards this thesis.

A special thanks to various members of the Department of Biology for their support and help in using their facilities and equipment. Thanks to Hamid Izadi, a student of Dr. Stark for helping me with techniques like TLC, and to Steve Giilck, a summer student in our lab and a good friend, whose editorial expertise was much appreciated. The daily smiling faces of all my lab members contributed to a truly encouraging work environment, and helped me to grow and mature as a student. Thank you all for your enthusiasm, and for sharing the good moments with me.

Thank you Swati for being a true and reliable friend. My son, Rahul, always appreciated your excellent baking and we thank you for your artistic rendition of him. The years we have spent together are very precious and will never be forgotten. Thank you for your support during the low times and for always encouraging me to be brave. This thesis would not have reached a successful completion without your support.

Thanks to my husband, Jit, for always encouraging me to further my studies and for supporting me. Also thanks to 'mummy' for taking excellent care of my son and for preparing meals for all family members along with doing other chores. Thanks to 'Papa' for his positive attitude towards my studies and giving rides to and from the university in the chilly winter nights. Thanks to my younger sister, Neha, for helping me out with the house when I was extremely busy with school. Special thanks to my son, Rahul, for understanding that mom was busy with school work and allowing me time to concentrate on my studies.

Dedication

For
Jit and Rahul

Table of Contents

List of Figures

List of Tables

Chapter 1
Introduction

1.1 Hypothesis

The transformation from a normal to a pathological state in an organ is accompanied by altered signaling leading to a compromised state. In the pathological state of obesity, oxidative stress and tissue pathology is a common occurrence. Zucker obese rats exhibit hepatic steatosis in adulthood. Furthermore, membrane structure has evolved from the concept of the lipid bilayer to a complex and dynamic system continuously changing in response to intra- and extra-cellular stimuli as well as changes in the physiology of the whole organism (Simons and Toomre, 2000). In keeping with this concept, a new functional domain in the membrane, known as a lipid raft, is receiving a great deal of attention. Lipid rafts have been implicated in controlling the concentration and activity of various important membrane bound receptors and enzymes. Based on the physiological state of the animal, liver steatosis is accompanied by disordered lipid metabolism, abnormality of cytokine, etc. Therefore, one could speculate that if lipid rafts are involved in the generation of signals leading to metabolic responses, significant changes in lipid raft structure pertaining to key functional components in a steatotic liver could be anticipated.

It is generally understood that obese states differ significantly from non-obese states in responding to drugs as well as nutrients. This causes one to question whether all drugs and cancer preventive agents are equally effective and safe in obese states in comparision to normal states. In one preliminary study in our laboratory, it was observed that piroxicam, a known and safe cancer inhibitory agent in F344 rats (non-obese rats), was hepatotoxic to Zucker obese rats; the key observation was enlarged and fatty marbled appearance of the livers in comparison to the livers of lean rats. This observation prompted the investigation of the potential role of TNF-α in liver steatosis.

Hypothesis: Hepatic steatosis noted in obese states with or without piroxicam treatment is associated with altered TNF alpha and NF-κB axis in whole tissue and in membrane lipid raft microdomains.

1.1.1 Specific Objectives of this Study

Objective : The primary objective of this research is to explore the role of TNF-α signaling in hepatic steatosis

Specific Aim 1: To examine the morphological and biochemical changes in whole steatotic and non-steatotic tissue with the following sub-aims:

A. Examine the changes in liver histology of Zucker obese, lean and piroxicam treated obese rats
B. Assess the changes in lipid composition between obese and lean rats
C. Investigate the levels of COX-1 and COX-2 proteins between obese and piroxicam treated obese rats
D. Evaluate the expression of key molecules involved in TNF alpha mediated signaling pathway

Specific Aim 2: To examine the TNF-α and associated molecules in steatotic and non steatotic hepatic lipid rafts with the following sub-aims:

A. Extract lipid rafts from hepatic tissues of Zucker obese and lean rats with or without piroxicam treatment
B. Confirm that the method of isolating lipid raft was satisfactory in analyzing the fractions for the following:
    I. Caveolin-1 and Flotillin-1 protein expression
    II. Cholesterol levels
C. Investigate if altered lipid structure/composition is associated with liver steatosis and toxicity by conducting following:
    I. Comparison of lipid raft structure between obese (hepatosteatotic) and lean rats
    II. Comparison of lipid raft structure between obese (hepatosteatotic) and piroxicam treated obese rats
    III. Comparison of the expressions of key molecules studied in whole homogenate with that of the lipid raft

These specific aims were achieved by conducting one study. Specific aim 1 and its sub-aims were met by analysing the whole tissue (Section 3.1, 3.2, 3.3, 4.1.1). Specific aim 2 and its sub-aims were achieved by extracting lipid raft from the whole tissue (Section 3.3, 3.4, 4.1.2).

To put this project in perspective, brief background information on hepatic steatosis, lipid raft and TNF-α pathway relevant to this thesis are provided.

1.2 Hepatic Steatosis

1.2.1 The Liver

The liver is the largest glandular organ and the central component of the body. It plays a major role in metabolism (anabolic and catabolic responses) including, drug detoxification, plasma protein synthesis, glucose and fat metabolism, hormone synthesis and urea production. The liver is also responsible for producing 80% of the body's cholesterol. Some of these products are excreted into the bile and others are metabolized in the liver (Silverthorn, 1998). Since metabolites are constantly moving in and out, liver hepatocytes play an extensive role in membrane trafficking such as exocytosis and endocytosis.

1.2.2 Characteristics of Hepatic Steatosis

Hepatic Steatosis is the presence of significant amounts of triglyceride (TG) in hepatocytes. Fat accumulation in the liver results from four different processes: 1) increased delivery of free fatty acids to the liver, 2) increased de novo synthesis of free fatty acids in the liver, 3) decreased oxidation of free fatty acids, and 4) decreased synthesis of secretion of very low-density lipoprotein (VLDL) (Browning and Horton, 2004). Hepatic Steatosis was thought to be mainly a symptom of alcoholic liver disease (ALD), but in recent years, has been found in the absence of alcohol abuse which has led to the definition of a series of disorders ranging from non-alcoholic fatty liver (NAFL) to non-alcoholic steatohepatitis (NASH). Hence, various factors are found to be associated with hepatic steatosis, including obesity, high alcohol consumption, type II diabetes, and hyperlipidaemia (Raman and Allard, 2006). Moreover, the pathogenesis of steatosis and cellular injury is thought to be related mostly to insulin resistance and oxidative stress. For example, non-alcoholic fatty liver disease (NAFLD) is 76% more likely to be found in an obese individual, and is almost universal within individuals who are morbidly obese and diabetic (Adams et al., 2005). Recently, the association between obesity and the development of NAFLD has been proposed by Day et al, as a 'two hit' model (1998).

1.2.3 The 'Two-Hit' Model

The primary abnormality or 'first hit' in patients with NAFLD is insulin resistance leading to hepatic steatosis. Accumulation of hepatic fat is closely linked to insulin resistance, which increases lipolysis of peripheral adipose tissue with a resultant increased fat influx into the liver in the form of free fatty

acids. Furthermore, insulin resistance promotes de novo triglyceride synthesis within the liver and inhibits fatty acid oxidation thereby promoting triglyceride accumulation (Siebler and Galle, 2006; Adams et al., 2005). Thus, accumulation of lipids in hepatocytes is a pathologic hallmark of ALD and NAFLD. The "second hit" involves multiple proinflammatory cytokines resulting in non-alcoholic steatohepatitis (NASH) (Adams and Angulo, 2006). In NASH, as in alcoholic hepatitis, oxidative stress and lipid peroxidation have emerged as the most likely candidates. This "hit" occurs via increased mitochondrial beta-oxidation of the free fatty acids, production of reactive oxygen species and depletion of antioxidants glutathione and vitamin E. This depletion of anti-oxidants hampers reactive oxygen species inactivation and increases the deleterious effects on the mitochondria. Oxidative stress also results in abnormal cytokine production, especially TNF-α, through up-regulation of nuclear translocation of transcription factor nuclear factor κB. This combination of lipid peroxidation and cytokine production results in hepatocyte death (Siebler and Galle, 2006).

1.2.4 Development of Hepatic Steatosis in Insulin-Resistant State

A series of molecular alterations resulting in accumulation of triglycerides in the liver occuring in insulin resistant state is summarized in figure 1.1 (Browning and Horton, 2004). In a normal physiologic state, a balance exits between the storage and release of free fatty acids (FFAs) and the metabolism of glucose in the adipose tissue, liver, striated muscle and pancreas. One of the proposed mechanisms for the abnormal fat deposition suggests that insulin stimulates glucose uptake and free fatty acid esterification in adipocytes and hepatocytes and suppresses hormone-sensitive lipase (HSL) in the adipose tissue (Boer et al., 2004). Because HSL regulates the release of FFAs from the adipose tissue, the net effect of insulin on the adipose tissue is fat storage in the form of triglycerides. However, in the presence of insulin resistance, increased adipocyte mass and increased hydrolysis of triglycerides (lypolysis) through increased hormone-sensitive lipase activity contributes to elevated plasma levels of FFAs. The rate of hepatic FFA uptake is unregulated and, therefore, directly proportional to plasma FFA concentrations. FFAs taken up by the liver are metabolized by three pathways: oxidation to generate ATP for energy, esterification with glycerol to produce triglycerides for storage, and secretion in the form of VLDL. With less oxidation or mere esterification, or when VLDL secretion is defective, these pathways can lead to hepatic steatosis (Browning and Horton, 2004).

Figure 1.1: Metabolic alterations resulting in hepatic triglyceride accumulation in insulin-resistant states. Insulin resistance is manifested by hyperinsulinemia, increased hepatic glucose production, and decreased glucose disposal. In adipocytes, insulin resistance increases hormone-sensitive lipase (HSL) activity, resulting in elevated rates of triglyceride lipolysis and enhanced FFA flux to the liver. FFAs can either be oxidized in the mitochondria to form ATP or esterified to produce triglycerides for storage or incorporation into VLDL particles. In the liver, hyperinsulinemia induces SREBP-1c (Sterol regulatory element-binding protein 1c) expression, leading to the transcriptional activation of all lipogenic genes. Simultaneously, hyperglycemia activates ChREBP (carbohydrate response element binding protein), which transcriptionally activates L-PK (liver-type pyruvate kinase) and all lipogenic genes. The synergistic actions of SREBP-1c and ChREBP activate the enzymatic machinery necessary for the conversion of excess glucose to fatty acids. A consequence of increased fatty acid synthesis is increased production of malonyl-CoA, which inhibits CPT-1, the protein responsible for fatty acid transport into the mitochondria. Thus, in an insulin resistance state, FFAs entering the liver from the periphery, as well as those derived from de novo lipogenesis, will be preferentially esterified to triglycerides. ACL, ATP citrate lyase; CPT-1, carnitine palmitoyl transferase-1; FAS, fatty acid synthase; LCE, long-chain fatty acyl elongase (Browning and Horton, 2004).

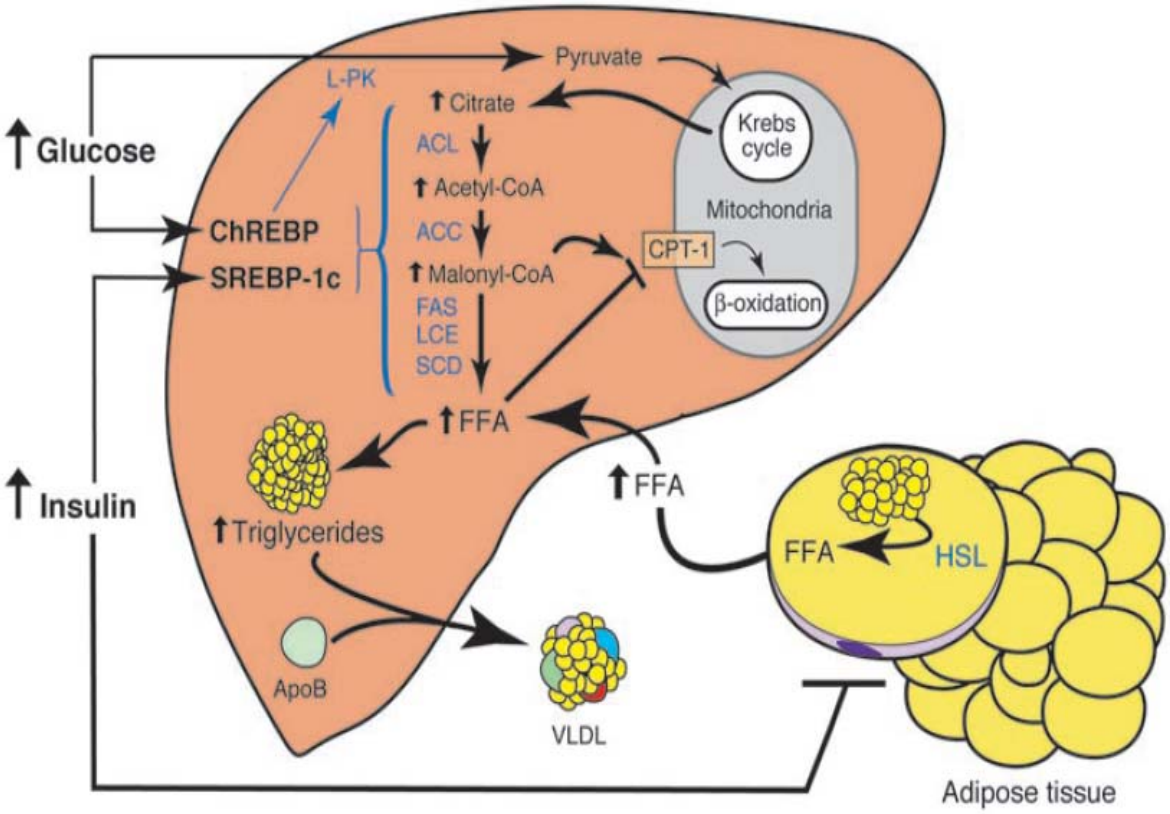
Pyruvate
L-PK
↑ Citrate
Krebs cycle
↑ Glucose
ACL
↑ Acetyl-CoA
Mitochondria
ChREBP
ACC
CPT-1
SREBP-1c
↑ Malonyl-CoA
β-oxidation
FAS
LCE
SCD
↑ FFA
↑ FFA
↑ Insulin
FFA
HSL
↑ Triglycerides
ApoB
VLDL
Adipose tissue

1.3 Lipid Raft

1.3.1 Isolation and Characterization of Lipid Raft

In 1972, Singer and Nicolson suggested the classical fluid mosaic model of the cell membrane based on the finding that most physiological phospholipids exhibit low melting temperatures and, therefore, most likely exist in a liquid disordered phase. However, this model has since been transformed into a more complex system wherein proteins and lipid rafts float laterally within the two dimensional liquid (Simons et al., 2002). Lipid rafts are specialized membrane microdomains enriched in cholesterol and sphingolipids. For example, there is a three to five fold increase in cholesterol in lipid rafts when compared to total membrane content and sphingomyelin, this represents 10-15% of the total lipids in the rafts (Pike, 2004). The fatty acid chains of lipids within the rafts tend to be extended and more tightly packed, creating domains with higher order. Due to the tight packing of lipids, lipid rafts are resistant to solublization by non-ionic detergents such as Triton X-100 at low temperatures, allowing their isolation as an insoluble membrane fraction (Pike, 2004). These liquid-ordered domains contain proteins that are involved in functions such as apoptosis, cell adhesion, signal transduction, endocytosis and cholesterol trafficking (Brown and London, 1998). Proteins with raft affinity include glycosylphosphatidylinositol (GPI)-anchored proteins and doubly acylated proteins such as the tyrosine kinases of the Src family (Simons and Toomre, 2000).

In the phospholipids rich plasma membrane, proteins are recruited through protein-protein interactions. However, in rafts, (Figure 1) this process takes place through interactions between lipids within the rafts and the transmembrane domain of integral membrane proteins (lipid-protein interaction) or the lipid moiety of proteins attached to the membrane by a lipid modification (lipid-lipid interaction). The recruitment of cytosolic proteins by protein-protein interactions can take place in both raft and non-raft membranes through modular domains (Src Homology domain 2 and 3) (Alonso et al., 2001). Thus, lipid rafts may function to bring different proteins into proximity with each other and thus promote interactions between receptors and signaling proteins.

Figure 1.2: **The structure and function of lipid rafts in the plasma membrane.** (A) The specialized membrane microdomains highly enriched in sphingolipids (dark-brown-headed structures) and cholesterol (red bean-shaped structures) float in a phospholipid-rich (light-brown-headed structures) environment. Glycolipids and sphingomyelin are restricted to the outer leaflet of the bilayer, whereas cholesterol and phospholipids are in both leaflets. Note that lipids in the rafts usually have long, saturated fatty acyl chains (red two-legged shapes), whereas those lipids excluded from these microdomains are shorter and unsaturated (green two-legged shapes). (B) In the model of recruitment of proteins in membrane lipid rafts, proteins excluded from rafts are in yellow, while proteins included in rafts are in blue (integral membrane proteins), light brown (GPI-anchored proteins) or pink (acylated, cytosolically-oriented, proteins such as Src family kinases, Ras and heterotrimeric G proteins) (Alonso et al., 2001).

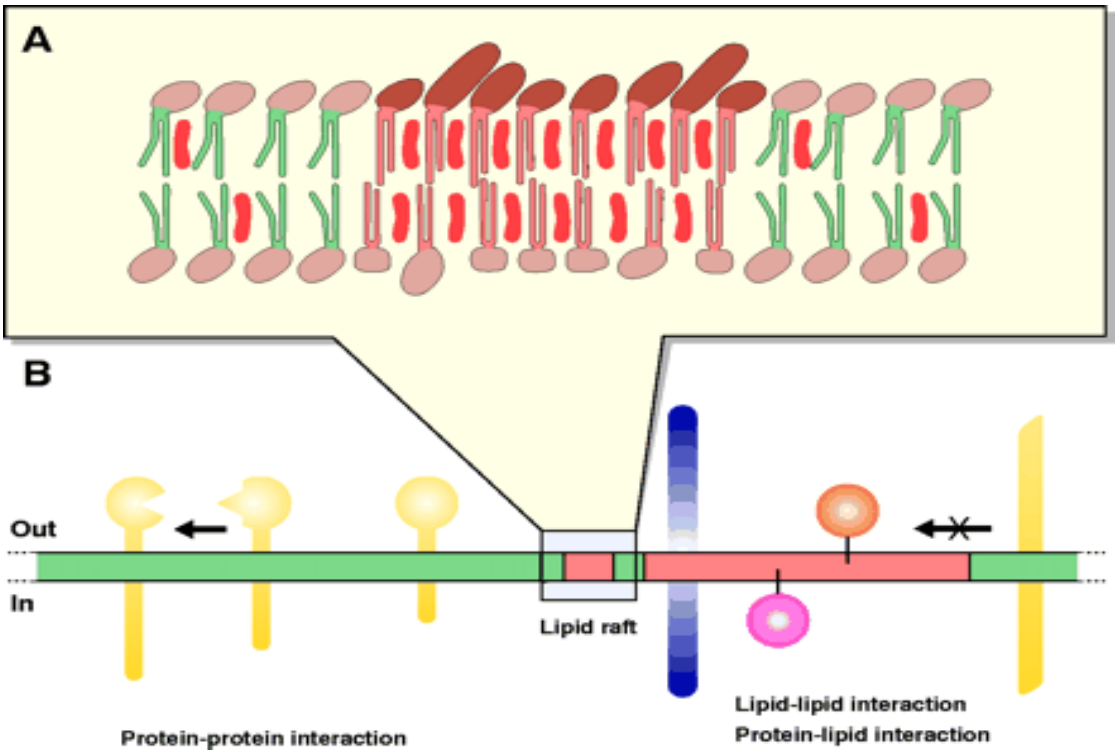
A
B
Out
In
Lipid raft
Protein-protein interaction
Lipid-lipid interaction
Protein-lipid interaction

1.3.2 Cholesterol and Lipid Raft

Cholesterol plays an important role in the phase partitions between raft and non-raft membrane domains by having a higher affinity towards the raft sphingolipids than to unsaturated phospholipids. Sphingolipids in the lipid raft interact with each other via hydrophilic interactions between the sphingolipid headgroups. However, cholesterol acts as a spacer, stabilizing bulky sphingolipid interactions via hydrogen bonds and hydrophobic van der Waal's interactions (Gulbins et al., 2006). It functions as the molecular glue that keeps the assembly together (Simons et al., 2002 and Alonso et al., 2001). However, lipid rafts can be easily modified with the simple approach of cholesterol depletion using methyl-β-cyclodextrin or through antibiotics such as filipin or nystatin or by inhibition of cholesterol biosynthesis with statins. β-Cyclodextrins remove cholesterol from the surface of cells and bind within their hydrophobic cavity. Hence, if cholesterol is depleted from membranes, lipid rafts are dissociated and previously associated proteins are no longer in the rafts (Dobrowsky, 2000).

1.3.3 Caveolae, Caveolin-1 and Lipid Raft

The morphologically identifiable raft-like domains called caveolae (CAV) were first discovered in the early 1950s using electron microscopy (Maguy, 2006). CAV are 50-100 nm flasked shaped non-clathrin-coated invaginations of the plasma membrane. They have been implicated as playing a critical role in transcytosis and endocytosis, cholesterol homeostasis, communication between cell surface membrane receptors and intracellular signaling protein cascades such as apoptosis and tumorigenesis. CAV are found in all cell types but are abundant in muscle cells, endothelial cells, adipocytes, and fibroblasts. These invaginated membrane structures are enriched in cholesterol and sphingolipids, along with the small cholesterol-binding protein "caveolin" (Brown and London, 1998 and Pike, 2004). Lipid rafts and CAV are controversial among researchers, as some researchers consider CAV to be a type of lipid raft that contains caveolin, whereas others consider the two microdomains to be completely separate entities (Brown and Waneck, 1992 and Smart et al., 1999).

Caveolin is a protein with a molecular mass of 21 kDa and was first identified as a substrate for the v-src tyrosine kinases which, like several other kinases, phosphorylates caveolin on Tyr 14. In mammals, this protein family is comprised of three members, caveolin-1, caveolin-2 and caveolin-3, of which caveolin-1 is the principal structural protein. Caveolins contain a highly hydrophobic 33-amino acid membrane-spanning core (Dobrowsky, 2000). The invaginated caveolar structure results from a core hairpin loop in caveolin (Quest et al., 2004). Besides the plasma cell membrane,

caveolins are also present in mitochondria, the endoplasmatic reticulum, the Golgi/trans-Golgi network, and secretory vesicles (Podar and Andersen, 2006).

Caveolins act as scaffolding proteins to cluster and regulate signaling molecules targeted to the caveolae, such as Src-family tyrosine kinases, H-Ras, G protein α subunits, endothelial nitric oxide synthase, protein kinase C, and epidermal growth factor (EGF) receptor. Interestingly, altered caveolin expression has been implicated in a variety of human diseases like Alzheimer, cancer and diabetes (Engelman et al., 1998). Moreover, Cav-1 has been implicated as acting as a tumor suppressor gene and an oncogene depending on the tumor type and tumor stage (Li et al., 1995 and Cohen et al., 2004). It has been demonstrated that transcriptional inactivation of caveolin-1 in human colon cancer cell lines (HT-29 and DLD-1) leads to increased tumor growth in nude mice, suggesting a tumor suppressor function for the protein (Bender et al., 2000). By contrast, studies with tissues from human prostate, breast, and colon adenocarcinoma have shown over expression of caveolin-1, suggesting a potential role as an oncogene (Yang et al., 1998 and Fine et al., 2001). Hence, the role of caveolin-1 in tumorigenesis is controversial.

1.3.4 Sphingolipid Signal Transduction and Lipid Raft

Recent evidence suggests that rafts are involved in aggregation and clustering of receptors upon ligand binding which is facilitated by receptor localization (Simons and Toomre, 2000). Sphingomyelin (SM) is exclusively located in the outer leaflet of the biological membrane and is a major component of lipid rafts, functioning to enhance the efficiency of membrane receptor signaling through ceramide generation (Gulbins et al., 2006). Ceramides usually accumulate in the plasma membrane upon receiving death- or stress-stimuli, and subsequently activate their acidic or neutral sphingomyelinases (Bollinger et al., 2005). The best model that describes the ceramide mediated raft clustering is Fas (CD95) stimulation in Jurkat T cells. In these cells (figure 1.3), Fas clustering with FADD (Fas-associated death domain) and caspase-8, occurs within seconds, translocating acid sphingomyelinase (aSMase) into membrane rafts where it hydrolyzes SM to ceramide and results in the formation of ceramide-enriched membrane platforms (Rotolo, 2005). Thus, it has been suggested that SM is important for Fas clustering through aggregation of lipid rafts, leading to Fas-mediated apoptosis.

Ceramide-mediated raft clustering also mediates stress stimuli triggered cell death other than Fas induced apoptosis. The natural phytoalexin resveratrol, a polyphenol found in grape skin known for its chemopreventive and antitumor activities, has shown the synergistic toxicity of resveratrol and

Figure 1.3: **The proposed model of Fas mediated apoptosis in lipid rafts.** The engagement by Fas ligand (FasL) leads to the binding of the Fas intracellular domain, called death domain (DD) to the cytoplasmic adaptor protein, Fas-associated death domain (FADD), and causes reactive oxygen species-dependent ceramide generation. This in turn aggregates the death receptors in lipid rafts and results in Fas induced apoptosis (Scheel Toellner et al., 2004; Miyaji et al., 2005)

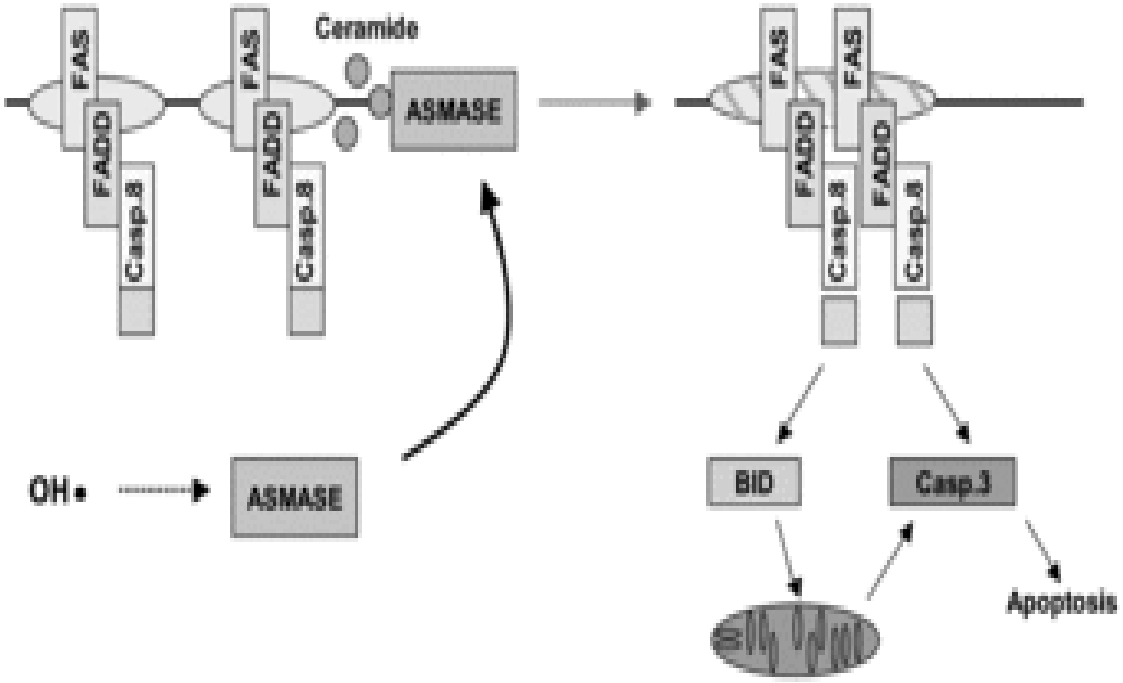
FAS
FADD
Casp.8
Ceramide
ASMASE
OH•
ASMASE
BID
Casp.3
Apoptosis

death receptor ligands in HT29 cells. In the resveratrol treated cells, tumor necrosis factor (TNF), CD95 and TNF-related apoptosis inducing ligand (TRAIL) binding death receptors (DR4 and DR5) is redistributed into the lipid raft and activates the caspase dependent death pathway upon death receptor stimulation (Delmas et al., 2004). Hence, ceramide-mediated raft clustering into macrodomains appears to represent a generic mechanism for transmembrane signaling rather than a specific mechanism for apoptosis induction.

1.3.5 Tyrosine Kinase Signal Transduction and Lipid Raft

Tyrosine kinases were among the first signal transduction molecules to be identified within lipid rafts/caveolae. Many membrane-bound tyrosine kinase receptors including epidermal growth factor (EGF), platelet-derived growth factor (PDGF), insulin, insulin-like growth factor (IGF), etc. have been shown to be localized to lipid rafts (Pike, 2004).

The insulin-like growth factor I receptor (IGF-IR) and the insulin receptor (IR) belong to the same subfamily of receptor tyrosine kinases, each with two extracellular alpha-subunits and two transmembrane beta-subunits. They share highly similar structure and play a major role in maintaining glucose homeostasis. Both receptors can stimulate glucose uptake in muscle and fat which in turn inhibits hepatic glucose production and serves as the primary regulator of blood glucose concentration (Saltiel and Kahn, 2001). Furthermore, the two receptors activate common intracellular pathways. Both receptors phosphorylate insulin receptor substrate (IRS) proteins on the same tyrosine residues. These IRS proteins then act as adaptor molecules to recruit and activate downstream signaling cascades such as the phosphatidylinositol 3-kinase and mitogen-activated protein kinase (MAPK) pathways (Entingh-Pearsall and Kahn, 2004). The insulin receptor-dependent tyrosine phosphorylation of both insulin receptor substrate IRS1 and IRS2 are critical in maintaining proper glucose homeostasis through their interaction with phosphatidylinositol-3-kinase (PI3K). Apart from activation of the PI3-kinase–dependent signaling pathway, compartmentalization of CAP/Cbl complex serves as a second signalling pathway required for insulin-stimulated glucose transport (Baumann et al., 2000).

Insulin like growth factor (IGF) also plays an important role in cancer development and progression**.** Remacle-Bonnet et al. note that IGF-1 shows an antiapototic effect from TNF induced apoptosis as well as a proapoptotic effect through FasL and TRAIL. However, the IGF-I proapoptotic effect appears to be mediated via activation of the PI3-K/Akt pathway when IGF-I

Figure 1.4: The suggested insulin pathway in glucose homeostasis. Two signaling pathways are required for the translocation of the glucose transporter Glut4 by insulin in fat and muscle cells. Tyrosine phosphorylation (Y-P) of the insulin receptor substrate (IRS) proteins after insulin stimulation leads to an interaction with and subsequent activation of the Src-homology 2 (SH2)-domain-containing protein phosphatidylinositol 3-kinase (PI3-K), producing the polyphosphoinositide phosphatidylinositol (3,4,5)-trisphosphate (PIP3), which in turn interacts with and localizes protein kinases such as phosphoinositide-dependent kinase 1 (PDK1). These kinases then initiate a cascade of phosphorylation events, resulting in the activation of Akt and/or atypical protein kinase C (PKC). A separate pool of the insulin receptor can also phosphorylate the substrates Cbl and APS. Upon insulin binding to its tyrosin receptor, substrate Cb1 (proto-oncogene product) gets phosphorylated and interacts with the adaptor protein CAP which can then binds to the lipid raft protein flotillin (Baumann et al., 2000). This interaction recruits phosphorylated Cbl into the lipid raft, resulting in the recruitment of CrkII along with guanine nucleotide exchange factor C3G. Upon this translocation, C3G activates TC10. Activation of TC10 is specific for insulin, and disruption of its activation blocks insulin-stimulated glucose transport and Glut4 translocation (Kimura et al., 2002). These events play crucial roles in the trafficking, docking and fusion of vesicles containing the insulin-responsive glucose transporter Glut4 at the plasma membrane (Saltiel and Pessin, 2002).

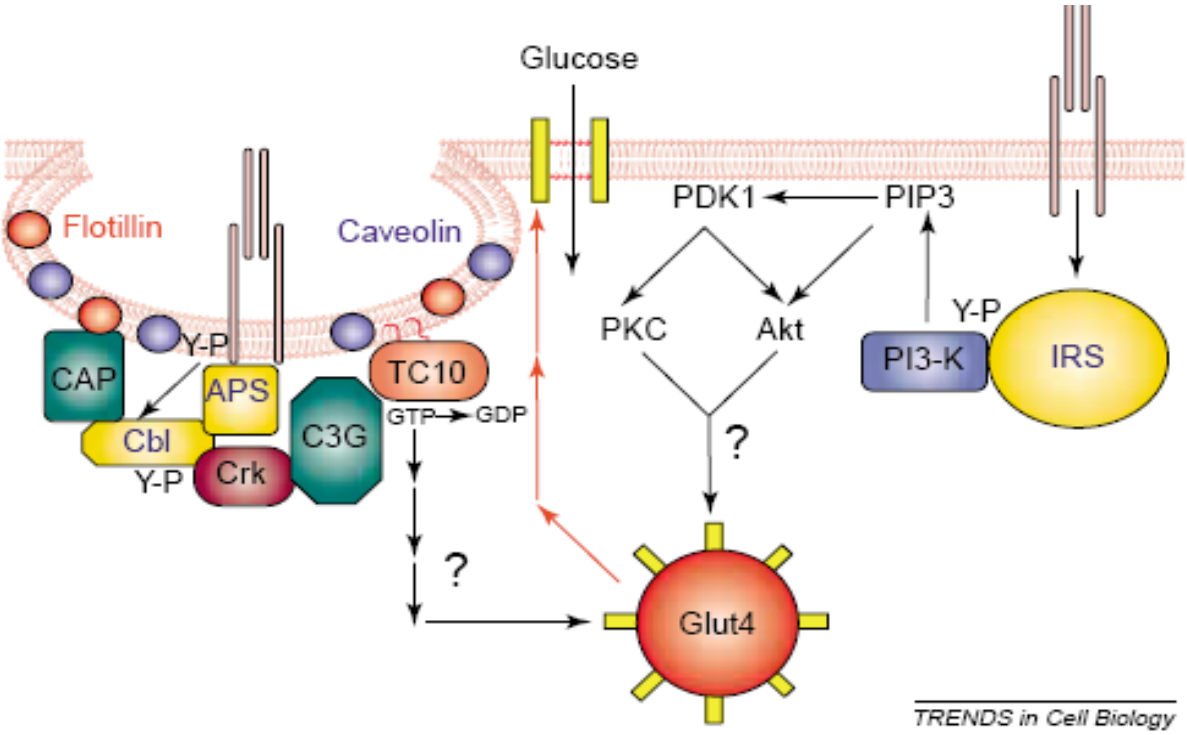
Glucose
Flotillin
Caveolin
PDK1
PIP3
PKC
Akt
Y-P
PI3-K
IRS
CAP
APS
TC10
GTP
GDP
Cbl
Y-P
Crk
C3G
?
?
Glut4
TRENDS in Cell Biology

shows an antiapototic effect from TNF induced apoptosis as well as a proapoptotic effect through FasL and TRAIL. However, the IGF-I proapoptotic effect appears to be mediated through activation of the PI3-K/Akt pathway when IGF-I receptors (IGF-IR) were located in lipid rafts. Furthermore, disruption of rafts by acute cholesterol depletion shifted IGF-IR to non-raft domains and inhibited the IGF-I-mediated proapoptotic effect. In contrast, activation of Erk 1/2 and p38 MAPK seems to suggest that the IGF-I anti-apoptotic signaling occurs outside of rafts. Thus, it has been proposed that segregation of IGF-IR in and out of lipid rafts may dynamically regulate the pro- and anti-apoptotic effects of IGF-I on apoptosis (2005).

1.4 TNF-α Pathway

TNF-α is a pro-inflammatory cytokine produced mainly by activated macrophages. TNF-α elicits a broad spectrum of biologic responses which are mediated by binding to a cell surface receptor. Upon binding to its receptor, TNF-α intiates signaling cascades mediating both cell death and survival. The TNF alpha receptors are members of the TNF superfamily and are denoted as TNF receptor I (TNF-RI) and TNF receptor II (TNF-RII), respectively. The two receptors have relatively conserved extracellular domains and have been found to self assemble via the extracellular pre-ligand assembly domain (PLAD).

1.4.1 TNF-RI Pathway

The schematic representation of TNF-RI pathway is presented in figure 1.5. Following the TNF-RI ligation, TNF Receptor associated death domain (TRADD), an adaptor molecule, is recruited by the death domains (DD) of TNF-RI to form the plasma membrane bound protein complex (Complex-1). TRADD then recruits the secondary adaptors like receptor activating protein (RIP) and TNF Receptor Associated factor 2 (TRAF2) (Varfolomeev and Ashkenazi, 2004). This TRADD-RIP1-TRAF2 complex has been implicated in the indirect activation of IκB kinase (IKK) complex, which consists of IKK α, β and γ. IKK phosphorylates IκB, and which leads to IκB degradation and allowing NF-κB to move to the nucleus to activate transcription. NF-κB activates the transcription of several survival genes, including antiapoptotic proteins c-FLIP (FLICE inhibitory protein), IAPs (inhibitor of apoptosis proteins), Bcl-XL, A1, TRAF1/2, etc. Moreover, the TRADD-RIP1-TRAF2 complex can also activate MAPK/JNK pathway (Ashkenazi and Dixit, 1998).

Complex I then undergoes modification and ligand-dissociated internalization with formation of cytoplasmic Complex II, also known as the DISC (death-inducing signaling complex). Complex II

recruits FADD (Fas-associated death domain) via interactions between conserved death domains (DD) and activates procaspase 8 via interaction between death effector domains (DED). Active caspase 8 cleaves Bid to *t*Bid, which translocates to mitochondria leading to mitochondrial permeabilization, dysfunction and apoptosis (Ashkenazi and Dixit, 1998; Micheau and Tschopp, 2003).

Hence, when NF-κB is activated by complex I, complex II harbors the caspase-8 inhibitor FLIP proteins and the cell survives. The secondary complex (complex II) initiates apoptosis, provided that the NF-κB signal from complex I fails to induce the expression of antiapoptotic proteins such as FLIP (Micheau and Tschopp, 2003).

1.4.2 TNF-R2 Pathway

In contrast to TNF-RI, TNF-RII does not contain a death domain (DD). Instead, TNF-RII directly binds to TNFR-associated factors (TRAFs) and, therefore, is able to activate NF-κB signaling directly. Although TNF-RII has shown instances of pro-apoptotic signaling, in most cellular interactions TNF-RII can be regarded as an anti-apoptotic signaling receptor through TRAF2 degradation (Varfolomeev and Ashkenazi, 2004).

1.4.3 TNF-α and Insulin Resistance

The indications that inflammatory pathways are stimulated in insulin resistance are presented by many researchers. High plasma concentrations of TNF-α (Bird and Raju, 2006) and high TNF-α gene expression in adipocytes are documented in some of the studies (Hotamisligil et al., 1993; Hoffman et al., 1994). However, with further investigation, they established that elevated levels of TNF-α in an obese state contributes to insulin resistance (Samad et al., 1999), with chronic elevations of TNF-RI and TNF-RII observed in obese human and animal studies (Samad et al., 1999; Hotamisligil et al., 1993).

In tissues obtained from Zucker fa/fa rats, which have steatosis, basal IκB kinase-β (IKK-β) activity was increased when compared with lean fa/fa$^+$ controls. In such animal models, various strategies that inhibit IKK-β reverse insulin resistance. For example, insulin resistance is improved by treating obese rats with high doses of NSAID, aspirin, due to decreased expression of IKK-β (Yuan et al., 2001). Yang et al. (1997) showed that obese mice with severe steatosis have much more sensitivity to bacterial endotoxin than do lean ones. They also revealed that liver injury appeared to be mediated by both TNF-α and interferon gamma. Hepatic expression of TNF-α is also increased in

alcohol-induced fatty liver disease, which closely resembles obesity-related hepatic steatosis (Lin et al., 1998). Indeed, another group reported that TNF-RI deficient mice are completely protected from steatohepatitis induced by alcohol, demonstrating the importance of TNF-α during the inflammatory stage of fatty liver disease (Yin et al., 1999).

1.5 Animal Models

The use of animal models allows researchers to investigate progression of disease in a physiologically relevant state to humans. Moreover, they have been used to test targeted therapies, cancer vaccines, preventive agents and combinations of chemopreventive and/or therapeutic agents, allowing large scale clinical trials to be based upon the data generated from this model. However, such studies should always be assessed in regard to how well it resembles human conditions (Green and Hudson, 2005).

With worldwide rises of metabolic disease incidences, rodent models such as OLETF (Otsuka Long-Evans Tokushima Fatty) rats, GK (Goto-Kakizaki) rats, db/db mice, Zucker rats and ob/ob mice are most commonly used in drug discovery. OLETF rats closely simulate the metabolic abnormalities of the human syndrome, especially the diabetic nephropathy. While the GK rat appears to be a suitable model for non-obese diabetes, Zucker rats are generally applied to studies of diabetes with obesity and cardiovascular complications due to the dyslipidaemia background (Chen and Wang, 2005). Moreover, genetically engineered mice have also been used for chemoprevention studies. For instance, Apc^{Min} mice model is widely used for colon carcinogenesis (Green and Hudson, 2005).

1.5.1 Obesity

Obesity is a problem of epidemic proportions in North America. Obesity is a chronic disease consisting of an increase in body fat stores and contributes directly to morbidity and mortality (Formiguera and Canton, 2004). There is a strong correlation between obesity and diseases like cardiovascular and liver disorders, dyslipidemia, insulin resistance, type-2 diabetes, hypertension, metabolic syndrome X and certain types of cancers (Raju and Bird, 2006).

Figure 1.5: Simplified representation of TNF-RI pathway. Upon binding of TNF-α to TNF-RI, Complex 1 forms which initiates a cell survival pathway via NF-κB. Dissociation of Complex 1 leads to formation of Complex 2, which is conjugated with Fas_L recruited FADD. Complex 2 then activates pro-caspase 8. Active caspase 8 cleaves Bid, a BH3 only proapoptotic Bcl2 family member, to a truncated form, *t*Bid. *t*Bid translocates to mitochondria, causing mitochondrial permeabilization and release of mitochondrial effectors of apoptosis, such as cytochrome c (Malhi et al., 2006).

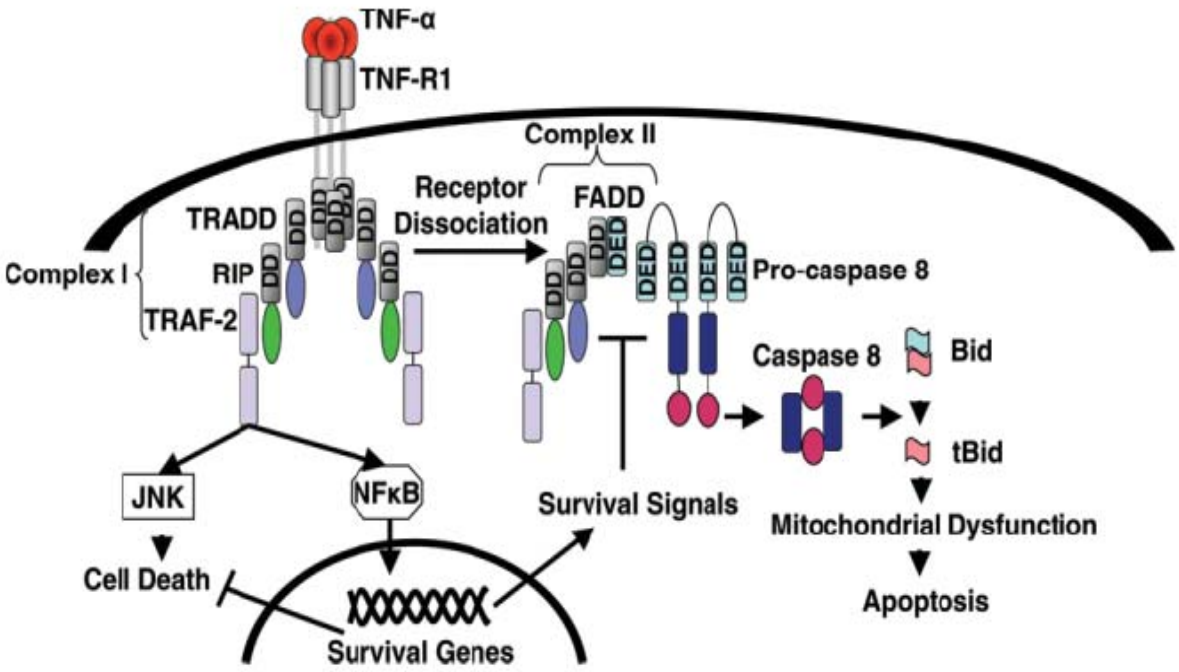
TNF-α
TNF-R1
Complex II
Receptor
Dissociation
FADD
TRADD
RIP
TRAF-2
Complex I
DD
DED
Pro-caspase 8
Caspase 8
Bid
tBid
JNK
NFκB
Survival Signals
Mitochondrial Dysfunction
Cell Death
Apoptosis
Survival Genes

1.5.2 Zucker-Obese Model

The Zucker obese rat is an excellent model most widely for the study of obesity. It has several characteristics in common with human obesity such as hyperphagia, hypertriacylglycerolemia, and hyperinsulinemia. All metabolic changes are present very early (three to five weeks of age) in the life of these animals. Zucker obese rats inherit obesity, as an autosomal Mendelian recessive trait (fa/fa, homozygous for nonfunctional leptin receptors) as compared with their lean (Fa/fa or Fa/Fa) counterparts (figure 1.6) (Zucker and Zucker, 1961). Leptin, the main hormone produced by adipose tissue which regulates body weight and fat metabolism by sending signals to the hypothalamus to suppress appetite (Moore and Dalley, 1999).

1.6 Nonsteroidal Anti-Inflammatory Drug

Nonsteroidal anti-inflammatory drugs (NSAIDs) are among the most widely used medications in the world and are used to treat arthritis and other inflammatory conditions. NSAIDs work by blocking the activity of the enzyme cyclooxygenase, also known as COX. COX is responsible for the conversion of arachidonic acid to prostaglandins, which are short-lived substances that act as local hormones (autocoids) important in normal physiology and pathologic conditions. Research has revealed that there are two cyclooxygenase isoforms known as COX-1 and COX-2 (Meric et al., 2006). COX-1 is involved in the homeostasis of various physiologic functions, such as protection of the gastric mucosa and regulation of platelet aggregation, and is constitutively expressed in many tissues and is responsible for general prostaglandin synthesis. In contrast, COX-2 is undetectable in most normal tissues but is induced by various inflammatory and mitogenic stimuli (Meric et al., 2006). COX-2 is found to be highly expressed in inflammatory disease states, premalignant lesions, and colorectal tumors in both humans and animals (Levi et al., 2001). NSAIDs affect both COX isoforms. Initial NSAIDs, such as aspirin, are non-selective Cox-2 inhibitors and have been shown to reduce the risk of heart attack by 44%. Second classes of COX inhibitors, which include Refecoxib, are selective for Cox-2 and have been shown to decrease renal injury in obese Zucker rats (Dey et al., 2004). In contrast to their therapeutic nature, NSAIDs have adverse effects such as gastrointestinal ulceration and bleeding, disturbance of platelet function, nephrotoxicity, hepatotoxicity and hypersensitivity reactions (Teoh and Farrell, 2003).

Figure 1.6: Zucker obese rat and its lean counterpart. Zucker obese rats are an excellent model of human obesity and provide an ideal opportunity to study hepatic steatosis in an altered physiological state. Zucker obese rats inherit obesity as an autosomal Mendelain recessive trait, fa/fa homozygous for nonfunctional leptin receptors, as compared with their lean (Fa/fa or Fa/Fa) counterparts.

Zucker Obese rats
fa/fa: homozygous
for nonfunctional
leptin receptors

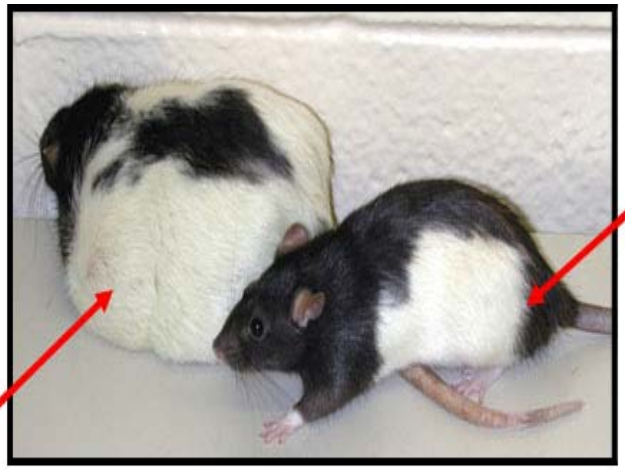

Zucker Lean rats
Fa/fa or Fa/Fa

1.6.1 Piroxicam

The NSAID-Piroxicam, a non-selective COX inhibitor, is used to reduce the pain, inflammation, and stiffness caused by rheumatoid arthritis and osteoarthritis. Reddy et al., has shown, in one study, that colon tumor multiplicity (tumors/animal; tumors/tumor-bearing animal) was significantly inhibited in animals fed diets containing 25 to 150 ppm piroxicam starting 1 and 13 wks after AOM (azoxymethane)-carcinogen administration in male F344 rats. The number of colon tumors/animal was inhibited by about 80% to 84% in animals fed the 150 ppm piroxicam diet (1987). It has been also demonstrated that piroxicam suppress tumor formation in the small intestine of Apc^{Min} mice (Corpet et al., 2003). On the other hand, treatment with 200 ppm piroxicam (~33mg/kg/day) in the Apc^{Min} mice for six or more days resulted in gross intestinal ulceration in >90% of the animals (Levi et al., 2001). Prolonged periods of piroxicam use has been reported to result in hepatotoxicity (Sherman and Jones, 1992).

Chapter 2
Methods and Materials

2.1 Materials

Unless otherwise stated, all chemicals and reagents were purchased from Sigma Chemical Co., Mississauga, Ontario.

Antibodies: Rabit polyclonal to TNF-RI, TNF-RII and NFκB p65 were ordered from Abcam Inc., Cambridge, MA, USA (Cat.# ab19139, ab15563 and ab7970, respectively). Moreover, rabbit anti-IκB-α, anti-IR-β, anti-Caveolin-1 and anti-Flotillin-1 were ordered from Santa Cruz Biotechnologies, Santa Cruz, CA, USA (Cat.# sc-371, sc-711, sc-894 and sc-25506, respectively). Mouse anti-IKK-β came from USBiological, Swampscott, MA, USA (Cat.# I3000-26). Mouse monoclonal to COX-1 and rabbit affinity purified polyclonal to COX-2 were purchased from Cayman Chemical, Ann Arbor, MI, USA (Cat.# 160110 and 160126, respectively). Monoclonal anti-TNF-α antibody produced in mice was used from (Cat.# T3198). Secondary anti-rabbit IgG, HRP-linked antibody was ordered from Cell Signaling Technology, Inc., Danvers, MA, USA (Cat.# 7074), and anti-mouse IgG, peroxidase conjugated antibody came from Sigma-Aldrich Ltd., St. Louis, MO, USA (Cat.# A9044).

2.2 Animal Care and Experimental Design

2.2.1 Animals

Five-week-old female Ob (fa/fa) rats (n=12) and their lean (Fa/Fa) counterparts (n=12) were obtained from Charles River Laboratories (Wilmington, MA, USA) and housed in suspended wire cages approximately 10cm above sawdust bedding trays with a 12-h light/12-h dark cycle, in the animal housing facility. Temperature and relative humidity were controlled at 22°C and 55%, respectively. All animals were acclimatized to the above conditions for one week with free access to standard laboratory rodent chow and *ad libitum* drinking water until initiation of the experiment. All animals were cared for according to the guidelines of the Canadian Council on Animal Care.

2.2.2 Diet, Body Weights and Termination

The experimental design for this study is presented in figure 2.1. Briefly, the control and piroxicam supplemented experimental diets were based on a semesynthetic AIN-93G standard diet formula containing 5% corn oil by weight. The piroxicam supplemented diet contained 150 parts per million powdered piroxicam and the control diet contained no piroxicam and was substituted with corn starch. The dose was selected on the observation that inhibits colon cancer. Diets were prepared twice each week and were stored in the dark at 4°C until used. Food cups were replenished every alternate day with fresh diets, and body weight and food intake monitored routinely on a daily basis. The rats remained on their respective diets for eight weeks, after which they were fasted for 12 h overnight, weighed, and terminated by CO_2 asphyxiation. Following termination, gross anatomy was observed and any pathologic abnormalities were recorded as a general observation. Weights of liver, kidney, spleen, adipose tissues were recorded and the samples frozen for biochemical analysis. For histological observation, segments of the liver were fixed in buffered formalin for a period of 48 h and processed for serial sectioning for haematoxylin and eosin staining.

2.3 Lipid Analysis

2.3.1 Lipid Extraction from Liver Tissue

Total lipids were extracted from liver samples using chloroform/methanol (2:1, vol/vol) with slight modification in Folch method (Folch et al., 1957). One gram of liver tissue was homogenized with 20 ml of chloroform/methanol (2:1) with PT2100 Polytron homogenizer, followed by the addition of 0.3% NaCl at a ratio of 0.2 times the volume of chloroform/methanol (2:1). In other words, 4 mL of 0.3% NaCl was added, and the mixture was vortexed and allowed to separate overnight at 4°C into two phases. The subnatant (bottom phase) was extracted with pasteur pipette and placed into previously weighed glass vials with aluminium lids. The lipid extract was then evaporated to dryness in a sand bath at 37°C. The yellow colour lipid was extracted and weighed on a per gram basis.

2.3.2 Separation of Phospholipids and Triglycerides by Thin Layer Chromatography

The major lipid classes contained in the lipid extract were separated by thin layer chromatography performed on Silica Gel G precoated plates (Alltech Assoc., Deerfield, IL)) in a solvent system containing hexane/diethylether/acetic acid (60:40:3 by volume). The location of various lipid classes was determined by spotting standard samples on the plate before development of the plate in the

Figure 2.1: Schematic representation of the experimental protocol. After one week of acclimatization, Zucker obese (fa/fa) rats and lean (Fa/Fa) rats were randomly divided into two sub-groups receiving either *ad libitum* (Ob or Ln) or 150 ppm piroxicam (Ob-Pirox or Ln-Pirox) diets. All groups were kept on the experimental diets for a period of eight weeks, after which all animals were fasted for 12 hrs and then euthanized by CO_2 asphyxiation.

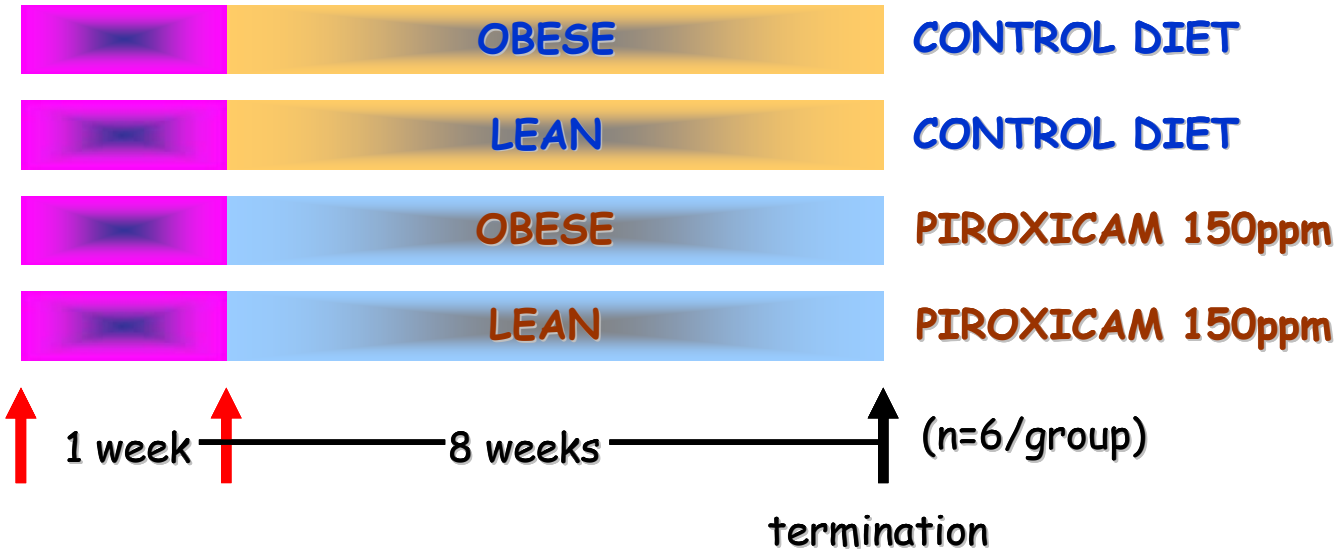
OBESE
CONTROL DIET
LEAN
CONTROL DIET
OBESE
PIROXICAM 150ppm
LEAN
PIROXICAM 150ppm
1 week
8 weeks
(n=6/group)
termination

solvent system, the plates were removed, dried and sprayed with 2', 7'- dichlorofluorescein (Sigma Chemical Co., Mississauga, Ontario). The location of the phospholipid and triglyceride bands was visualized under an ultraviolet lamp.

2.3.3 Fatty Acid Analysis

Bands representing phospholipids and triglycerides as visualized under an ultraviolet lamp were scraped into test tubes and methyl esters were prepared according to the method developed by Morrison and Smith (1964). One mL of boron triflouride in methanol (14% wt/vol; Alltech Assoc., Deerfield, IL) and 300 µL of hexane were added to each lipid sample. Each test tube containing this mixture was tightly capped and heated at 95°C for one hr in the presence of internal standard 17:0 methyl esters. The samples were cooled to room temperature, one mL of distilled water was added to each test tube and the mixture was vortexed and then allowed to stand until the layers had separated. The hexane layer containing the fatty acid methyl esters was removed and dried under pure nitrogen and reconstituted in small volumes of hexane. The reconstituted fatty acid methyl esters were analyzed by capillary gas chromatography according to Salem et al. (1996) on a Shimadzu GC-17A gas chromatograph (Shimadzu, Columbia, MD) with a DB-FFAP 30m × 0.25 mm i.d. × 0.25 µm film thickness column (J&W Scientific from Agilent Technologies, Mississauga, ON).

2.4 Sample Preparation

2.4.1 Preparation of Whole Extract from Liver Tissue

One gram of liver tissue stored at -80°C was chopped and mixed with 3 mL of ice-cold RIPA buffer (50 mM Tris-HCl, 1% NP-40, 0.25% Sodium deoxycholate, 150 mM NaCl, 1 mM EDTA, 1 mM NaF) with freshly added protease inhibitors (1 µg/mL of Aprotinin, Leupeptin, Trypsin Inhibitor, Sodium Orthovandate) and then homogenized in ice using PT2100 Polytron homogenizer. The mixture was transferred into the microcentrifuge tubes, and lipids and cell debris were removed by centrifugation at 15,000 rpm for 20 min at 4°C. The top lipid layer was removed and the supernatant (lysate) was collected and aliquoted in small amounts into pre-chilled eppendorf tubes and stored in -80°C for further analysis. Equal amounts of protein were used for western blot analysis and enzymatic assays.

2.4.2 Preparation of Nuclear Extract from Liver Tissue

Nuclear extraction was carried out using the stock solutions of 10X Buffer A (100 mM HEPES, pH 7.9; 100 mM KCl; 100 mM EDTA) and 5X Buffer B (100 mM HEPES, pH 7.9; 2 M NaCl; 5 mM EDTA; 50% glycerol). Half a gram of liver tissue was weighed and collected in a pre-chilled tube with 1.2 mL of Buffer A mix (1X Buffer A, 1 mM DTT, 0.4% IGEPAL, protease inhibitor cocktail) and then the tissue was homogenized in ice using PT2100 Polytron homogenizer. The homogenate was centrifuged at 9,600 rpm into the microcentrifuge tubes for 10 min at 4°C. The supernatant with the lipid layer was discarded and the pellet was homogenized again into 1 mL of Buffer A mix. Upon incubation on ice for 15 min, the homogenate was centrifuged at 15,000 rpm for 5 min at 4°C. The supernatant (cytosolic fraction) was aliquoted and stored at -80°C. The remaining pellet was resuspended in 150 μL of Buffer B mix (1X Buffer B, 1 mM DTT, protease inhibitor cocktail). The pellet was resuspended by vortexing at high speed for 10-15 sec, and then centrifuged for 5 min at 15,000 rpm. The supernatant (nuclear fraction) was collected into pre-chilled tubes and stored at -80°C for further analysis. Equal amounts of protein were used for western blot analysis.

2.4.3 Isolation of Detergent Resistant Membranes from Liver Tissue

To isolate the low-density membrane rafts, discontinuous sucrose gradient ultracentrifugation was performed. Breifly, 0.5 grams of Zucker rat liver was chopped and mixed with 1 mL of ice-cold MEB lysis buffer (as described earlier) and homogenized with PT2100 Polytron homogenizer. The liver homogenates were transferred into ultracentrifuge tubes and mixed with 1 mL Triton X-100 free MEB buffer (250 mM NaCl, 20 mM Mes pH 6.5) containing 90% (w/v) sucrose. The lysates were sequentially overlaid by 6 mL Triton X-100 free MEB buffer containing 30% (w/v) sucrose and then with 4 mL Triton X-100 free MEB buffer containing 5% (w/v) sucrose, respectively. The discontinous sucrose gradients were centrifuged for 18 hours at 4°C in Beckmann SW40 Ti swinging rotor at 39,500 rpm. A light-scattering band was observed at the 5%-30% sucrose interface. 1-ml fractions were then collected from top to bottom for a total of 12 fractions and 60 μM η-octyl-β-D-glucopyranoside (ODG) was added to each fraction. ODG is a gentle nonionic detergent that is very efficient in solubilizing proteins associated with rafts (Simons and Toomre, 2000). Equal volume from each fraction was used for western blot analysis and enzymatic assays.

Figure 2.2: Schematic representation of isolation of lipid raft from liver tissue. 0.5 grams of liver tissue was homogenized in lysis buffer and then sucrose density gradient was prepared. The tubes were then ultracentrifuged for 18-20 hours. After unltracentrifugation, a light-scattering band at the 5%-30% sucrose interface was observed. Total 12 fractions, 1 mL each was collected from top to bottom in an eppendorf tube.

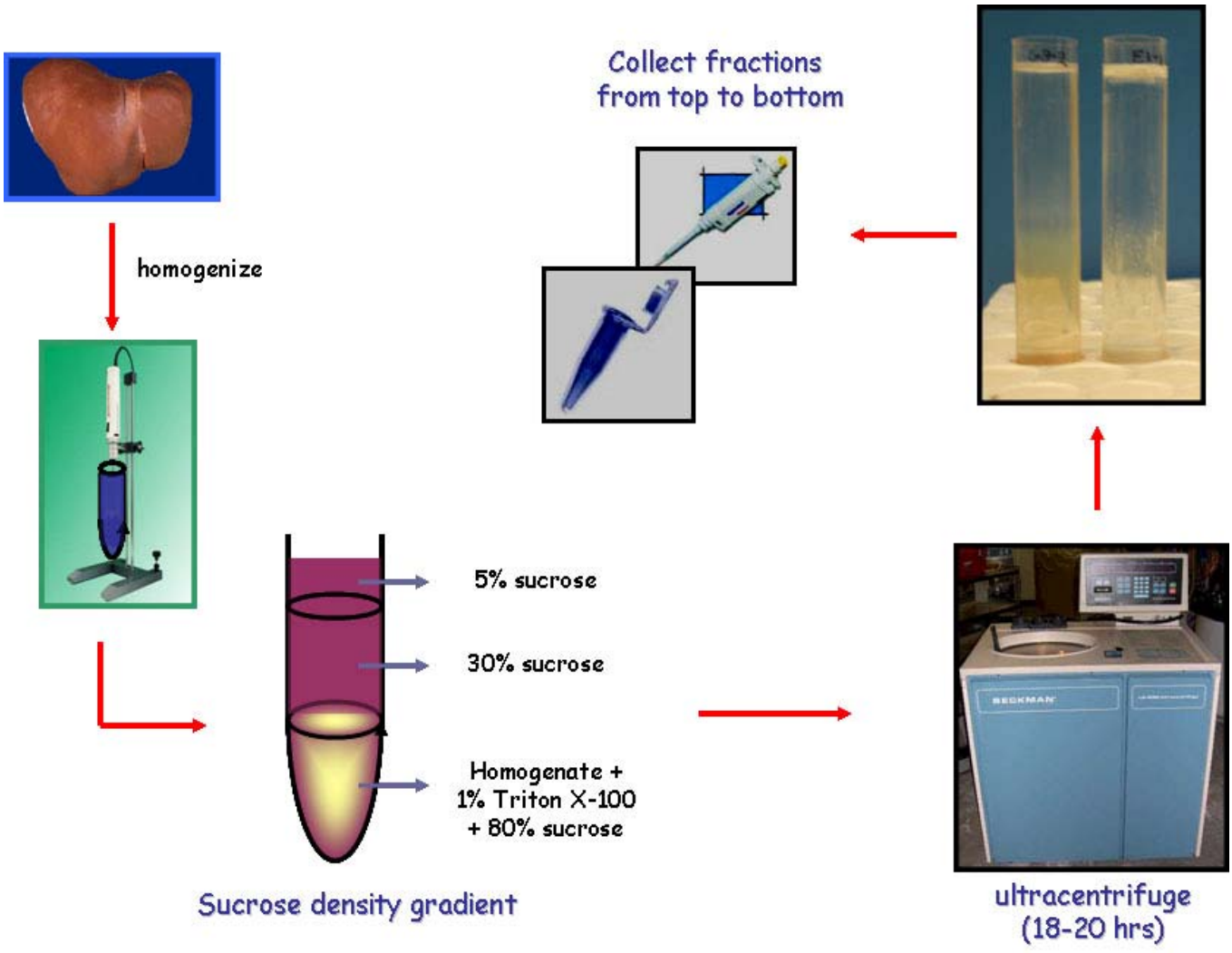
Collect fractions
from top to bottom
homogenize
5% sucrose
30% sucrose
Homogenate +
1% Triton X-100
+ 80% sucrose
Sucrose density gradient
ultracentrifuge
(18-20 hrs)

2.5 Western Blot Analysis

2.5.1 Protein Quantification

A Bio-Rad protein assay, based on Bradford's method, was used to determine the total protein content using bovine serum albumin as a standard. Protein solutions were assayed in duplicate in 96 well plates and the absorbance was measured using Bio-Rad 3550-UV Microplate Reader at a wavelength of 595 nm.

2.5.2 Sodium Dodecyl Sulfate-Polyacrylamide Gel Electrophoresis (SDS-PAGE)

The protein samples were subjected to 8%, 10% or 12% (depending on the molecular weight of protein of interest) SDS-PAGE using the Mini-Protean-BioRad II apparatus (Bio-Rad Laboratories Ltd, Canada). Samples were mixed with equal volumes of 2x SDS Laemmli buffer and boiled for 5 min at 90°C. The separating gel was made with 30% Acrylamide/Bis solution (Bio-Rad Laboratories Ltd, Canada), 1.5 M Tris-HCl (pH 8.8), 10% SDS, 10% Ammonium persulfate and 0.05% TEMED (Bio-Rad Laboratories Ltd, Canada). The 4% stacking gel was made of using all of the above except the Tris-HCl buffer was 1 M with pH 6.8. Equal amounts (50 μg) of liver protein or equal volumes (3 μL or 6 μL) of lipid raft fractions were loaded and run through SDS-PAGE at 120V for 90 mins. The proteins from the gel were then transferred onto PVDF membranes in order to detect the bands with specific antibodies.

2.5.3 Western Blot

Following SDS-PAGE, proteins were transferred onto 15 min methanol soaked 0.45 μm PVDF membranes (Pall Corp. FI, USA) using the Trans-Blot Semi-Dry transfer cell (Bio-Rad Laboratories Ltd, Canada). Briefly, the protein gel was placed on the top of the thick sponge (Bio-Rad Laboratories Ltd, Canada) onto the anode platform of the Semi-Dry system. The PVDF membrane was placed directly onto the gel and another sponge was placed on the membrane. The whole sandwich was then transferred at 20V for 30 mins followed by rolling a test-tube onto the sandwich to remove of the bubbles. The membranes and gels were then stained with Ponceau-S and Coomassie Brilliant Blue for equal loading and proper transfer, respectively. After washing the blots briefly in TBS-T, they were next incubated with TBS-T containing 5% skim milk powder for 1 hour at room temperature to block the non-specific binding, then probed with respective primary antibodies for one hour at room temperature, followed by overnight incubation at 4°C. The immunoblots were washed three times with TBS-T and then incubated with peroxidase conjugated secondary antibodies in a 1% blocking

solution for one hour. After the blots were washed three times in TBS-T, they were incubated for 5 mins with ECL Plus substrate (Amersham Biosciences Canada, GE Healthcare Bio-Sciences Inc., Quebec, Canada) and developed using X-ray film (Fisher Scientific Company, Ottawa, ON, Canada). A positive control was included in all the gels to minimize background and gel-to-gel variability. As well, equal loading of each gel was verified by comparison with the immunoblotting of beta-actin. Finally, densitometric analysis of protein bands was conducted using AlphaEaseFC software (Alpha Innotech Corporation, CA, USA).

2.6 Enzymatic Assays

2.6.1 Transcriptionally Active p65 NF-κB Colorimetric Assay

NF-κB transcription factor activation was monitored using TransAM NF-κB p65 kit (Active motif, Carlsbad, CA) according to the manufacturer's protocol. NF-κB DNA binding activity is detected in ELISA format, where a 96-well plate is coated with the oligonucleotide containing the NF-κB consensus site (5' –GGGACTTTCC- 3'). The active form of NF-κB contained in the nuclear extract specifically binds to this oligonucleotide. The primary antibody used to detect NF-κB recognizes an epitope on p65 that is accessible only when NF-κB is activated and bound to its target DNA. An HRP-conjugated secondary antibody provides a sensitive colorimetric readout that is easily quantified by spectrophotometry.

Briefly, microwells precoated with a double-stranded oligonucleotide containing the NF-κB consensus sequence were incubated with 2 μg of nuclear extracts for 1 hour at room temperature with mild agitation. The microwells were washed three times with a washing buffer to remove any unbound proteins. The captured active transcription factor bound to the consensus sequence was incubated for 1 hour with a specific primary antibody, then for an additional hour with a secondary horseradish peroxidase-conjugated antibody. After washing, the wells were exposed to a developing solution for 10 mins before adding stopping solution. The optical density of each well was determined at 450 nm using Asys UVM 340 spectrophotometer (Montreal Biotech, Montreal, QB, Canada).

2.6.2 Cholesterol Assay

The Amplex Red Cholesterol Assay Kit (Molecular Probes, Eugene, OR) provides a simple fluorometric method for the sensitive quantitation of cholesterol using a fluorescence microplate reader. In this enzymatic assay, cholesteryl esters are hydrolyzed by cholesterol esterase (CE) into

cholesterol, which is then oxidized by cholesterol oxidase (CO) to yield the corresponding ketone and hydrogen peroxide (H_2O_2) coproducts. Thus, the enzymatic methods for assaying cholesterol are based on the measurement of H_2O_2 by way of horseradish peroxidase (HRP)-coupled oxidation of H_2O_2-sensitive probes. In the presence of HRP, Amplex Red reagent reacts with H_2O_2 to produce highly fluorescent resorufin.

To measure cholesterol, 6 µL of lipid raft fraction or 25 µg of liver homogenate was analyzed with the Amplex Red cholesterol fluorescence assay kit according to the manufacturer's instruction. In brief, the assay was conducted in a 96-well microplate using a total of 100 µl reaction volume per well. In addition to membrane fractions or liver homogenates, reaction mixtures contained 300 µM Amplex Red, 2 U/ml HRP, 2 U/mL cholesterol oxidase and 0.2 U/mL cholesterol esterase. The reaction mixtures were incubated at 37°C for 30 mins, and the fluorescence intensities were measured with a filter set for excitation and emission at 560±10 and 590±10 nm, respectively.

2.6.3 Sphingomyelinase Assay

The activity of neutral and acidic sphingomyelinase was measured using the Amplex Red Sphingomyelinase Assay Kit (Molecular Probes, Eugene, OR). In the first step, the enzymatic hydrolysis of sphingomyelin to ceramide and phosphorylcholine is carried out by sphingomyelinase. Then, with the action of alkaline phosphatase, phosphorylcholine is hydrolyzed to choline, which is then oxidized by choline oxidase to betaine and H_2O_2. Finally, H_2O_2 in the presence of horseradish peroxidase reacts with the Amplex Red reagent to generate highly fluorescent resorufin.

The activity of neutral sphingomyelinase was analyzed using 20 µL of lipid raft fraction or 50 µg of liver homogenate through a continuous sphingomyelinase assay method according to the manufacturer's instruction. Briefly, 100 µL of sample was added to a 100 µL assay solution containing 100 µM Amplex Red, 2 U/ml HRP, 0.2 U/mL cholesterol oxidase, 8 U/mL alkaline phosphatase, 0.5 mM sphingomyelin (made in 2% Triton X-100) with 0.1 M Tris-HCl and 10 mM $MgCl_2$, pH 7.4. After preincubation for 1 hr at 37° C, the fluorescence was measured using excitation at 560±10 nm and detection at 590±10 nm. The basal level of neutral sphingomyelinase was measured in the same way as described above except that the reaction mixture did not contain any sphingomyelin.

The 20 µL of lipid raft fraction or 50 µg of liver homogenate (adjusted to pH 5.0) was assayed for acidic sphingomyelinase activity in a two-step reaction system. First, to generate phosphocholine and ceramide, 0.5 mM sphingomyelin was added to the 100 µL sample and incubated

for 60 min at 37 °C. The reaction was then placed on ice and the reaction mixture containing 100 μM Amplex Red, 2 U/ml HRP, 0.2 U/mL cholesterol oxidase, 8 U/mL alkaline phosphatase, with 100 mM Tris-HCl, pH 8, was added and further incubated at 37° C for 1 hr to generate H_2O_2. The fluorescence intensities were measured with a filter set for excitation and emission at 560±10 and 590±10 nm, respectively. The basal level of acidic sphingomyelinase was measured in the same way as described above except that the 100 μL sample was incubated for 60 min at 37 °C without any sphingomyelin.

2.7 Statistical Analysis

Statistical analysis of the data was performed using SPSS statistical software (SPSS Inc., Chicago, IL, USA). A comparison between the groups of interest was performed and differences were determined using ANOVA in conjunction with LSD post-hoc analysis at a significance level of $P < 0.05$ and $P < 0.1$.

Chapter 3
Results

3.1 Hepatic Steatosis and Hepatotoxicity in Obese Rats

3.1.1 Body and Organ Weights of Zucker Rats

Administration of piroxicam at the level of 150 ppm did not significantly affect the observed eating habits or behavior of obese or lean rats. Independent of piroxicam treatment, the body weights were significantly higher in Zucker obese rats than in their lean counterparts (table 3.1). Moreover, a great difference was observed in food intake, calculated as mean weight of food (g) per animal per day, between obese and lean rats. Piroxicam administration significantly elevated the mean body weight and mean liver weight only in obese rats as depicted in table 3.1.

3.1.2 The Gross Pathological Changes Associated with Liver Steatosis

In addition to the weight of the organs, any other visible changes were recorded. Obese animals generally had pale livers, and their kidneys frequently had a cystic and enlarged appearance. Gross appearance of the livers of obese rats treated with piroxicam revealed markedly yellowish marbled appearance. In the obese group three rats had cystic kidneys whereas in the piroxicam treated obese group seven out of eight rats had enlarged cystic kidneys. Piroxicam did not exert any overt toxicity assessed by gross examination of the organs in lean rats. Moreover, quantification of total lipid in hepatic tissue (table 3.1) revealed significantly higher amounts of lipid in obese compared to lean livers. Furthermore, piroxicam significantly increased the amount of lipid per gram of liver only in obese rats without any effect on the level of cholesterol. However, obese rats had significantly higher levels of cholesterol in the hepatic tissue compared to their lean counterparts (table 3.1).

Table 3.1: Body weight, liver weight and food intake of Zucker rats[a]

	Ob	Ob-Pirox	Ln	Ln-Pirox
Body Weight (g)	480.3 ± 8.8 ^{x}	564.2 ± 16.8 ^{y}	260.0 ± 10.2 ^{z}	247.3 ± 14.5 ^{z}
Liver Weight (g)	37.6 ± 1.5 ^{x}	52.4 ± 4.5 ^{y}	8.9 ± 0.3 ^{z}	8.7 ± 0.6 ^{z}
Lipid Weight (g) (per gram of liver)	0.20 ± 0.02 ^{x}	0.32 ± 0.01 ^{y}	0.08 ± 0.00 ^{z}	0.06 ± 0.03 ^{z}
Cholesterol (mmol)	0.45 ± 0.08 ^{x}	0.36 ± 0.04 ^{x}	0.18 ± 0.04 ^{y}	0.33 ± 0.04 ^{x}
Kidney Weight (g)	3.0 ± 0.1 ^{x}	3.9 ± 0.1 ^{y}	1.8 ± 0.05 ^{z}	1.8 ± 0.08 ^{z}
Food intake (g/animal/day)	31.3 ± 0.3 ^{x}	34.5 ± 0.5 ^{y}	23.6 ± 0.8 ^{z}	23.8 ± 1.7 ^{z}

[a]Body and organ weights collected from animals terminated at eight weeks are shown in this table, as is the table, as is the lipid that was extracted from one gram of liver by the folch method using chloroform/methanol (2:1, vol/vol) solvent system. Cholesterol was measured from the hepatic tissues of Zucker rats using the Amplex Red Fluorescence Assay Kit. Equal amounts of liver protein (25 μg) were used to detect cholesterol levels. The enzymatic assay was based on hydrolyzing cholesteryl esters into cholesterol, then oxidizing cholesterol into ketone and H_2O_2. In the presence of horseradish peroxidase (HRP)-coupled oxidation of H_2O_2, Amplex Red reagent reacts with H_2O_2 to produce highly fluorescent resorufin. All values are means ± s.e., n=8/dietary group. Values in a row without a common letter (^{x,y,z}) differ significantly, $P < 0.05$, as determined by ANOVA in conjunction with LSD post-hoc analysis. Ob: Obese, Ob-Pirox: Piroxicam supplemented Obese, Ln: Lean, Ln-Pirox: Piroxicam supplemented Lean.

3.1.3 The Progression of Hepatic Steatosis to Hepatotoxicity

Hepatic steatosis was observed in obese control as well as obese-piroxicam treated rats, with a significant increase in lipid accumulation and steatotic progression in the latter (figure 3.1). Well defined hepatocyte nuclei were evident in the normal lean liver while, the hepatocyte structure of obese livers was irregular and had marked lipid accumulation as indicated by the arrow in figure 3.1b. Overall, 60%-70% of the cells showed lipid accumulation with droplets of varying sizes scattered throughout the liver mass. This condition was exacerbated in piroxicam treated liver tissue (figure 3.1c versus 3.1b) and lipid droplets were more abundant than hepatocyte nuclei and occupied 80% of liver mass. Many smaller lipid droplets appeared to fuse together forming larger droplets.

3.2 Lipid Analysis

3.2.1 Fatty Acid Composition of Total Triglycerides and Phospholipids in Liver

The fatty acid composition of liver phospholipid and triglyceride fractions from obese and lean rats is presented in table 3.2. It should be noted that only pertinent fatty acids are presented in this table while the rest are shown in tables B1 and B2 (Appendix). Total phospholipid fractions of control obese rats were noted to contain significantly higher ($p<0.05$) percentages of saturated (except 18:0) fatty acids and significantly lower percentages ($p<0.05$) of 18:2 n-6 and 20:4 n-6 unsaturated fatty acids. Piroxicam supplementation caused a significant decrease ($p<0.05$) in the percentage of 16:0 fatty acids and a significant increase in 20:4 n-6 fatty acid levels in obese rats, while having the opposite effect in lean rats. Triglyceride fractions of lean rats were observed to contain increased saturated and n-6 fatty acids as compared to obese rats. Piroxicam supplementation showed no changes in saturated fatty acid levels but increased significantly ($p<0.05$) the level of 20:4 n-6 in both obese and lean rats. Moreover, obese had significantly high concentration of total fatty acids in the triglyceride fractions compare to lean. Piroxicam further increased its level significantly in obese.

Figure 3.1: Haematoxylin and eosin stained liver histology of Zucker rats. After termination, the segment of liver was fixed in buffered fomalin and was sectioned for histological observation. Transverse sections (4 μm) were made and stained with heamatoxylin (stains nuclei black) and eosin (stains cytoplasm pink). (a) Zucker obese (Ob) rat liver tissue showing different sizes of lipid droplets in hepatocytes (arrow); (b) Zucker lean (Ln) rat liver tissue displaying normal liver architecture; (c) piroxicam fed Zucker obese rat (Ob-pirox) liver tissue showing deterioration of hepatocytes containing increased lipid accumulation. Magnification used x 100.

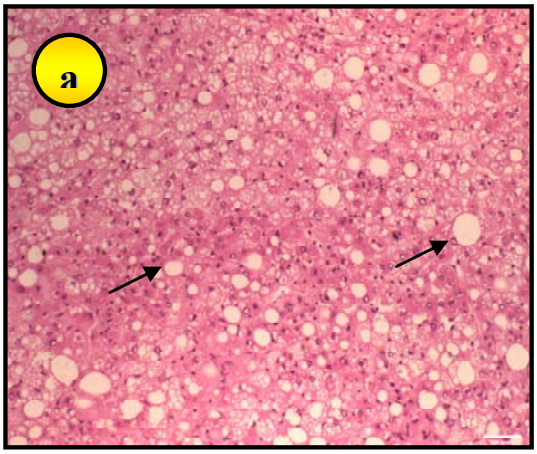

Ob

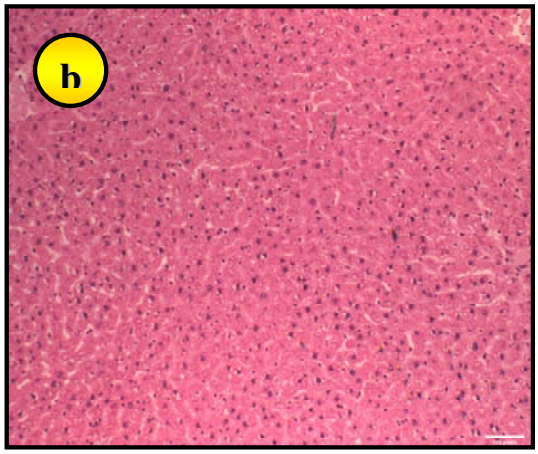

Ln

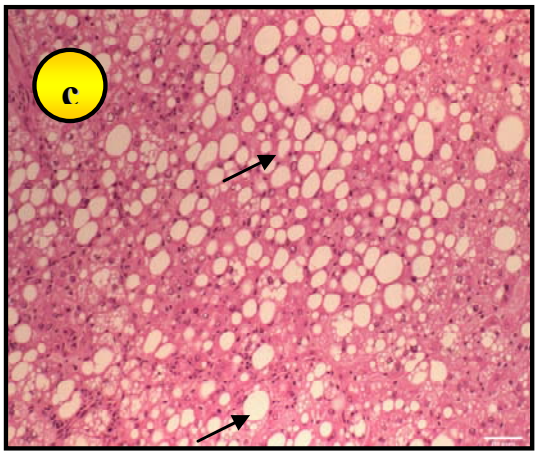

Ob-pirox

Table 3.2: Percent fatty acid composition of total phospholipids and triglycerides in liver[a]

	Ob	Ob-Pirox	Ln	Ln-Pirox
Phospholipid				
C14:0	0.49 ± 0.01^{x}	0.24 ± 0.01^{y}	0.15 ± 0.01^{z}	0.27 ± 0.00^{y}
C16:0	20.47 ± 0.73^{x}	16.43 ± 0.69^{y}	13.44 ± 0.42^{z}	17.08 ± 0.90^{y}
C18:0	22.55 ± 0.48^{x}	28.57 ± 0.71^{y}	32.69 ± 0.71^{z}	26.81 ± 1.52^{y}
C18:1 n-9	13.92 ± 0.75^{x}	5.98 ± 0.34^{y}	2.16 ± 0.12^{z}	6.41 ± 0.26^{y}
C18:2 n-6	4.60 ± 0.25^{x}	3.68 ± 0.17^{x}	7.90 ± 0.25^{y}	11.31 ± 0.64^{z}
C20:4 n-6	20.60 ± 0.67^{x}	28.86 ± 0.39^{y}	25.71 ± 0.21^{z}	22.43 ± 0.55^{w}
Total (mg/g)	17.38 ± 0.64^{x}	12.13 ± 0.74^{y}	17.30 ± 0.66^{x}	15.71 ± 0.49^{x}
Triglyceride				
C14:0	1.32 ± 0.06^{x}	1.46 ± 0.03^{x}	0.97 ± 0.13^{y}	0.86 ± 0.07^{y}
C16:0	34.97 ± 0.32^{x}	33.11 ± 0.83^{x}	35.59 ± 1.31^{x}	35.00 ± 1.23^{x}
C18:0	2.92 ± 0.23^{x}	3.17 ± 0.21^{x}	5.36 ± 0.34^{y}	3.27 ± 0.42^{x}
C18:1 n-9	34.93 ± 1.13^{x}	38.20 ± 1.29^{x}	23.57 ± 2.15^{y}	27.26 ± 0.84^{y}
C18:2 n-6	4.31 ± 0.20^{x}	3.65 ± 0.34^{x}	16.00 ± 1.69^{y}	22.33 ± 2.20^{z}
C20:4 n-6	0.28 ± 0.02^{x}	0.40 ± 0.07^{y}	1.06 ± 0.17^{z}	1.72 ± 0.18^{w}
Total (mg/g)	185.93 ± 11.79^{x}	231.32 ± 10.19^{y}	9.28 ± 2.42^{z}	33.54 ± 6.10^{z}

[a]Total lipids were extracted from liver samples using a chloroform/methanol (2:1, vol/vol) solvent system. Phospholipids and triglycerides were separated by thin-layer chromatography. The corresponding phospholipid and triglyceride bands were transmethylated and converted to methyl esters. These fatty acid esters were analyzed by capillary gas chromatography. All values are means ± s.e., n=4/dietary group. Values in a row without a common letter (^{x,y,z}) differ significantly, $P < 0.05$, as determined by ANOVA in conjunction with LSD post-hoc analysis. Ob: Obese, Ob-Pirox: Piroxicam supplemented Obese, Ln: Lean, Ln-Pirox: Piroxicam supplemented Lean.

3.3 Protein Expression Patterns in Liver Tissue

3.3.1 COX-1 and COX-2 Protein Expressions

COX-1 protein (figure 3.2) levels were higher in obese rat livers compared to those of lean rats. Piroxicam treatment caused a significant ($p<0.05$) increase in the level of COX-1 protein only within lean rats. COX-2 protein levels (figure 3.2) were similar in both obese and lean rats. Piroxicam treated groups were observed to have significantly ($p<0.05$) lower hepatic COX-2 levels compared to the corresponding control rats.

3.3.2 TNF-α, TNF-RI and TNF-RII Protein Expressions

TNF-α specific antibody identified two major bands with 17 and 80 kDa as shown in figure 3.3. Both bands were quantified knowing that TNF-α could exist in the free and bound form. The soluble form at 17 kDa showed variability between obese and lean rats ($p<0.1$). In this context, obese livers were observed to have lower levels of the soluble 17 kDa form than lean livers. Piroxicam further decreased the level of TNF-α in lean rats but not in obese rats, significance ($p<0.05$). The membrane bound (higher molecular band) 80 kDa protein was more consistent within the group and it was observed that obese rats had higher levels of the protein than lean rats. Moreover, piroxicam consistently lowered the levels of TNF-α in both obese and lean rats.

The anti-TNF-RI antibody also recognized two closely associated bands (55 and 57kD). The levels of TNF-RI protein (figure 3.3) in obese and lean livers were differed significantly, with lean rat livers having lower levels than obese. Piroxicam treatment affected the level of TNF-RI differently depending on the genotype of the animals. In the lean rats, piroxicam treatment resulted in a moderate but significant increase in TNF-RI levels compared to those noted in control livers ($p<0.05$). An opposite effect, however, was observed in piroxicam treated obese animals as the group had lower TNF-RI levels than the control obese group ($p<0.1$).

TNF-RII levels were significantly lower (figure 3.3) in obese rat hepatic tissue compared to lean. A significant ($p<0.05$) increase in TNF-RII levels was noticed in lean piroxicam treated hepatic tissue compared to control hepatic tissue. An opposite effect of piroxicam was noted in the obese rats. Piroxicam treated obese animals had a reduced level of TNF-RII ($p<0.08$).

Figure 3.2: Western blot analysis of COX-1 and COX-2 protein expressions from liver homogenates of Zucker rats. Equal amounts of liver protein (50 μg) was separated by 8% SDS-PAGE gel and transferred onto PVDF membranes. Following incubation with primary antibodies at a final dilution of 1:1000 and corresponding HRP-conjugated secondary antibodies at a final dilution of 1:5000, the blots were developed on X-ray film using ECL Plus substrate. The blots were first identified by immunoblotting with anti-rabbit affinity purified polyclonal COX-2 antobody. The same membranes were then reprobed with anti-mouse monoclonal COX-1 antibody. Equal loading of each gel was verified by comparison with the immunoblotting of beta-actin. (A) Representative western blots of COX-1, COX-2 and β-actin using 50 μg of liver protein from Zucker obese (Ob) and lean rats with or without piroxicam treatment. (B) Ponceau S staining of membranes containing 50 μg of liver homogenate from all four groups of Zucker rats. (C) Bar graphs represents levels of COX-1 and COX-2 protein. Densitometric values were corrected for gel-to-gel variability using equal amounts of a common liver homogenate as a positive control in each blot. All values are means ± s.e., n=4/dietary group. Bars without a common letter ($^{x, y, z}$) differ significantly, $p<0.05$, as determined by ANOVA in conjunction with LSD post-hoc analysis. Ob: Obese, Ob-Pirox: Piroxicam supplemented Obese, Ln: Lean, Ln-Pirox: Piroxicam supplemented Lean.

A

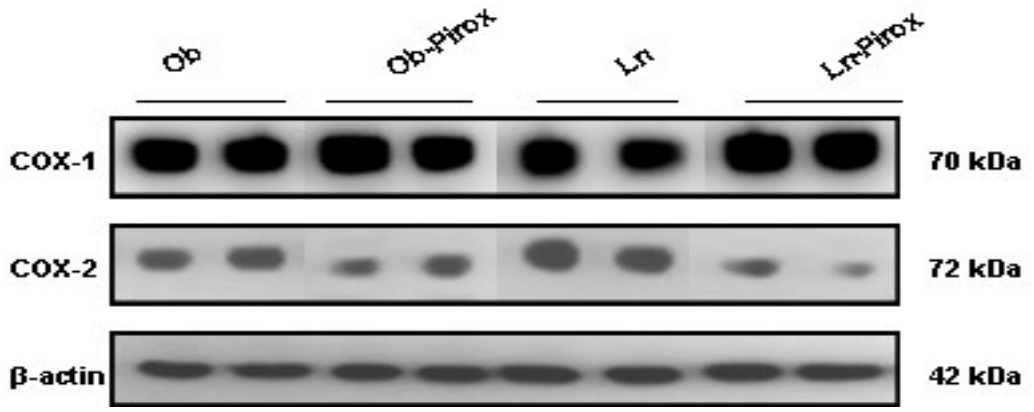
Ob
Ob-Pirox
Ln
Ln-Pirox
COX-1
70 kDa
COX-2
72 kDa
β-actin
42 kDa

B

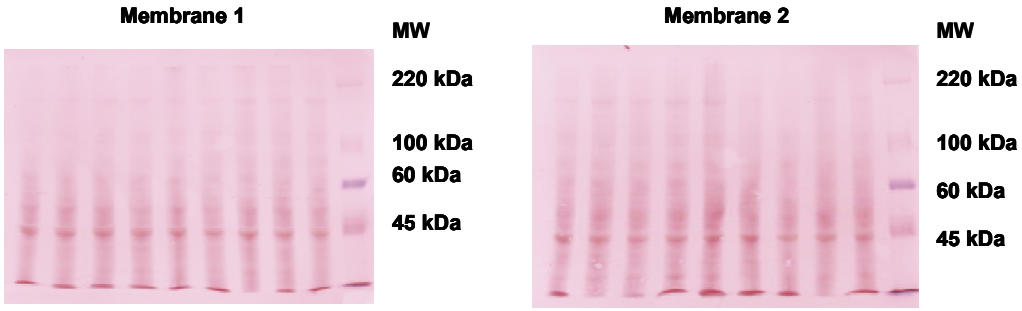
Membrane 1
MW
220 kDa
100 kDa
60 kDa
45 kDa
Membrane 2
MW
220 kDa
100 kDa
60 kDa
45 kDa

C

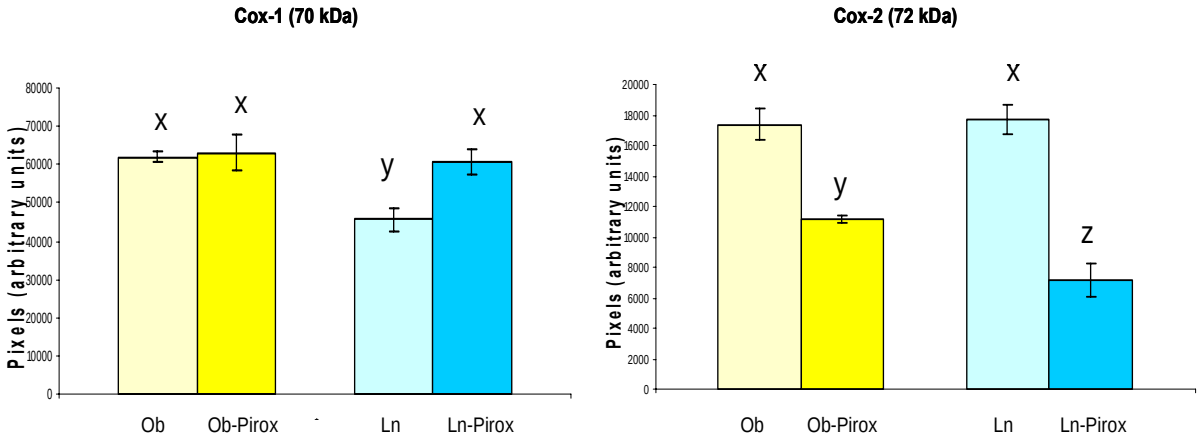
Cox-1 (70 kDa)
Pixels (arbitrary units)
80000
70000
60000
50000
40000
30000
20000
10000
0
x
x
y
x
Ob
Ob-Pirox
Ln
Ln-Pirox
Cox-2 (72 kDa)
Pixels (arbitrary units)
20000
18000
16000
14000
12000
10000
8000
6000
4000
2000
0
x
y
x
z
Ob
Ob-Pirox
Ln
Ln-Pirox

Figure 3.3: Western blot analysis of TNF-α protein expression from liver homogenates of Zucker rats. About 50 μg of liver protein was loaded into a 10% acrylamide gel and transferred to a PVDF membrane. The membrane was probed with primary TNF-α monoclonal antibody at a concentration of 1:1000. After washing, the membrane was probed with secondary anti-mouse antibody at 1:5000 concentration. The blots were developed on X-ray film using ECL Plus substrate. Equal loading of each gel was verified by comparison with the immunoblotting of beta-actin. (A) Representative western blots of TNF-α and β-actin using 50 μg of liver protein from Zucker obese (Ob) and lean rats with or without piroxicam treatment. (B) Ponceau S staining of membranes containing 50 μg of liver homogenate from all four groups of Zucker rats. (C) Bar graphs represents levels of TNF-α protein. Densitometric values were corrected for gel-to-gel variability using equal amounts of a common liver homogenate as a positive control in each blot. All values are means ± s.e., n=4/dietary group. Bars without a common letter ($^{x, y, z}$) differ significantly, $p<0.05$ and $p<0.1$, as determined by ANOVA in conjunction with LSD post-hoc analysis. Ob: Obese, Ob-Pirox: Piroxicam supplemented Obese, Ln: Lean, Ln-Pirox: Piroxicam supplemented Lean.

A

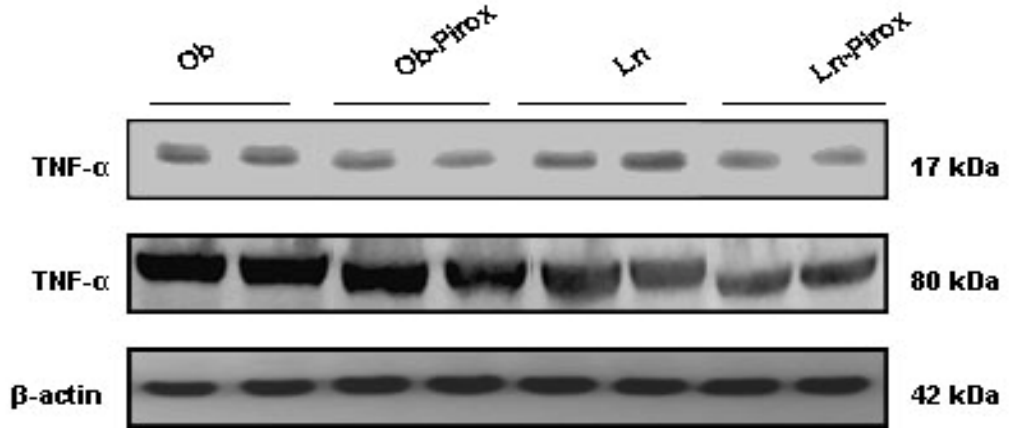
Ob
Ob-Pirox
Ln
Ln-Pirox
TNF-α
17 kDa
TNF-α
80 kDa
β-actin
42 kDa

B

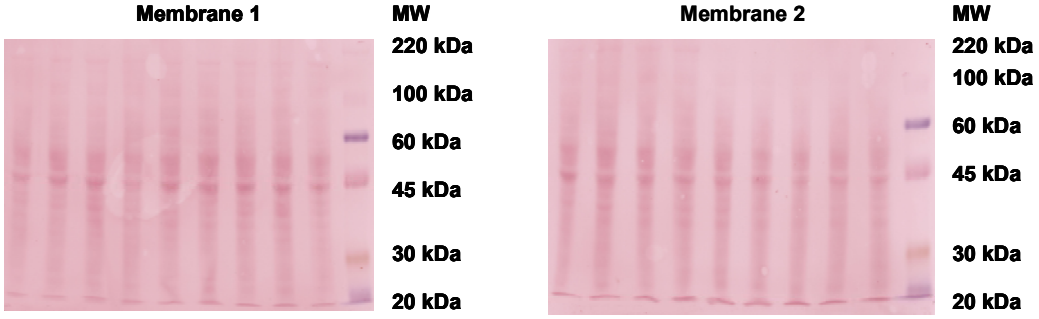
Membrane 1
MW
220 kDa
100 kDa
60 kDa
45 kDa
30 kDa
20 kDa
Membrane 2
MW
220 kDa
100 kDa
60 kDa
45 kDa
30 kDa
20 kDa

C

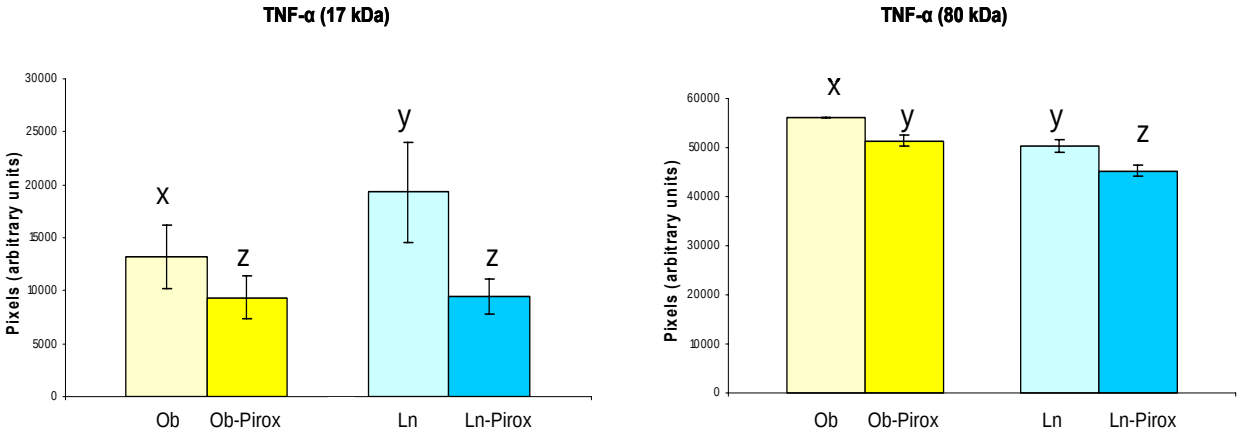
TNF-α (17 kDa)
Pixels (arbitrary units)
30000
25000
20000
15000
10000
5000
0
x
y
z
z
Ob
Ob-Pirox
Ln
Ln-Pirox
TNF-α (80 kDa)
Pixels (arbitrary units)
60000
50000
40000
30000
20000
10000
0
x
y
y
z
Ob
Ob-Pirox
Ln
Ln-Pirox

Figure 3.4: **Western blot analysis of TNF-RI and TNF-RII protein expressions from liver homogenates of Zucker rats.** Equal amounts of liver protein (50 μg) was separated by 8% SDS-PAGE gel and transferred onto PVDF membranes. Following incubation with primary antibodies at a final dilution of 1:1000 and corresponding HRP-conjugated secondary antibodies at a final dilution of 1:5000, the blots were developed on X-ray film using ECL Plus substrate. The blots were first identified by immunoblotting with anti-rabbit polyclonal TNF-RI antibody. The same membranes were then reprobed with anti-rabbit polyclonal TNF-RII antibody. Equal loading of each gel was verified by comparison with the immunoblotting of beta-actin. (A) Representative western blots of TNF-RI, TNF-RII and β-actin using 50 μg of liver protein from Zucker obese (Ob) and lean rats with or without piroxicam treatment. (B) Ponceau S staining of membranes containing 50 μg of liver homogenate from all four groups of Zucker rats. (C) Bar graphs represents levels of TNF-RI and TNF-RII protein. Densitometric values were corrected for gel-to-gel variability using equal amounts of a common liver homogenate as a positive control in each blot. All values are means ± s.e., n=4/dietary group. Bars without a common letter ($^{x, y, z}$) differ significantly, $p<0.05$, $p<0.08$ and $p<0.1$, as determined by ANOVA in conjunction with LSD post-hoc analysis. Ob: Obese, Ob-Pirox: Piroxicam supplemented Obese, Ln: Lean, Ln-Pirox: Piroxicam supplemented Lean.

A

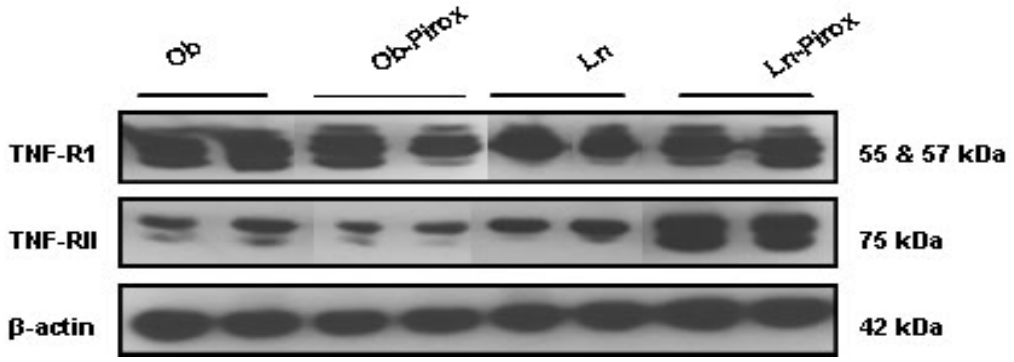
Ob
Ob-Pirox
Ln
Ln-Pirox
TNF-R1
55 & 57 kDa
TNF-RII
75 kDa
β-actin
42 kDa

B

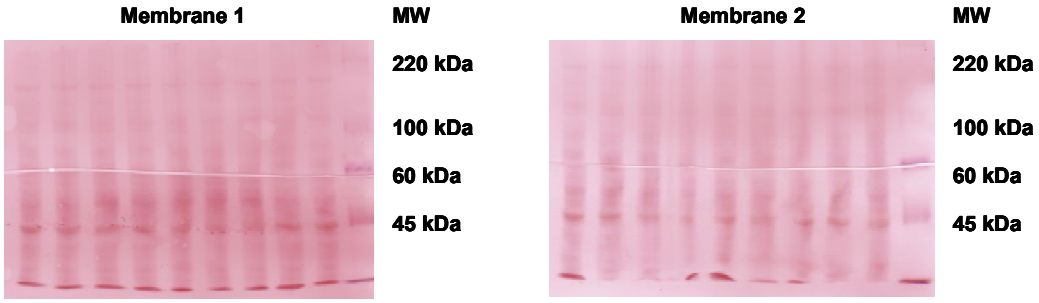
Membrane 1
MW
220 kDa
100 kDa
60 kDa
45 kDa
Membrane 2
MW
220 kDa
100 kDa
60 kDa
45 kDa

C

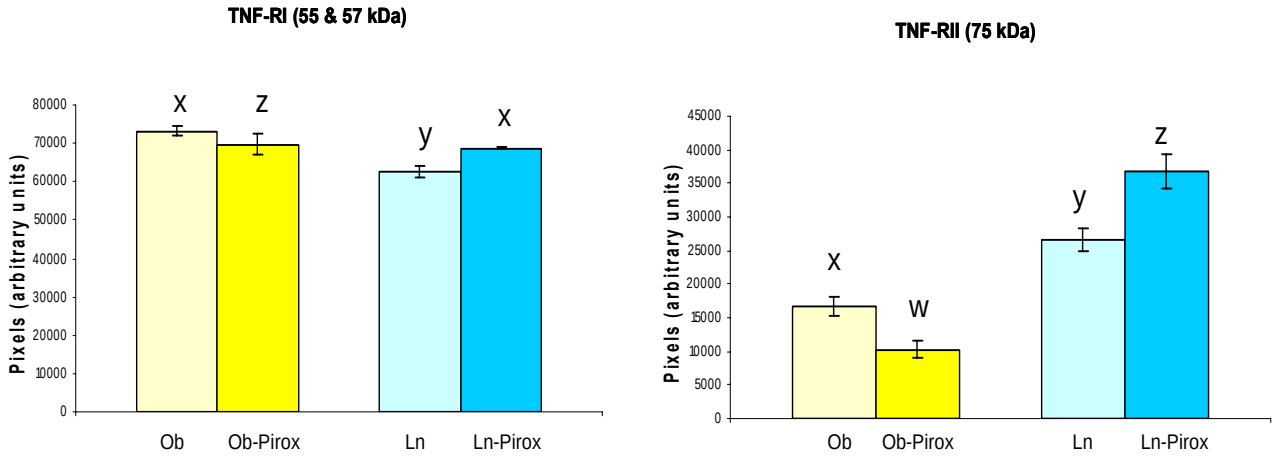
TNF-RI (55 & 57 kDa)
Pixels (arbitrary units)
80000
70000
60000
50000
40000
30000
20000
10000
0
x
z
y
x
Ob
Ob-Pirox
Ln
Ln-Pirox
TNF-RII (75 kDa)
Pixels (arbitrary units)
45000
40000
35000
30000
25000
20000
15000
10000
5000
0
x
w
y
z
Ob
Ob-Pirox
Ln
Ln-Pirox

3.3.3 NF-κB Protein Expression

Obese animals had significantly elevated levels of both whole homogenate (liver tissue) and nuclear NF-κB protein levels compared to their lean counterparts as shown in figure 3.5 and figure 3.7 respectively. Moreover, a 5-6 fold difference of the p65 NF-κB protein level is observed in the nuclear fraction between obese and lean rats. Piroxicam treatment resulted in lowering the NF-κB level in the lean liver tissue only. Significant differences in NF-κB protein levels were not observed between piroxicam treated obese and obese control animals. Piroxicam treated obese animals, however, had a moderate but statistically significant elevation in nuclear NF-κB levels compared to the obese control animals. A significant trend was not observed between piroxicam treated lean and lean control animals in the nuclear rich fraction.

To determine the level of transcriptionally active NF-κB in the nuclear fraction, the DNA binding activity was assessed through an ELISA kit (figure 3.8). No significant trend was observed between obese and lean rats. Increased active NF-κB was observed in piroxicam treated obese animals as compared to their obese control counterparts. However, the differences in abundance were not as large as those noted in the nuclear fraction by western blot analysis. A significant difference ($p<0.05$) in active NF-κB was not observed between piroxicam treated lean and lean control rats.

3.3.4 IκB-α Protein Expression

Western blots were performed to assess relative whole homogenate (liver tissue) and nuclear extract protein levels of IκB-α in all groups (figures 3.12 and 3.13). A significantly increased level of IκB-α protein was observed in obese compared to lean rat liver tissue. Piroxicam treated obese rats had lower levels of IκB-α protein than obese control rats. A significant trend ($p<0.05$) was not observed in piroxicam lean vs. lean control animals. Surprisingly, in the nuclear rich fraction IκB-α was present in significantly higher amounts in the livers of obese rats compared to those of lean ones. The effect of piroxicam in the nuclear extract was seen in the lean liver only. Similar levels of nuclear IκB-α protein were observed in both obese and obese piroxicam treated rats.

3.3.5 IKK-β Protein Expression

Obese livers had higher levels of IKK-β protein than lean livers. Increased levels of IKK-β protein were observed in lean piroxicam treated rats compared to lean control rats. No apparent differences in IKK-β protein levels were noticed between piroxicam treated obese rats and their obese control counterparts (figure 3.14).

Figure 3.5: **Western blot analysis of NF-κB and IκB-α protein expression from liver homogenates of Zucker rats**. Equal amounts of liver protein (50 μg) were separated by 8% SDS-PAGE gel and transferred onto PVDF membranes. Following incubation with primary antibodies at a final dilution of 1:1000 and corresponding HRP-conjugated secondary antibodies at a final dilution of 1:5000, the blots were developed on X-ray film using ECL Plus substrate. The blots were first identified by immunoblotting with anti-rabbit polyclonal NF-κB antibody. The same membranes were then reprobed with anti-rabbit polyclonal IκB-α antibody. Equal loading of each gel was verified by comparison with the immunoblotting of beta-actin. (A) Representative western blots of NF-κB, IκB-α and β-actin using 50 μg of liver protein from Zucker obese (Ob) and lean rats with or without piroxicam treatment. (B) Ponceau S staining of membranes containing 50 μg of liver homogenate from all four groups of Zucker rats. (C) Bar graphs represents levels of NF-κB and IκB-α protein. Densitometric values were corrected for gel-to-gel variability using equal amounts of a common liver homogenate as a positive control in each blot. All values are means ± s.e., n=4/dietary group. Bars without a common letter ($^{x, y, z}$) differ significantly, $p<0.05$, as determined by ANOVA in conjunction with LSD post-hoc analysis. Ob: Obese, Ob-Pirox: Piroxicam supplemented Obese, Ln: Lean, Ln-Pirox: Piroxicam supplemented Lean.

A

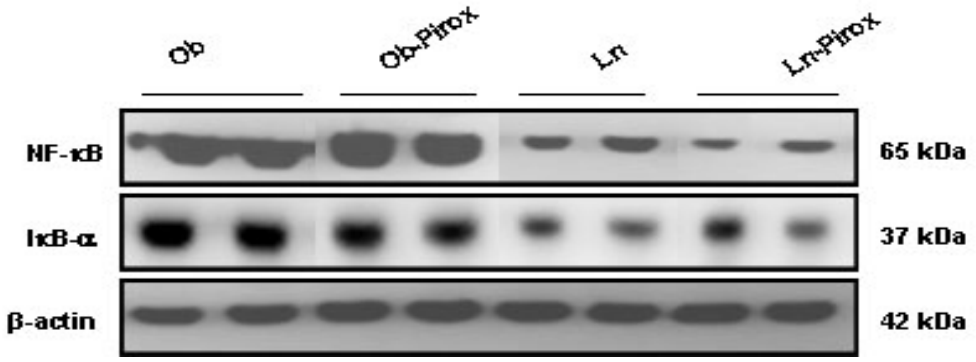
Ob
Ob-Pirox
Ln
Ln-Pirox
NF-κB
IκB-α
β-actin
65 kDa
37 kDa
42 kDa

B

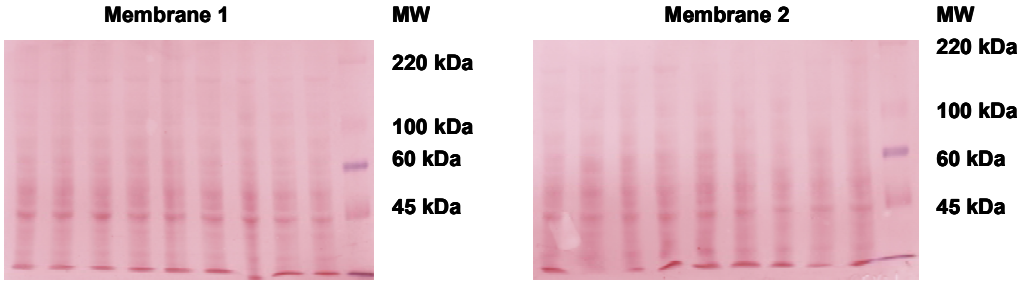
Membrane 1
MW
220 kDa
100 kDa
60 kDa
45 kDa
Membrane 2
MW
220 kDa
100 kDa
60 kDa
45 kDa

C

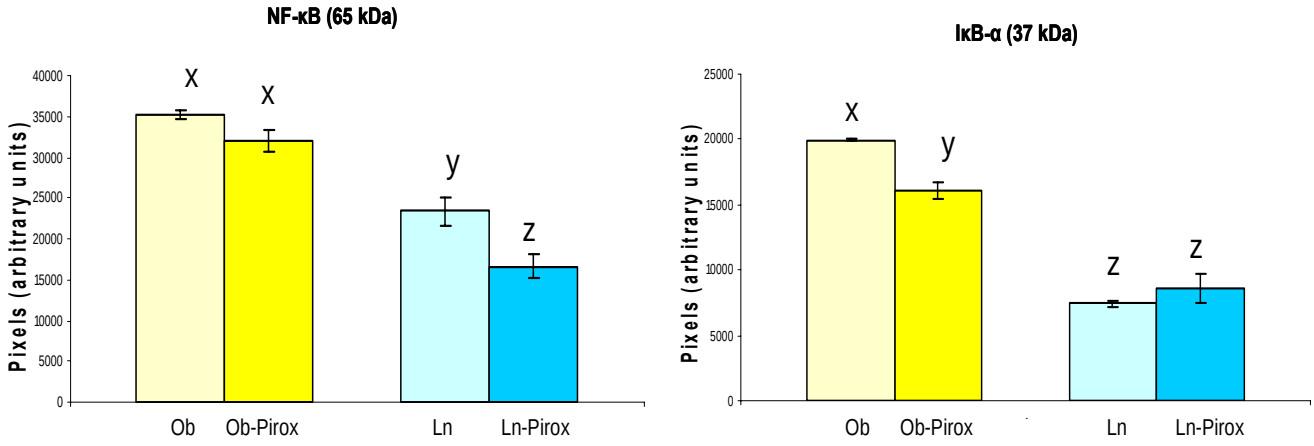
NF-κB (65 kDa)
Pixels (arbitrary units)
40000
35000
30000
25000
20000
15000
10000
5000
0
x
x
y
z
Ob
Ob-Pirox
Ln
Ln-Pirox
IκB-α (37 kDa)
Pixels (arbitrary units)
25000
20000
15000
10000
5000
0
x
y
z
z
Ob
Ob-Pirox
Ln
Ln-Pirox

Figure 3.6: **Western blot analysis of IKK-β protein expression from liver homogenates of Zucker rats.** Equal amounts of liver protein (50 μg) were separated by 8% SDS-PAGE gel and transferred onto PVDF membranes. Following incubation with primary IKK-β antibody at a final dilution of 1:1000 and corresponding HRP-conjugated secondary anti-mouse antibody at a final dilution of 1:5000, the blots were developed on X-ray film using ECL Plus substrate. Equal loading of each gel was verified by comparison with the immunoblotting of beta-actin. (A) Representative western blots of IKK-β and β-actin using 50 μg of liver protein from Zucker obese (Ob) and lean rats with or without piroxicam treatment. (B) Ponceau S staining of membranes containing 50 μg of liver homogenate from all four groups of Zucker rats. (C) Bar graphs represents levels of IKK-β protein. Densitometric values were corrected for gel-to-gel variability using equal amounts of a common liver homogenate as a positive control in each blot. All values are means ± s.e., n=4/dietary group. Bars without a common letter ($^{x, y, z}$) differ significantly, $p<0.05$, as determined by ANOVA in conjunction with LSD post-hoc analysis. Ob: Obese, Ob-Pirox: Piroxicam supplemented Obese, Ln: Lean, Ln-Pirox: Piroxicam supplemented Lean.

A

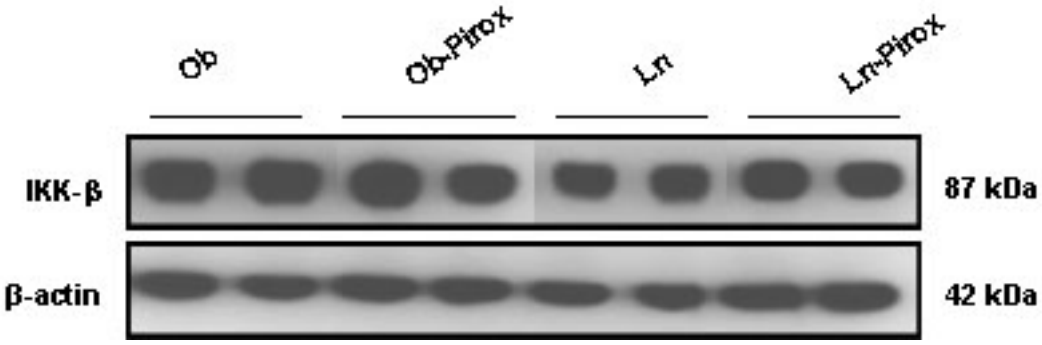
Ob
Ob-Pirox
Ln
Ln-Pirox
IKK-β
87 kDa
β-actin
42 kDa

B

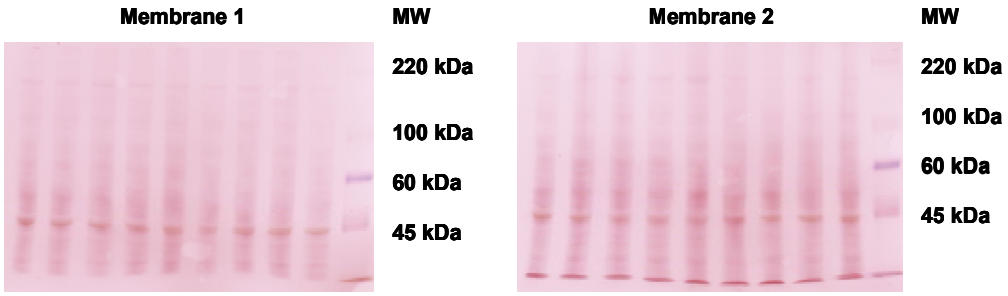
Membrane 1
MW
220 kDa
100 kDa
60 kDa
45 kDa
Membrane 2
MW
220 kDa
100 kDa
60 kDa
45 kDa

C

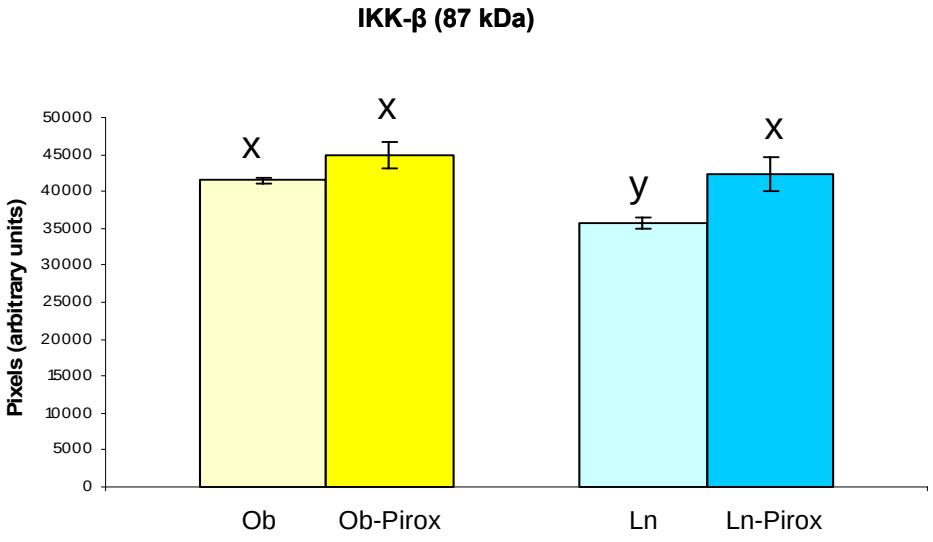
IKK-β (87 kDa)
Pixels (arbitrary units)
50000
45000
40000
35000
30000
25000
20000
15000
10000
5000
0
x
x
y
x
Ob
Ob-Pirox
Ln
Ln-Pirox

Figure 3.7: **Western blot analysis of NF-κB and IκB-α protein expressions in nuclear rich extracts from liver of Zucker rats.** Equal amounts of nuclear rich lysate (50 μg) were separated by 8% SDS-PAGE gel and transferred onto PVDF membranes. Following incubation with primary antibodies at a final dilution of 1:1000 and corresponding HRP-conjugated secondary antibodies at a final dilution of 1:5000, the blots were developed on X-ray film using ECL Plus substrate. The blots were first identified by immunoblotting with anti-rabbit polyclonal NF-κB antibody. The same membranes were then reprobed with anti-rabbit polyclonal IκB-α antibody. (A) Representative western blots of NF-κB, IκB-α and β-actin using 50 μg of nuclear protein from Zucker obese (Ob) and lean rats with or without piroxicam treatment. (B) Bar graphs represent levels of NF-κB and IκB-α protein. Densitometric values were corrected for gel-to-gel variability using equal amounts of a common liver homogenate as a positive control in each blot. All values are means ± s.e., n=4/dietary group. Bars without a common letter ($^{x, y, z}$) differ significantly, $p<0.05$, as determined by ANOVA **in** conjunction with LSD post-hoc analysis. Ob: Obese, Ob-Pirox: Piroxicam supplemented Obese, Ln: Lean, Ln-Pirox: Piroxicam supplemented Lean.

A

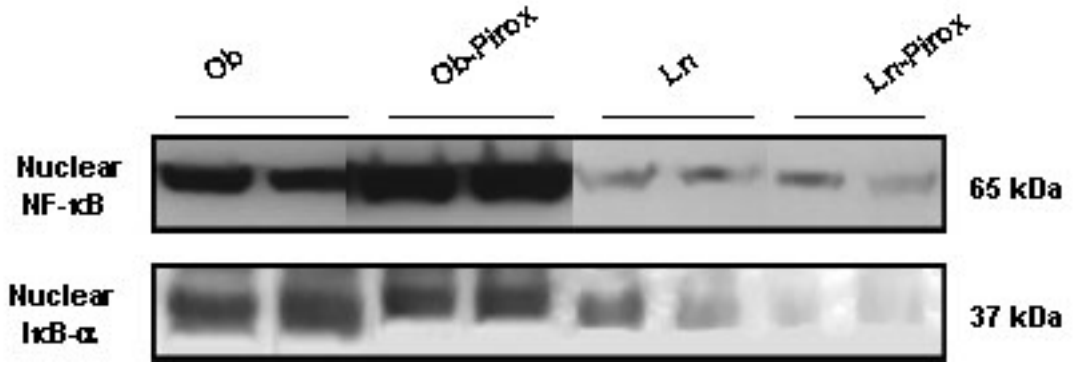
Ob
Ob-Pirox
Ln
Ln-Pirox
Nuclear NF-κB
65 kDa
Nuclear IκB-α
37 kDa

B

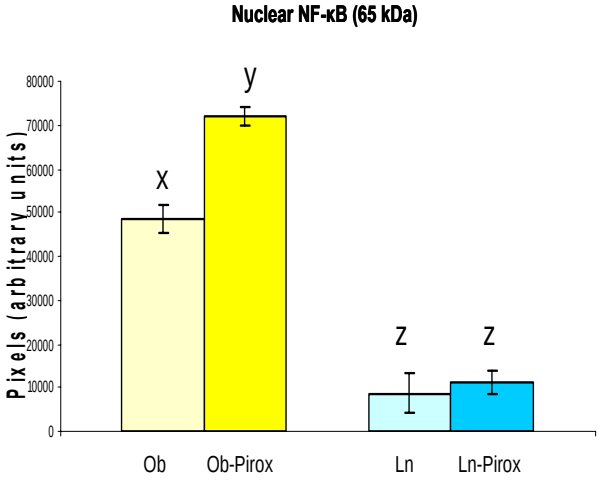
Nuclear NF-κB (65 kDa)
Pixels (arbitrary units)
80000
70000
60000
50000
40000
30000
20000
10000
0
x
y
z
z
Ob
Ob-Pirox
Ln
Ln-Pirox

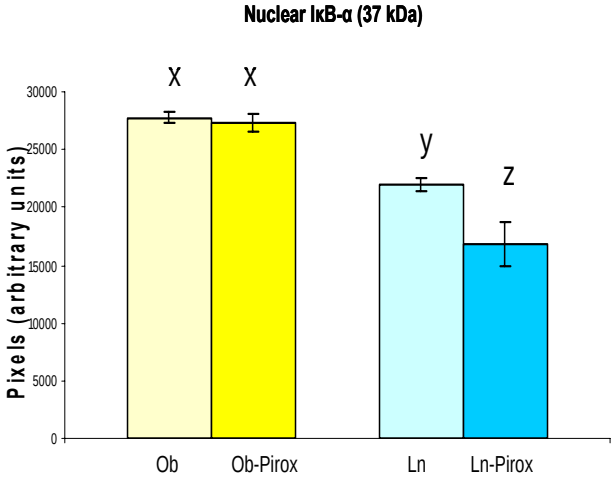
Nuclear IκB-α (37 kDa)
Pixels (arbitrary units)
30000
25000
20000
15000
10000
5000
0
x
x
y
z
Ob
Ob-Pirox
Ln
Ln-Pirox

Figure 3.8: **Colorimetric measurement of transcriptionally active p65 NF-κB levels in nuclear rich extracts of liver from Zucker rats.** Nuclear rich lysates were extracted from the livers of Zucker obese (Ob) and lean rats with or without piroxicam treatment. Active levels of p65 NF-κB were measured by a transcription factor ELISA (Active Motif) by loading nuclear rich extracts, 2 μg of nuclear protein per sample, in a 96 well plate coated with 5′-GGGACTTTCC-3′ oligonucleotide sequence. Incubation with primary antibody specific to the p65 NF-κB subunit was followed by exposure to HRP-conjugated secondary antibody and developing solution. Absorbance was read at 450 nm along with a reference at 655 nm. Samples were tested with n=4/dietary group and expressed as a percentage of positive control (jurkat nuclear rich extract) provided with the kit. This was done to minimize inter-assay variation. All values are means ± s.e. Bars without a common letter (x, y, z) differ significantly, $p<0.05$, as determined by ANOVA in conjunction with LSD post-hoc analysis. Ob: Obese, Ob-Pirox: Piroxicam supplemented Obese, Ln: Lean, Ln-Pirox: Piroxicam supplemented Lean.

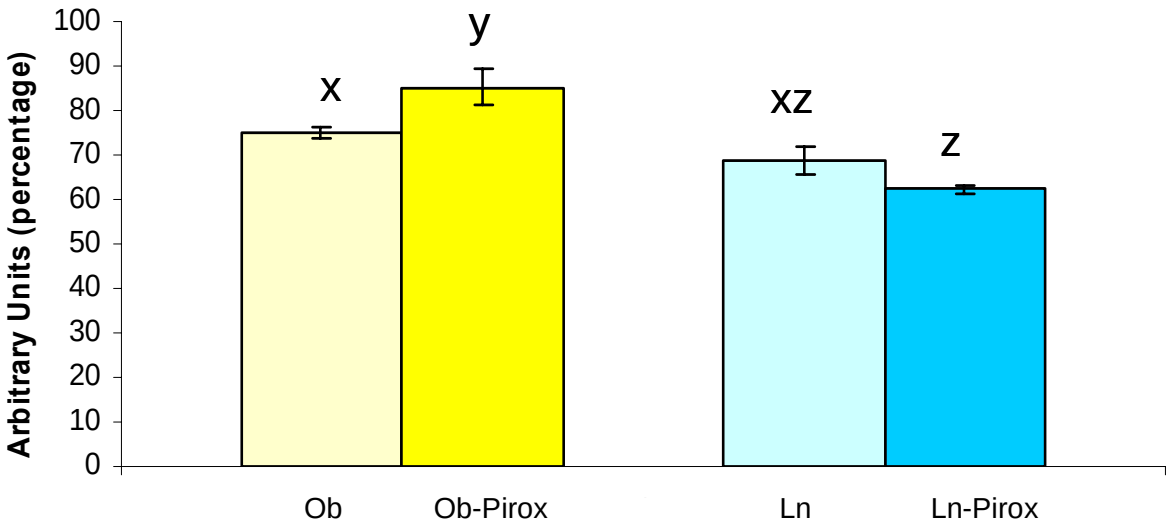
Arbitrary Units (percentage)
100
90
80
70
60
50
40
30
20
10
0
x
y
xz
z
Ob
Ob-Pirox
Ln
Ln-Pirox

3.4 Lipid Raft Isolation

3.4.1 Cholesterol Detection in Lipid Raft

The Amplex Red fluorescent cholesterol assay was used to quantify the level of cholesterol in all fractions. As shown in figure 3.9, it was apparent that lipid raft fractions 5, 6, and 7 contained the most significant amount of cholesterol compared to other fractions. Fractions 5, 6, and 7 contained more than 50% of the total cholesterol (present in all 12 fractions) and only ~ 25% of the total protein (figure 3.9A). On the other hand, the fractions 10, 11, and 12 contained more than 50% of the total protein and only ~ 20% of the total cholesterol. The lean and lean-piroxicam treated liver show a higher level of cholesterol compared to obese and obese-piroxicam , indicating the specificity for the lipid raft fraction (figure 3.9B).

3.4.2 Detection of Lipid Raft Marker Proteins

All 12 fractions obtained following sucrose gradient centrifugation were analyzed for raft marker proteins caveolin-1 and flotillin-1 (figure 3.10) through immunoblotting. As expected, caveolin-1 and flotillin-1 were present primarily in the lipid raft fractions 5, 6 and 7, the 6^{th} fraction having the highest level. This confirmed that fractions 5, 6 and 7 contained lipid raft. The lipid raft marker proteins were expressed as per μg of protein (figure 3.10C). Lipid raft fractions from lean piroxicam treated animals contained significantly lower levels of caveolin-1 compared to all the other groups. No significant trend was observed between obese and lean or obese and piroxicam treated obese groups. Obese piroxicam (figure 3.10C) contained significantly higher levels of flotillin-1 compared to the other groups. No apparent trend was observed between obese and lean or obese and piroxicam treated obese rats.

Figure 3.9: **Distribution of percent cholesterol and protein in 12 fractions of liver tissues from Zucker obese and lean rats with or without piroxicam treatment.** The cholesterol assay was performed on all 12 fractions extracted by sucrose density gradient ultracentrifugation from the liver of Zucker rats. The assay was carried out according to the manufacturer's instruction. In brief, 6 µL of equal volume was used from each fraction of all four groups in order to detect the cholesterol level. The enzymatic assay was based on hydrolyzing cholesteryl esters into cholesterol, then oxidizing cholesterol into ketone and H_2O_2. Thus, in the presence of horseradish peroxidase (HRP)-coupled oxidation of H_2O_2, Amplex Red reagent reacts with H_2O_2 to produce highly fluorescent resorufin. (A) % cholesterol and % protein in the lipid raft fractions of all four groups of Zucker rats. All values are means ± s.e., n=4/dietary group. (B) The change in % cholesterol level of fraction 6 of obese, lean, piroxicam treated obese and piroxicam treated lean rats. All values are means of n=4 per group. Ob: Obese, Ob-Pirox: Piroxicam supplemented Obese, Ln: Lean, Ln-Pirox: Piroxicam supplemented Lean.

A

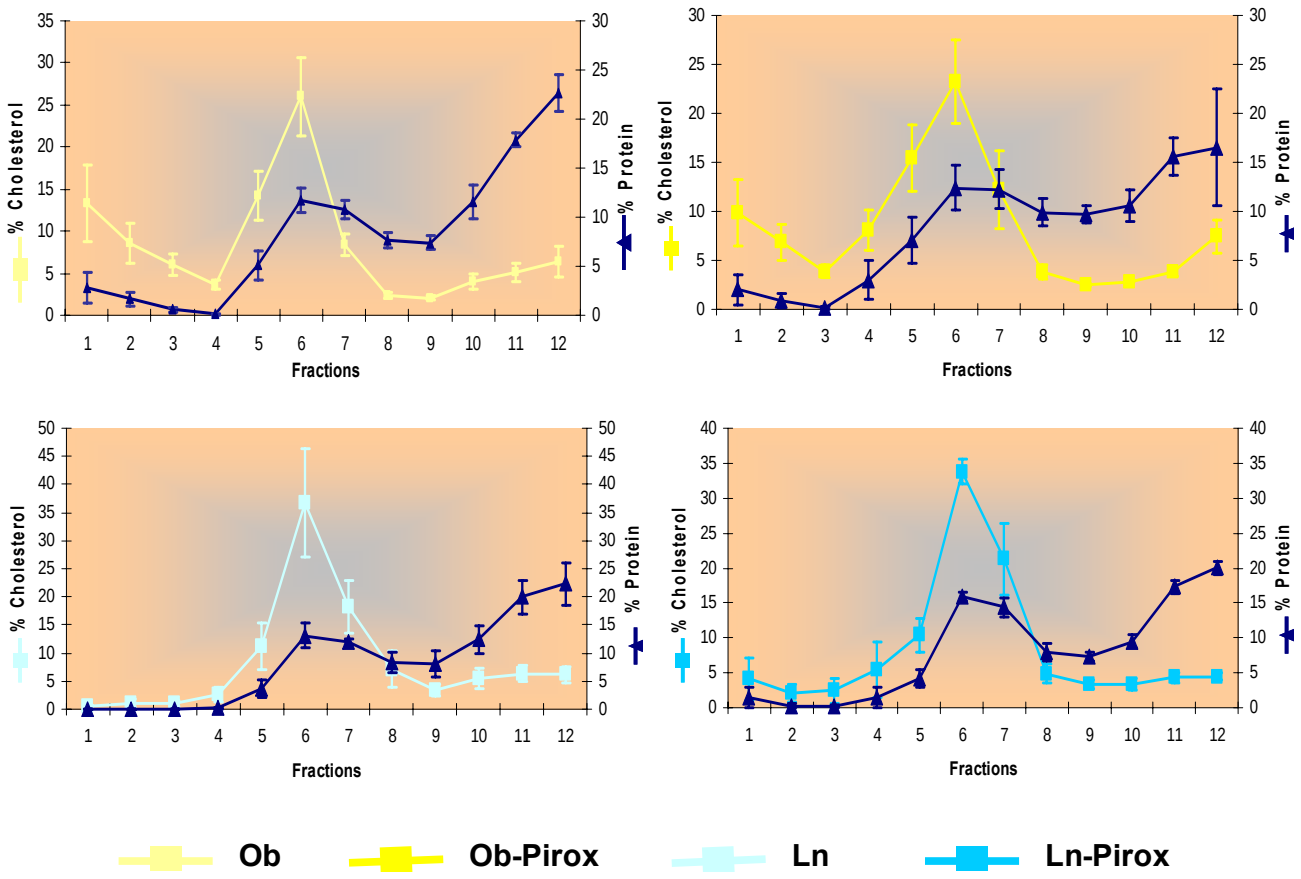
% Cholesterol
% Protein
Fractions
Ob
Ob-Pirox
Ln
Ln-Pirox

B

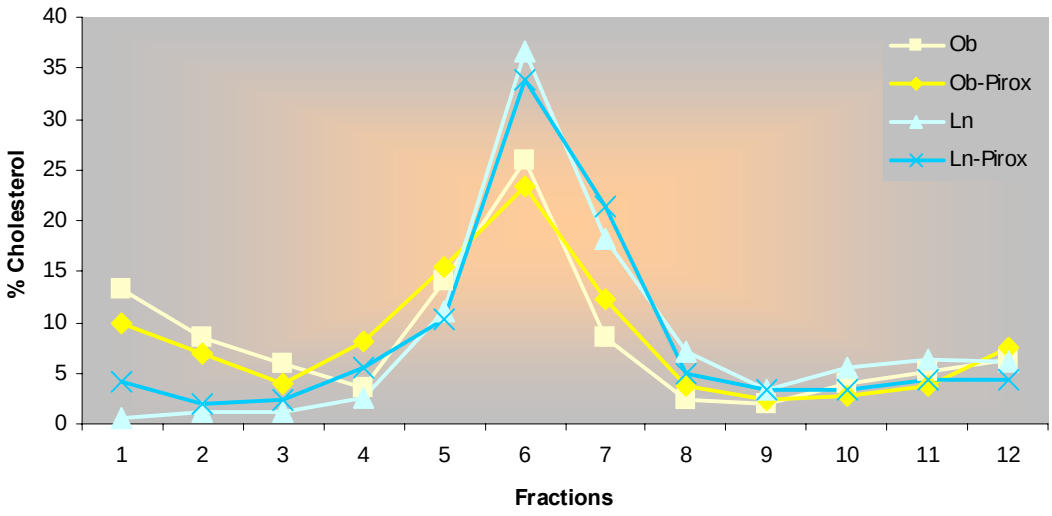
% Cholesterol
Fractions
Ob
Ob-Pirox
Ln
Ln-Pirox

Figure 3.10: Western blot analysis of caveolin-1 and flotillin-1 in lipid raft fractions of Zucker rat livers. Lipid rafts from rat livers were isolated after discontinuous sucrose gradient ultracentrifugation. After ultracentrifugation, the sucrose gradient was fractionated from top to bottom. Equal volumes of 3 µL raft fraction proteins were separated on 12% SDS-PAGE gel and immunoblotted with rabbit anti-caveolin-1 and rabbit anti-flotillin-1 raft marker proteins. The primary antibodies were added at a final dilution of 1:1000; the secondary antibodies were added at a final dilution of 1:5000 and the blots were developed on X-ray film using ECL Plus substrate. (A) Representative western blots of caveolin-1 using 3 µL from lipid raft fractions of Zucker obese (Ob) and lean rats. (B) Representative western blots of caveolin-1 and flotillin-1 using 3 µL from lipid raft fractions of Zucker obese (Ob) and lean rats with or without piroxicam treatment. (C) Levels of caveolin-1 and flotillin-1 in fraction 6 expressed as per µg of protein. All values are means ± s.e., n=4/dietary group. Bars without a common letter ($^{x, y}$) differ significantly, $p<0.05$, as determined by ANOVA in conjunction with LSD post-hoc analysis. Ob: Obese, Ob-Pirox: Piroxicam supplemented Obese, Ln: Lean, Ln-Pirox: Piroxicam supplemented Lean.

A

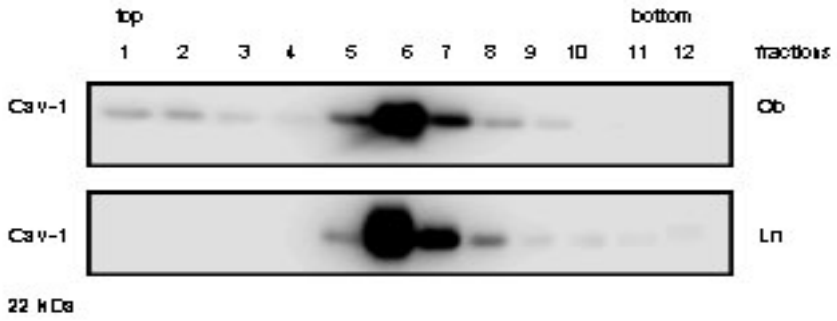
top
bottom
1 2 3 4 5 6 7 8 9 10 11 12
fractions
Cav-1
Ob
Cav-1
Ln
22 kDa

B

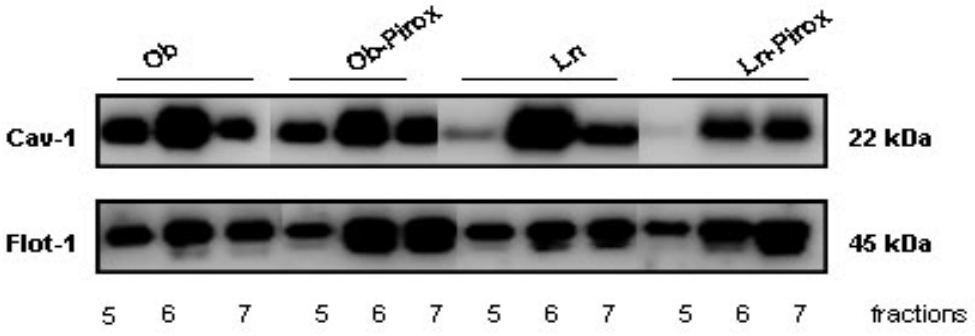
Ob
Ob-Pirox
Ln
Ln-Pirox
Cav-1
22 kDa
Flot-1
45 kDa
5 6 7 5 6 7 5 6 7 5 6 7
fractions

C

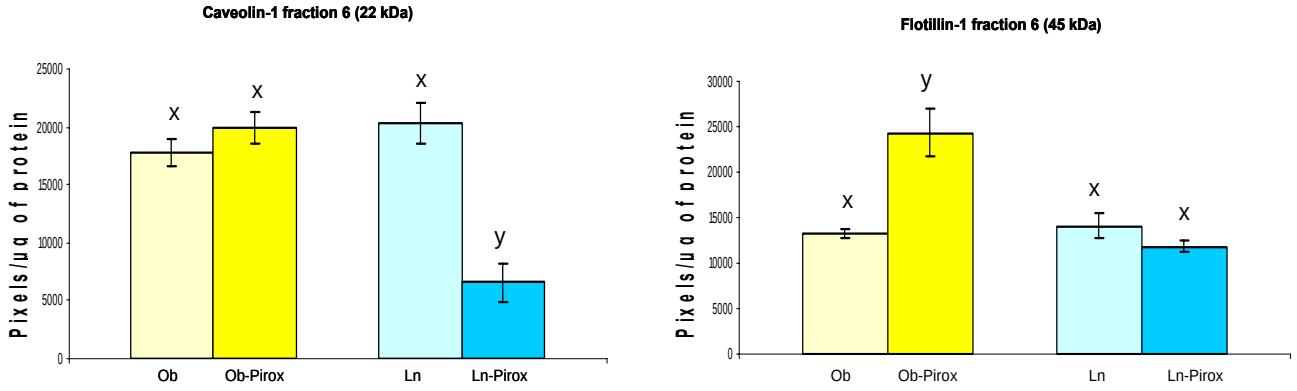
Caveolin-1 fraction 6 (22 kDa)
Pixels/ug of protein
25000
20000
15000
10000
5000
0
x
x
x
y
Ob
Ob-Pirox
Ln
Ln-Pirox
Flotillin-1 fraction 6 (45 kDa)
Pixels/ug of protein
30000
25000
20000
15000
10000
5000
0
x
y
x
x
Ob
Ob-Pirox
Ln
Ln-Pirox

3.5 Protein Expression Patterns in Lipid Raft

3.5.1 COX-2 Protein Expression

Lipid raft fractions were analyzed by western blot to determine the level of COX-1 and COX-2 proteins. COX-1 was undetectable with western blot in lipid raft fraction. Fraction 5, 6 and 7 showed the presence of COX-2 (figure 3.11A). When equal volume loaded western blots were quantified, fraction 6 and 7 contained almost the same level of COX-2 protein (Appendix; figure C5). The variation within the samples of the same group was large and hence the levels of COX-2 were calculated on per μg of protein. Fraction 6 was chosen as a representative lipid raft fraction. COX-2 levels of lipid raft fraction 6 were similar in both obese and lean rats (figure 3.11B). Furthermore, piroxicam significantly ($p<0.05$) increased the level of COX-2 protein only in lean rats.

3.5.2 TNF-RI and TNF-RII Protein Expressions

TNF-RI specific antibody detected two closely associated bands (55 & 57 kDa) in the lipid raft fractions. It was noted that 55 kDa band (figure 3.12A) was more prominent than the 57 kDa band. Quantified levels of equal volume loaded western blots suggests that fraction 6 and 7 contained almost the same level of the 55 kDa band of TNF-RI, but the 57 kDa band is specific for lipid raft fraction 6 (Appendix; figure C6). Again, the variation within the samples of the same group was large and, hence, the levels of TNF-RI were calculated on per μg of protein. Fraction 6 was chosen as a representative lipid raft fraction. No significant ($p<0.05$) differences were found with the TNF-RI level (55 kDa) between control obese and lean rats. Piroxicam treatment decreased the level of TNF-RI (55 kDa) significantly in the lean rats. However, in the piroxicam treated groups, TNF-RI (57 kDa) levels of lipid raft fraction 6 were significantly ($p<0.05$) lower than corresponding control obese and lean rats. Therefore the difference in 55 and 57 kDa bands was noted.

TNF-RII was also present in the lipid raft fraction 5, 6 and 7 as shown in figure 3.12A. When analyzed with equal amounts of protein (1 μg), as shown in figure 3.12B, obese piroxicam treated rats contained significantly higher levels of TNF-RII compared to all the other groups. No apparent trends were observed between obese and lean or obese and piroxicam treated obese rats.

Figure 3.11: Western blot analysis of COX-2 protein expression in lipid raft fractions of Zucker rat livers. After isolation of lipid raft through ultracentrifugation, the sucrose gradient was fractionated from top to bottom. Equal volumes (6 μL) of raft fraction proteins were loaded to an 8% acrylamide gel and transferred to a PVDF membrane. Later, the membrane was probed with a primary antibody at a concentration of 1:1000. After washing, the membrane was probed with a secondary antibody at 1:5000 concentration. The blots were developed on X-ray film using ECL Plus substrate. (A) Representative western blots of COX-2 using 6 μL from lipid raft fractions of Zucker obese (Ob) and lean rats with or without piroxicam treatment. (B) Levels of COX-2 in fraction 6 expressed as per μg of protein. All values are means ± s.e., n=4/dietary group. Bars without a common letter ($^{x, y, z}$) differ significantly, $p<0.05$, as determined by ANOVA in conjunction with LSD post-hoc analysis. Ob: Obese, Ob-Pirox: Piroxicam supplemented Obese, Ln: Lean, Ln-Pirox: Piroxicam supplemented Lean.

A

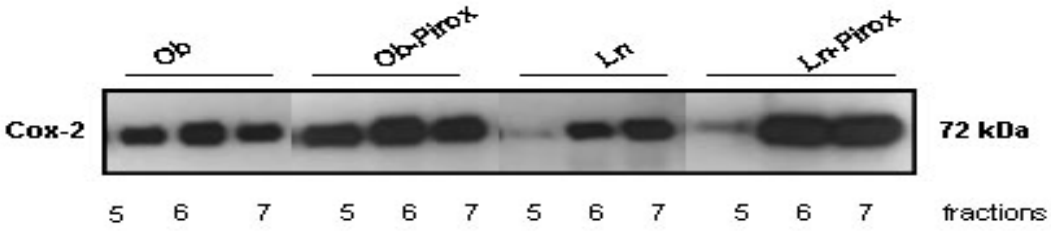
Ob
Ob-Pirox
Ln
Ln-Pirox
Cox-2
72 kDa
5 6 7 5 6 7 5 6 7 5 6 7
fractions

B

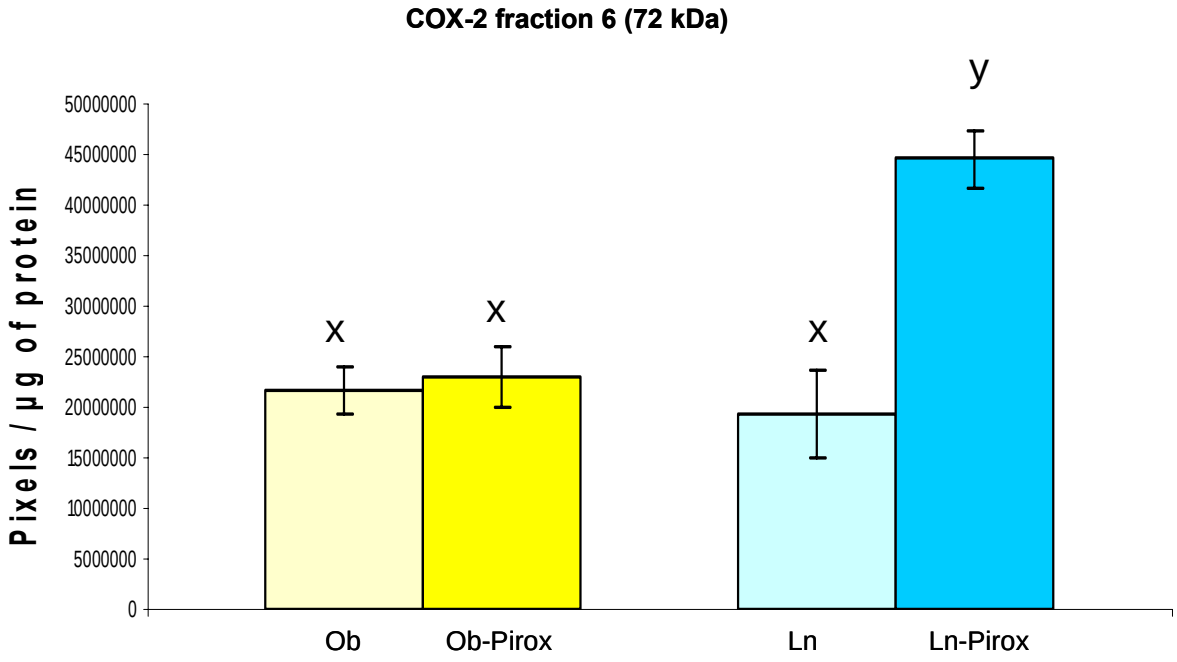
COX-2 fraction 6 (72 kDa)
Pixels / µg of protein
50000000
45000000
40000000
35000000
30000000
25000000
20000000
15000000
10000000
5000000
0
x
x
x
y
Ob
Ob-Pirox
Ln
Ln-Pirox

Figure 3.12: Western blot analysis of TNF-RI and TNF-RII protein expressions in lipid raft fractions of Zucker rat livers. Equal volumes (6 μL) of lipid raft fractions were subjected to 8% SDS-PAGE gel and were identified by immunoblotting first with rabbit anti-TNF-RI polyclonal antibody. The same membranes were then reprobed with anti-rabbit TNF-RII polyclonal antibody. The primary antibodies were added at a final dilution of 1:1000, the secondary antibodies were added at a final dilution of 1:5000, and the blots were developed on X-ray film using ECL Plus substrate. (A) Representative western blots of TNF-RI and TNF-RII using 6 μL from lipid raft fractions of Zucker obese (Ob) and lean rats with or without piroxicam treatment. (B) Levels of TNF-RI and TNF-RII in fraction 6 expressed as per μg of protein. All values are means ± s.e., n=4/dietary group. Bars without a common letter ($^{x, y, z}$) differ significantly, $p<0.05$, as determined by ANOVA in conjunction with LSD post-hoc analysis. Ob: Obese, Ob-Pirox: Piroxicam supplemented Obese, Ln: Lean, Ln-Pirox: Piroxicam supplemented Lean.

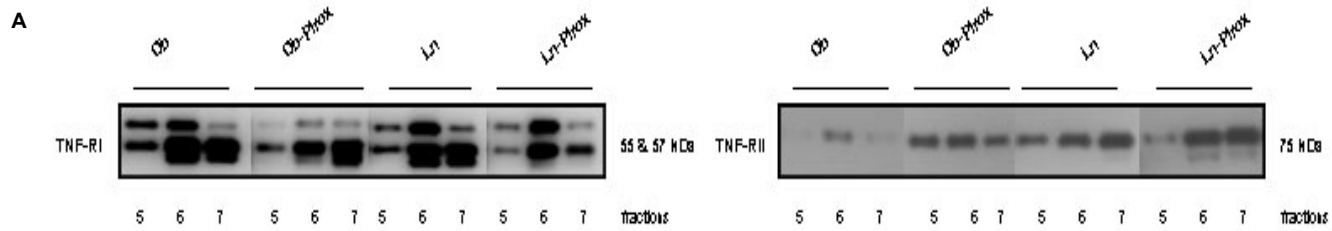
A
Ob
Ob-Pirox
Ln
Ln-Pirox
TNF-RI
55 & 57 kDa
TNF-RII
75 kDa
5 6 7 5 6 7 5 6 7 5 6 7 fractions
5 6 7 5 6 7 5 6 7 5 6 7 fractions

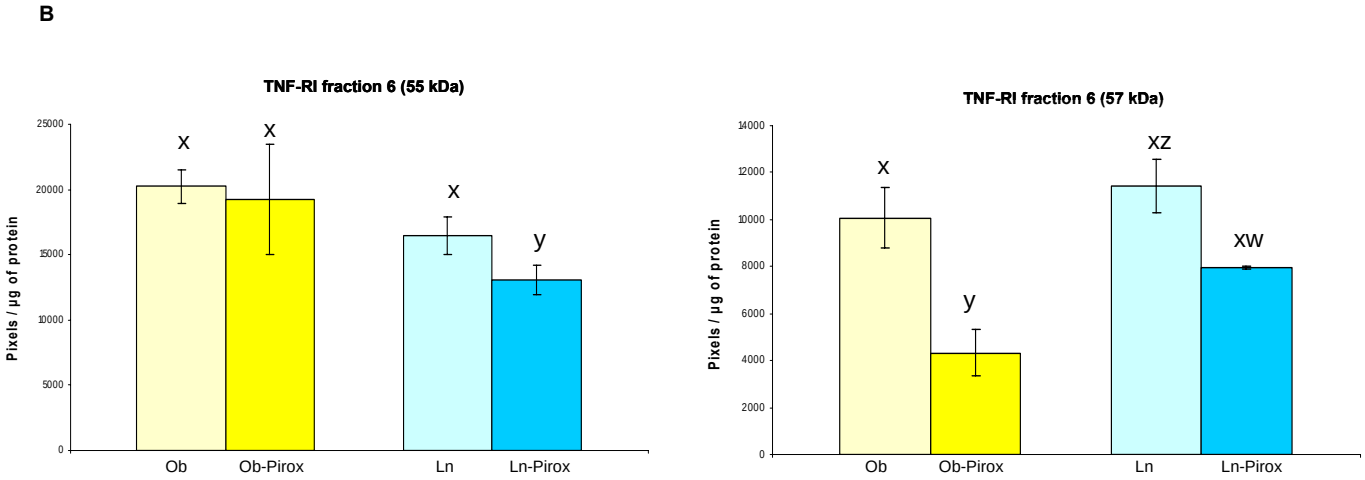
B
TNF-RI fraction 6 (55 kDa)
Pixels / µg of protein
25000
20000
15000
10000
5000
0
x
x
x
y
Ob
Ob-Pirox
Ln
Ln-Pirox
TNF-RI fraction 6 (57 kDa)
Pixels / µg of protein
14000
12000
10000
8000
6000
4000
2000
0
x
y
xz
xw
Ob
Ob-Pirox
Ln
Ln-Pirox

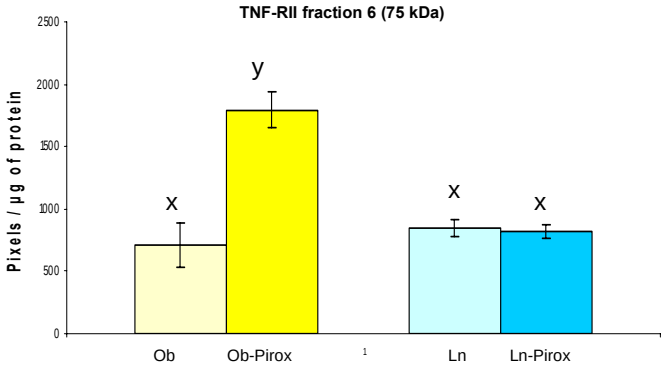
TNF-RII fraction 6 (75 kDa)
Pixels / µg of protein
2500
2000
1500
1000
500
0
x
y
x
x
Ob
Ob-Pirox
Ln
Ln-Pirox

Chapter 4
Discussion

4.1 Liver Tissue and Lipid Raft

4.1.1 Liver Tissue

NSAIDs are commonly noted for their analgesic and anti-inflammatory properties, and are more recently being used as anti-cancerous agents, namely, to reduce the incidence and progression of pre-cancerous lesions within the colon (Jalving et al., 2005; Reddy et al., 1987). The purported anti-cancerous effects of specific NSAIDs or COX inhibitors such as piroxicam have been implicated as treatment options for obese and lean individuals alike. Given the correspondence between disease states such as obesity and heart disease or cancer, the pharmacological activities and physiological consequences of drugs such as NSAIDs must be studied under co-occuring pathological states. Although NSAID administration to obese individuals has been used to evaluate insulin re-sensitizing effects (Yuan et al., 2001), to our knowledge, no studies have documented the effects of NSAIDs, specifically piroxicam, on susceptibility to hepatotoxicity and hepatopathology.

In the present study, we assessed whether the COX inhibitor piroxicam could be used safely as a cancer preventive agent in an animal model of obesity, a state known to be at higher risk for developing colon cancer than its lean counterpart. Obese animals are in a chronic state of inflammation and, as such, the use of a COX inhibitor was deemed appropriate. This study also investigated TNF-α signaling proteins in both obese and lean rat liver tissue and evaluated piroxicam's affect on this pathway. The main findings of the study pertain to the differences between the obese steatotic and lean livers, as well the ability of piroxicam to alter the levels of specific proteins. The principle findings of this study are that: 1) obese rats responded to piroxicam more adversely than lean rats, elevating whole liver weights and the severity of hepatic steatosis; 2) COX-2 protein (figure 3.2) levels were significantly lower in the piroxicam treated livers than their control counterparts; 3) the level of TNF-RII protein (figure 3.4) was significantly lower in obese rat liver tissue compared to lean rat liver tissue, and piroxicam further lowered the receptors abundance in obese but not in lean rat liver tissue; 4) IκB-α protein (figure 3.5) abundance was significantly higher in the obese compared to lean rat liver tissue, and piroxicam treatment lowered its abundance in obese

but not in lean rat liver tissue; 5) IκB-α (figure 3.7) was present in the nuclear rich fraction of hepatic tissue, and this nuclear IκB-α was significantly elevated in obese compared to lean rat hepatic tissue; 6) IKK-β (figure 3.6) levels were higher in obese compared to lean rat livers, and piroxicam further increased the level of IKK protein in lean but not in obese rat liver tissue; 7) the nuclear fraction of obese rat livers had 5-6 fold higher levels of NF-κB p65 protein than in the lean liver; and 8) active NF-κB (figure 3.8) was higher in obese compared to lean liver nuclei, however, the difference was not nearly as extreme as that observed between lean and obese in total nuclear NF-κB protein as assessed by western blot.

Zucker obese rats exhibit hepatic steatosis. This abnormality is attributed to insulin resistance, increased levels of TNF alpha, increased lipogenesis and decreased mobilization of triacylglycerol from the liver, and possibly, increased uptake and retention of circulating lipids by hepatic tissue (Adams and Angulo, 2006; Yang et al., 1997). Hepatic steatosis could also occur due to chemical toxicity or nutritional deficiency of choline and/or methionine (Bykov et al., 2006). In all cases, involvement of uncontrolled generation of reactive oxygen species has been suggested. Interestingly, Zucker obese rats are in a state of chronic inflammation and are often reported to have elevated levels of reactive oxygen species.

Piroxicam treatment for eight weeks caused a conspicuous increase in macrovesicular lipid accumulation and peripheral translocation of hepatocyte nuclei (figure 3.1), as well as an increase in total liver weight and triglycerides (table 3.1); aberrations characteristic of steatosis. These observations parallel to those made by Bykov et al. (2006), wherein treatment with celecoxib, a selective COX-2 inhibitor, enhanced the hepatosteatotic effects induced by ethanol consumption. This suggests a possible common protective role for COX-2 against liver pathogenesis. The observed piroxicam-induced increase in lipid accumulation, a sign of augmented toxicity, is the result of many factors and interactions, some of which are outlined below.

It was interesting to note that, overall, the proportion of 18:2 (table 3.2) was significantly lower in obese rat livers compared to those of lean rats suggesting a higher utilization of 18:2 by obese animals since all animals were on the same diet. What is happening with linoleic acid in obese rat livers remains an enigma. We have shown previously, that total phopholipid content of lipid is not altered in obese rats. One possibility for this is that because the pool of triglycerides is increased substantially, 18:2 is sequestered in triglyceride. Moreover, 20:4 n-6 fatty acid was accumulated in a significant amount in phospholipid fraction with piroxicam treated obese compared to control obese

rats. This increase suggests reduced mobilization of 20:4 for prostaglandin synthesis possibly due to reduced COX-1 and COX-2 activity.

Even though the main objective was to explore TNF-α signaling molecule, a preliminary study was conducted to determine if sphingolipid signaling could also be involved. TNF ligand-receptor binding can activate the sphingo-ceramide pathway leading to the production of ceramide via acidic sphingomyelinases present in cell endosomes (Schutze 1995). Ceramide may then induce NF-κB activation via IκB degradation leading to apoptosis (Yang et al. 1993). In a preliminary study, we observed that the neutral and acidic sphingomyelinase activity (Appendix; figure C3) were significantly higher in obese compared to lean rats, suggesting that the role of sphingomyelinase should be considered in future studies while investigating the role of TNF-α.

All the proteins discussed here are closely related, either metabolically, or through their constituent signaling function. TNF-α, TNF-RI and II, IκB-α, and IKK-β are involved in the generation of p65 NF-κB which, in turn, regulates either pro- or anti-apoptotic signaling by inducing several genes including TNF-α, IκB-α and IKK-β. One of the genes induced by active NF-κB is COX-2. Levels of active NF-κB and COX-2, among several other proteins, are elevated in colonic tumors and are implicated in tumor cell survival. Piroxicam lowered the level of COX-2, but not COX-1 (figure 3.2), suggesting a specific effect on the synthesis or turnover of this protein. Furthermore, a putative mechanism by which piroxicam inhibits colon tumorigenesis may be by reducing the COX-2 expression. One could propose that piroxicam may inhibit colon tumorigenesis by blocking the COX-2 and NF-κB pathways needed for tumor cell survival (Bykov et al., 2006). Despite the obvious importance of disrupting this pathway for restricting tumor growth, it exerts highly adverse effects on the already hepato-compromised obese state**.**

In the two-hit model described by Day et al. (1998), the inciting event in the progression of non-alcoholic fatty liver disease (NAFLD) is directly related to apoptosis, rupture of steatotic hepatocytes, and the subsequent release of toxic fatty acids and triglycerides. We speculate that piroxicam treatment in this study acts as the 'second hit', affecting liver steatosis and cell death. We further speculate that the consequences of the 'second hit' are related to piroxicam's influence on TNF signaling, and the production of inflammatory molecules and ROS in hepatic tissue. Characteristically decreased IR-β levels (Appendix; figure C2) were observed in Zucker obese rats, compared to lean. Interestingly, piroxicam treatment significantly reduced IR levels in obese and lean animals alike. This result is inconsistent with previous studies that have shown an insulin re-

sensitizing effect of NSAID treatment on obese (fa/fa) rats through a reduction of IKK-β levels but not through COX-1 or COX-2 levels (Reddy et al., 1987).

In this study, our findings allude to the possibility that piroxicam is affecting TNF-α mediated signalling and, subsequently, the presence and effects of NF-κB in the process. It has been reported that obese rats have higher levels of plasma TNF-α (soluble form) than their lean counterparts, but obese rats exhibit lower levels of hepatic TNF-α (Raju and Bird, 2006). Our findings are consistent with these results as we observed lower levels of the 17 kDa soluble TNF-α protein (figure 3.3) in obese compared to lean hepatic tissues. However, the 80 kDa membrane bound TNF-α protein (figure 3.3) was observed in higher abundance within obese rather than lean hepatic tissue. Nonetheless, piroxicam treatment decreased hepatic levels of membrane bound and soluble TNF-α protein in both obese and lean animals. The mechanism by which TNF-α forms regulate TNF receptors in steatotic as opposed to non-steatotic livers, however, remains to be elucidated.

Within the cytoplasm, NF-κB is bound by an inhibitory molecule IκB-α, and is inactive. Upon receptor signaling, the kinase IKK cleaves the inactivating IκB-α from NF-κB allowing the active form of NF-κB to travel to the nucleus and act as a transcription factor (Ashkenazi and Dixit, 1998). In this study, obese animals were found to have drastically elevated nuclear NF-κB protein levels (figure 3.7), possibly reflecting the existence of constant inflammation, characteristic to the obese state. In addition, obese piroxicam treated animals had elevated levels of nuclear NF-κB protein, as compared to their obese control counterparts. Coupled with the concomitant decrease in the repressive IκB-α protein in obese piroxicam treated animals, these results are suggestive of elevated NF-κB signaling within the obese-piroxicam state. The observed increase in hepatic NF-κB could be due to an increase in expression or alteration of protein turnover rate. The exact role of the observed aberrant increase in NF-κB signaling in the hepatic disease state, however, will require further investigation. Although it is difficult to directly correlate changes in the levels of specific proteins with NF-κB regulation, it is clear that TNF/NF-κB signaling is significantly involved in the hepatotoxicity observed in piroxicam treated animals. It is apparent that active NF-κB may be is exerting different effects in obese as opposed to lean livers. Based on the pathological state of the liver, it is speculated that proapoptotic activity of NF-κB is more dominant in obese than in lean rats.

It was noted that the obese liver had significantly higher levels of total NF-κB protein in the nuclear fraction compared to lean nuclei. Only a moderate increase, however, was observed in transcriptionally active NF-κB (figure 3.8) within obese piroxicam treated animals when compared to their lean counterparts. These results strongly suggest that of the total NF-κB present in the tissue the

relative proportion of active form was significantly higher in the lean liver. The presence of higher levels of cytoplasmic IκB-α is consistent with the idea that an elevation in the abundance of this protein will interfere in the activation of NF-κB. Unexpectedly, piroxicam decreased the level of this protein only in the obese tissue. It is possible that piroxicam reduced the activity of NF-κB via an alternate mechanism which in turn resulted in lower expression of genes regulated by NF-κB, one of which being the IκB-α gene.

The presence of IκB-α protein in the nuclear compartment was also unexpected. It has been demonstrated that cytoplasmic IκB-α could serve as a shuttle system to drive the nuclear NF-κB out of the nuclear compartment or to retain it in an inactive bound form, thus compromising its nuclear activity (Hayden and Ghosh, 2006). The obese state seems to predispose the cell to increased nuclear IκB-α levels and subsequently compromises NF-κB signaling. To our knowledge, this is the first demonstration that hepatic nuclear fractions contain IκB-α. Further investigation as to its biological significance is needed. Thus, we implicate piroxicam in compromising the pro-survival activity of NF-κB, allowing intracellular toxic constituents to be more effective in exerting hepatic toxicity, visualized by an augmented steatotic response in obese hepatic tissue.

The other possibility not investigated in the present study, is the ability of piroxicam to increase pro-inflammatory responses mediated by the lipoxygenase (LOX) pathway (Bykov et al., 2006). The primary pharmacological function of piroxicam, like other NSAIDs, is the inhibition of the COX enzyme. A reduction in the functional COX enzyme would shift the equilibrium toward an increase in the amount of arachadonic acid (AA) available to the LOX enzyme for processing into leukotrienes (LTs). The LOX enzyme functions to catalyze the production of LTs and, in so doing, commonly produces reactive oxygen intermediates (ROI) from AA (Heslin et al., 2005; Bonizzi et al., 1999).

In addition to increasing its activity, LOX, as any enzyme, exhibits a certain degree of saturation. Not all of the available AA will be metabolized into LTs, causing an accompanying increase in free AA. Free AA is able to stimulate sphingomyelinase, catalyzing the hydrolysis of sphingomeline to ceramide, which subsequently acts as an activating second messenger to many apoptotic pathways. Furthermore, it has been shown that AA can affect mitochondrial permeability, causing apoptosis through the release of cytochrome C (Bykov et al., 2006; Cao et al., 2000). Therefore, the increased LOX activity and increased free AA that could result from piroxicam induced COX inactivation represents a possible aberrant source of pro-apoptotic signaling.

When we look at the overall changes in protein levels involved in TNF-alpha mediated signaling, there are a number of salient observations which deserve special attention. From our study it is apparent that the steatotic liver differs from the non-steatotic liver with respect to a low abundance of TNF-RII and higher levels of total nuclear NF-κB and nuclear IκB-α. Piroxicam treatment lead to a lower level of COX-2 and TNF-RII in the obese rat liver, and higher levels of TNF-RII in the lean rat liver. Further studies are needed to explore whether and how several of these proteins are involved in integrating signaling that leads to hepatic steatosis and/or resisting any adverse effect of piroxicam.

4.1.2 Lipid Raft

Liquid-ordered microdomains enriched in cholesterol and sphingolipids form a distinct plasma membrane compartment. They have been termed 'lipid rafts' based on their ability to float in a discontinuous density gradient after lysis in non-ionic detergents (Pike, 2004). The proteins located in these microdomains are severely limited in their ability to freely diffuse over the plasma membrane, meaning that raft association tends to concentrate specific proteins within plasma membrane microdomains, and this could affect protein function (Simons and Toomre, 2000). It is known that the functional properties of lipid raft are determined by the levels of caveolins, cholesterol, proteins, phopholipids, sphingolipids and the amount and types of fatty acids. In the presence study, we only measured the level of cholesterol (figure 3.9) and caveolin-1 (figure 3.10). The cholesterol was lower in 5, 6 and 7 fractions in obese and obese-piroxicam rats compared to lean and lean-piroxicam. When caveolin-1 was quantified, only lean-piroxicam lowered the level of caveolin-1 compared to other groups. In contrast, the flotillin-1 level was increased only in obese-piroxicam. Because of the pathological state of the tissue, one would suggest the lowering of cholesterol in 5, 6 and 7 fractions was not a favorable effect. Moreover, it is possible that the ratio between caveolin and cholesterol in lipid raft fraction is critical.

Many studies in recent years have indicated that lipid rafts are merged into large membrane domains upon sphingomyelinase dependent hydrolysis of sphingomyelin and generation of ceramide within rafts (figure 4.1). Sphingomyelinases are characterized by their pH optimum, and an acid, neutral, and alkaline sphingomyelinase were described. Clustering of plasma membrane rafts into ceramide-enriched platforms serves as an important transmembrane signaling mechanism for cell surface receptors. Ceramides have been also implicated in apoptosis, stress signaling cascades as well as ion channels (Bollinger et al., 2005). Experimental studies have demonstrated TNF-α signaling via

ceramide-rich membrane rafts; acid sphingomyelinase released ceramide is essential for TNF-α clustering as well as apoptosis induction. Moreover, raft destruction of surface ceramide prevented TNF-α clustering and apoptosis (Grassme et al., 2001). Since lipid rafts are enriched in sphingomyelin, the activity of neutral and acidic sphingomyelinase was also measured in the lipid raft using the Amplex Red fluorescent assay kit. Moreover, stimulated (addition of sphingomyelin) and basal (without addition of external sphingomyelin) levels of neutral and acidic sphingomyelinase were investigated (Appendix; figure C8). The basal level of neutral sphingomyelinase was higher in obese-piroxicam compared to obese rats, however, an opposite trend was observed with the lean and lean-piroxicam groups. Significant stimulation was noted only in the lean group suggesting that sphingomyelinase level exceeds the hydrolysable sphingomyelin. If basal sphingomyelinase reflects its activity on raft sphingomyelin, then one can say that obese-piroxicam has more sphingomyelin than obese whereas lean-piroxicam has significantly lower sphingomyelin compared to lean. The basal level of acidic sphingomyelinase was higher in lean compared to obese, obese-piroxicam and lean-piroxicam. Upon stimulation, obese-piroxicam showed a significant increase in acidic sphingomyelinase levels. However, lean showed hardly any change in level upon stimulation, suggesting that lean has overall higher sphingomyelin as a substrate for acidic sphingomyelinase. Some of these changes with acidic and neutral sphingomyelinase are worth noting, but it is difficult to explain these differences as they pertain to sphingomyelin or ceramide levels or the pathological state of the tissue.

It has been proposed that lipid rafts serve as signaling platforms for antigen receptors such as BCR, TCR, and Fcε, bringing them into proximity with activating kinases that are constitutive residents of lipid rafts (Dykstra et al., 2003). Recent findings have also determined the roles for lipid rafts in TNF-RI signaling. However, discrepancies exist regarding the localization of TNF-RI within lipid rafts. For instance, in the human fibrosarcoma cell line HT1080, within two mins of TNF stimulation, TNF-R1 translocates to lipid rafts, where RIP1 (receptor-interacting protein), TRADD (TNF receptor-associated death domain), and TRAF2 (TNF receptorassociated factor-2) are recruited (Legler et al., 2003). When lipid rafts are disrupted by cholesterol depletion, phosphorylation of IκBα in response to TNF is inhibited and apoptosis is induced (Legler et al., 2003). In the myeloid cell line U937, TNF-R1 was reported to localize to lipid rafts upon unstimulation of U937 cells. However, with the cholesterol depletion of U937 cells, TNF-RI surface expression and consequently TNF-α mediated apoptosis was reduced (Ko et al., 1999).

In vitro studies have shown that lipid rafts also play a crucial role in signal transduction of death receptors, such as TNFR1 (Ko et al., 1999; Legler et al., 2003). Whether signals induced by TNFR family members *in vivo*, specifically in the compromised state of liver tissue, also depend on these specialized membrane microdomains, has not been analyzed to our knowledge. Our study tried to investigate the level of TNF-R1 and TNF-R2, two members of the TNFR superfamily implicated in pro- and anti-apoptotic events, in lipid raft fractions of steatotic and non-steatotic livers. It was anticipated that, if these proteins are involved in hepatic steatosis, then we will see changes in the lipid raft.

Lipid raft-containing fractions were confirmed by the enrichment of the cholesterol binding protein, caveolin-1, and the dendritic lipid raft marker, flotillin-1 (figure 3.10). We were able to detect TNF-RI and TNF-R2 in lipid raft fraction 6 of all four groups of Zucker rats (figure 3.12). Since similar levels of TNF-RI were noted in the lipid raft fraction of obese and lean, one can suggest that the physiological level of TNF-α may not directly affect the levels of TNF-RI in the lipid raft. Piroxicam treatment lowered the level of TNF-RI in both obese and lean rats. This effect suggest that either TNF-RI is migrated to other fractions, or that it is turning over in the lipid fraction much more rapidly in piroxicam treated rats compared to their controls. The presence of TNF-R2 in the lipid raft was consistent in all groups. This is the first time the presence of TNF-R2 is noted *in vivo* in the intact tissue lipid raft fractions. This may be because TNF-RI has received more attention in signal transduction than TNF-R2. It is interesting to note that TNF-R2 is higher in obese colonic tumors (previous study done in our lab, but unpublished) and also in the obese liver treated with anti-steatotic agent, alluding that TNF-R2 is involved in survival signal. However, our results show that TNF-R2 is higher in piroxicam obese rats (an inflammed state) in the lipid raft fraction compared to its level in intact tissue relative to other groups. It could be that TNF-R2 in lipid raft is less accessible and may represent an inactive state. Our results are contradictory to the observations by Lotocki et al (2006). They have shown that in the normal cerebral rat cortex, a portion of TNFR1 was present in lipid raft microdomains, where it was associated with the adaptor proteins TRADD, TRAF-2, the Ser/Thr kinase RIP, TRAF1, and cIAP-1 (cellular inhibitor of apoptosis protein-1), forming a survival signaling complex. They went on to show that moderate traumatic brain injury resulted in rapid recruitment of TNFR1, but not TNFR2, to lipid rafts and induced alterations in the composition of signaling intermediates. However, these findings may be tissue specific. Moreover, in the present research, a chronic exposure of liver tissue to piroxicam or TNF-α was carried out for several weeks and the changes in lipid raft or in tissue reflected alterations that reached a steady state level.

The NSAID piroxicam, a non-selective COX inhibitor, was used as a treatment group in our study. Therefore, it was of interest to investigate the presence of COX-1 and COX-2 in the lipid rafts of Zucker rat livers. The levels of COX-2 (figure 3.11) were not significantly different between obese, obese-piroxicam and the lean groups. Piroxicam treated lean rats showed higher levels of COX-2 compared to all other groups. However, COX-1 was undetectable through western blot in the lipid raft of Zuker rat livers. In 2001, Liou and coworkers reported that COX-2 was co-localized with Cav-1 in human fibroblasts. In addition, it has also been reported that COX-1 was also co-localized with Cav-1 and Cav-2 in human embryonic kidney (HEK 293) cells (Cha et al., 2004). In a recent study evidence has been presented to confidently argue for COX-2 association with Cav-3 in primary cultured rat chondrocytes (Kwak et al., 2006). Therefore, it is suggested that due to co-localization of caveolins with COX-1 and COX-2 in caveolae, caveolins may play an important role in regulating the function of COX-1 and COX-2. The co-localization experiments in the previous studies used immuno-precipitation and confocal microscopic techniques, while in our study, the western blot technique with commercially available COX-1 and COX-2 specific antibody was used. Moreover, it is important to know that we investigated just the levels of protein and not their activites. The presence of COX-2 in lipid raft suggests the movement and migration of the proteins from one fraction to another nevertheless could occur and affect its function.

4.2 General Discussion

The main objective of this research was to determine whether steatotic livers will exhibit differences in the level of TNF-α signaling molecules compared to their non-steatotic counterparts. The underlying hypothesis was that, in the obese state, increased plasma TNF-α is responsible for inducing liver steatosis, and that NF-κB plays an important role in mitigating TNF-α effects. TNF-α induces pro- or anti-apoptotic responses by interacting with its receptor TNF-RI and R2 which, in turn, could activate NF-κB. NF-κB, serving as a transcription factor, induces several genes leading to a specific biological outcome such as cell death or cell survival. Steatotic livers exhibit elevated levels of lipids and hepatocytes show signs of necrosis. In the present research we used piroxicam, a COX inhibitor and cancer preventive agent, to determine if this drug could be used safely in obese rats known to be at high risk for developing colon cancer. We observed that piroxicam was highly toxic and augmented liver steatosis. The assessment of the TNF-α signaling molecule carried out at the tissue level as well as in the membrane lipid rafts, known to be gate keeper of signaling events. The secondary objective was to determine if the findings from the whole tissue will reflect the

findings from the assessment of specific proteins such as TNF-RI and RII and COX-1 and COX-2 in lipid rafts. A summary of the key findings follows:

The main findings were that piroxicam treatment elevated the level of COX-1 protein only in the lean liver, otherwise COX-1 levels were similar in the livers of obese, obese-piroxicam and lean livers of Zucker rats. COX-2 levels were similar in obese and lean livers however; piroxicam treatment significantly lowered the level of this protein in both obese and lean rat livers. TNF-RII showed a trend which was inversely proportional to the pathological state of the tissue. The obese-piroxicam liver had the lowest level of TNF-RII and the lean liver had the highest. The total NF-κB level was higher in the obese and obese-piroxicam groups compared to the lean or lean-piroxicam groups. It was interesting to observe that piroxicam treatment lowered the level of NF-κB in obese as well as lean livers. IκB-α was higher in obese than in lean livers. IκB-α did not show a distinct change which could be attributed to the pathological state of the tissue.

The nuclear level of NF-κB by western blot analysis showed the same pattern as noted in the whole tissue homogenate. However, the difference in the level was marked. The obese nuclei contained two to three fold higher levels of NF-κB protein than in the lean liver nuclei. In the case of IκB-α, the level was significantly higher in obese liver tissues and nuclei than their lean counterparts. NF-κB activity in the nuclear fraction was higher in the obese livers than in the lean livers, but the difference between the obese and lean groups was not as marked as was noted for the level of NF-κB assessed by western blot. This suggested that the proportion of active NF-κB present in the nuclear fraction was much higher in the lean than in the obese nuclei as discussed previously.

Lipid raft was extracted successfully from obese and lean livers and fractions 5, 6 and 7 were identified as lipid raft enriched fractions due to the concentration of lipid raft specific proteins, caveolin-1 and flotillin-1, and higher levels of cholesterol compared to other fractions. These findings corroborated the findings of previous studies. The novel finding our research generated, was the fact that, total caveolin as well as flotillin levels was significantly higher in the liver lipid rafts of the obese-piroxicam than that of the other groups. This is the group also exhibited higher steatosis. Piroxicam treatment significantly decreased the level of caveolin-1 in the lean liver and significantly increased the level of flotillin-1 in the obese liver. COX-1 was not detectable, however, the level of COX-2 in the lipid raft was opposite to the level noted in the whole tissue homogenate. There was an approximate two fold increase in the level of COX-2 in the lean-piroxicam group than in the lean or obese groups. Again TNF-RII levels were opposite to the levels noted in the whole tissue homogenate. TNF-RII was highest in the obese-piroxicam lipid raft and lowest in the lean-piroxicam

lipid raft. These findings demonstrate that TNF-α signaling molecules are altered in obese steatotic livers than in lean non-steatotic livers. TNF-RII, COX-2 and NF-κB proteins stand out as the molecules profoundly affected by the pathological state of the tissue and piroxicam treatment. The reason for an increased level of TNF-RII in the lipid raft compared to the lowest level in the same group at the whole tissue level, suggest that movement of this protein, from other sites to lipid raft occurred. Whether this movement is a protective response or lipid raft is sequestering this protein making the tissue more vulnerable to damage, remains to be investigated. A similar reason could be provided for the abundance of COX-2 in the lean lipid raft. Why these proteins are localized in lipid raft fractions is puzzling.

When we look at the over all changes in the protein level of hepatic tissue or in lipid raft, it is reasonable to suggest that TNF-RII plays an important role in the pathogenicity of steatosis. Possibly, this receptor is important in protecting the tissue, as suggested by others (Fontaine et al. 2002), and its lower level in the obese-piroxicam group renders the tissue more susceptible to piroxicam toxicity. The findings on the levels of COX-1 and COX-2 suggest that piroxicam affected the level of COX-2 but not COX-1, suggesting that piroxicam is affecting the level of this protein by inhibiting the expression of the COX-2 gene which, in turn, may be due to inhibition of NF-κB. Piroxicam may also be inhibiting NF-κB. COX-2 expression is associated with cell survival. It is interesting to note that the COX-1 level went up in piroxicam treated lean livers but not in obese livers suggesting that increased COX-1 levels in lean livers is possibly compensating for the reduced COX-2 which did not occur in the obese liver. COX metabolites are reported to be cytoprotective (Bykov et al., 2006). Even though the level of transcriptionally active NF-κB is higher in the obese groups, it may not be sufficient to counteract the toxic effect of piroxicam or proinflammatory molecules. One additional observation worth noting is the presence of IκB-α in the nuclear compartment of obese livers and a higher level in the nuclei and whole tissue. This is the first report of this type. However, it has been suggested that IκB-α could serve as a transport protein for NF-κB to the nucleus or from the nucleus to cytoplasm. It is also possible that higher levels of IκB-α in the nuclear compartment affect the NF-κB's transcriptional activity. It should be noted that NF-κB transcribes genes for TNF-α, TNF receptors, COX-2, IκB-α and IKK-β along with several anti- and proapoptotic genes.

The network of signaling involved in mitigating TNF- α and/or NF-κB mediated response is complex, but the straight forward mechanism by NF-κB is depicted in figure 4.1. This research has unraveled selected phenomena associated with the pathological state of steatosis. Whether the changes are a cause or an effect of the pathological state remains to be seen. Nevertheless, this

research has emphasized that compartmentalization of specific proteins in the cells and tissues occur, and further analysis of specific proteins and their activities at the sub-cellular level may provide a better understanding of their involvement in eliciting biological responses.

4.3 Conclusion

In conclusion, we demonstrate that TNF-α signaling is altered in steatotic liver and anlaysis of lipid raft provide an insight into the activity and movement of proteins in causation and prevention of pathological states.

4.4 Future Directions

For future studies, it would be important to evaluate the role of NSAID in affecting NF-κB activity. In particular, gene and protein expressions of certain proapoptotic molecules like caspases, p53, Fas and antiapoptotic molecules like Bcl-2, Bcl-XL, FLIP, IAP, TRAF1/2 known to be regulated by NF-κB transcription must be evaluated in the pathological state of obesity. It would be important to investigate how the function and localization of these proteins are affected by exogenous, pro- and anti-growth stimuli in the whole tissue.

Figure 4.1: Possible mechanisms for apoptosis and survival mediated by NF-κB family members. NF-κB induces apoptosis by trancriptionally upregulating pro-apoptotic targets while repressing anti-apoptotic targets or vice-versa depending on equilibrium. This scheme presents the view that NF-κB activation could lead to at least a main outcome at the cellular level. The balance between the survival and apoptotic pathways is crucial. Piroxicam, or the production of very high levels of ROS or pro-inflammatory molecules, may activate NF-κB; however the transcriptional activity may produce proteins which could be counterproductive. Piroxicam in the obese animals appear to distort the balance in favour of enhanced toxicity possibly by inhibiting the survival pathway and this could be the mode of action underlying cancer preventive effects of piroxicam.

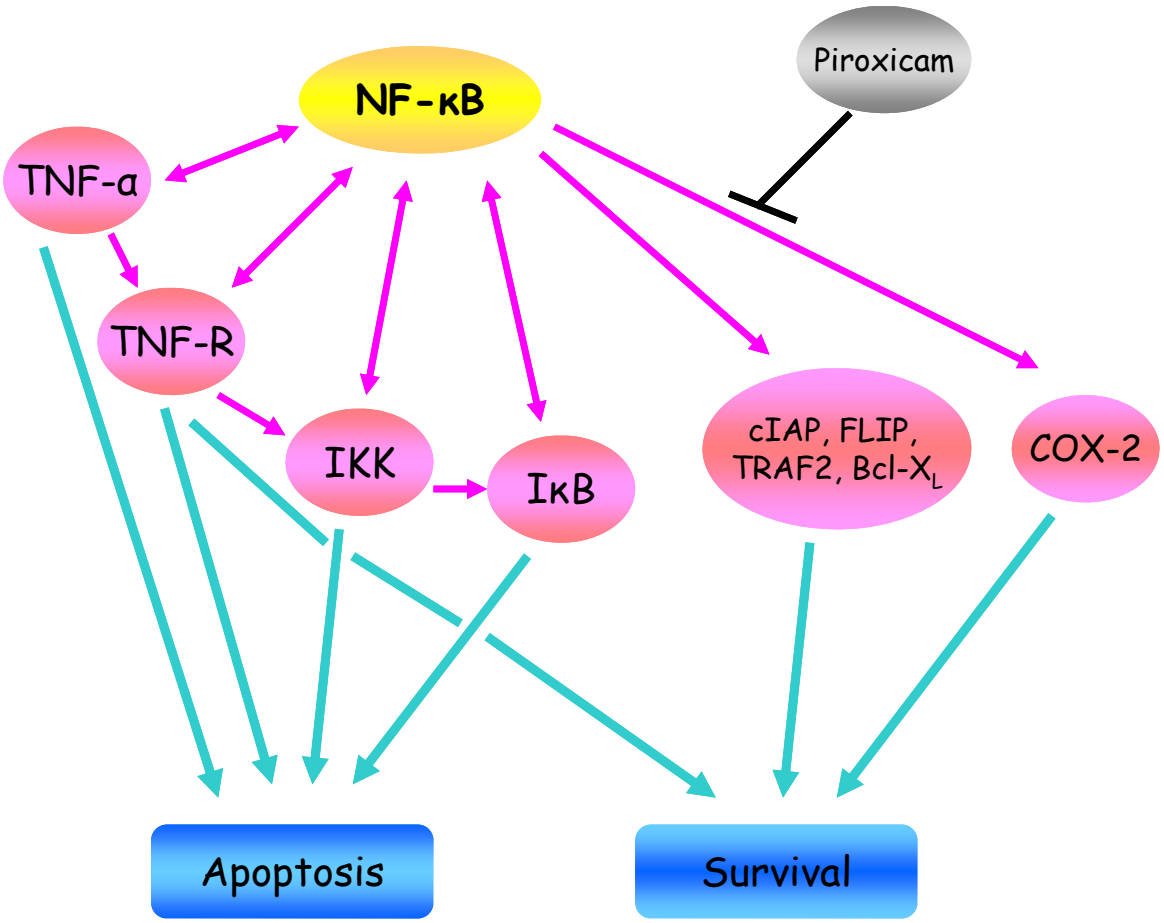
Piroxicam
NF-κB
TNF-α
TNF-R
IKK
IκB
cIAP, FLIP,
TRAF2, Bcl-X$_L$
COX-2
Apoptosis
Survival

Appendix A
Abbreviations

ACL	ATP citrate lyase
ALD	alcoholic liver disease
ANOVA	analysis of variance
ASMASE	acidic sphingomyelinase
CAV	caveolae
Cav-1	caveolin-1
Cav-2	caveolin-2
Cav-3	caveolin-3
COX-1	cyclooxygenase-1
COX-2	cyclooxygenase-2
CPT-1	carnitine palmitoyl transferase-1
ChREBP	carbohydrate response element binding protein
DD	death domain
DED	death effector domain
EGF	epidermal growth factor
ELISA	enzyme linked immunosorbent assay
FADD	Fas associated death domain
FAS	fatty acid synthase
Fas_L	Fas ligand
FFA	free fatty acid
$FLIP_L$	FLICE inhibitory protein
Flot-1	flotillin-1
GPI	glycosyl phosphatidylinositol
GK	Goto-Kakizaki
H&E	hematoxylin and eosin
HRP	horseradish peroxidase
HSL	hormone sensitive lipase
IAP	inhibitor of apoptosis proteins
IFN	interferon

IGF-1	insulin like growth factor-1
IGF-IRα	insulin like growth factor-I-receptor-α
IκB	inhibitor of NF-κB
IKK	IκB kinase
iNOS	inducible nitric oxide synthase
IR	insulin receptor
IRS	insulin receptor substrate
JNK	c-Jun amino-terminal kinase
LCE	long-chain fatty acyl elongase
L-PK	liver-type pyruvate kinase
MAPK	mitogen activated protein kinase
MW	Molecular weight marker
NAFL	nonalcoholic fatty liver
NAFLD	nonalcoholic fatty liver disease
NASH	nonalcoholic steatohepatitis
NF-κB	nuclear transcription factor-κB
NSAID	Nonsteroidal Anti-Inflammatory Drug
ODG	η-octyl-β-D-glucopyranoside
OLETF	Otsuka Long-Evans Tokushima Fatty
PARP	poly (ADP ribose) polymerase
PDGF	platelet-derived growth factor
PDK1	phosphoinositide-dependant kinase 1
PI3K	phosphatidylinositol-3-kinase
PKC	protein kinase C
RIP	receptor interacting protein
ROS	reactive oxygen species
SDS-PAGE	Sodium Dodecyl Sulfate Polyacrylamide Gel Electrophoresis
SH2	src-homology 2
SM	sphingomyelin
S1P	sphingosine-1-phosphate
SREBP-1c	sterol regulatory element binding protein 1c
TG	triglyceride

TNF-α	tumor necrosis factor-α
TNFR1	tumor necrosis factor receptor 1
TNFR2	tumor necrosis factor receptor 2
TRADD	TNF Receptor I associated death domain
TRAF	TNF Receptor associated factor
TRAIL	TNF-related apoptosis-inducing ligand
TLC	thin layer chromatography
Ob	Zucker obese rats
Ob-Pirox	Zucker obese rats supplemented with piroxicam
Ln	Zucker lean rats
Ln-Pirox	Zucker lean rats supplemented with piroxicam

Appendix B

Tables

Table B 1: Percent fatty acid composition of total phospholipids in liver[a]

	Ob	Ob-Pirox	Ln	Ln-Pirox
C14:0	0.49 ± 0.01^{x}	0.24 ± 0.01^{y}	0.15 ± 0.01^{z}	0.27 ± 0.00^{y}
C16:0	20.47 ± 0.73^{x}	16.43 ± 0.69^{y}	13.44 ± 0.42^{z}	17.08 ± 0.90^{y}
C16:1 n-7	3.11 ± 0.19^{x}	1.57 ± 0.05^{y}	0.26 ± 0.02^{z}	0.50 ± 0.01^{z}
C18:0	22.55 ± 0.48^{x}	28.57 ± 0.71^{y}	32.69 ± 0.71^{z}	26.81 ± 1.52^{y}
C18:1 n-9	13.92 ± 0.75^{x}	5.98 ± 0.34^{y}	2.16 ± 0.12^{z}	6.41 ± 0.26^{y}
C18:1 n-7	2.46 ± 0.07^{x}	2.54 ± 0.09^{x}	1.53 ± 0.06^{y}	1.51 ± 0.06^{y}
C18:2 n-6	4.60 ± 0.25^{x}	3.68 ± 0.17^{x}	7.90 ± 0.25^{y}	11.31 ± 0.64^{z}
C18:3 n-6	0.26 ± 0.02^{x}	0.18 ± 0.01^{xy}	0.15 ± 0.02^{y}	0.47 ± 0.05^{z}
C18:3 n-3	0.01 ± 0.00^{x}	0.00 ± 0.00^{y}	0.01 ± 0.00^{xy}	0.05 ± 0.01^{z}
C20:2 n-6	0.12 ± 0.00^{x}	0.17 ± 0.03^{x}	0.36 ± 0.02^{y}	0.18 ± 0.03^{x}
C20:3 n-6	0.34 ± 0.03^{x}	0.40 ± 0.01^{y}	0.01 ± 0.01^{z}	0.00 ± 0.00^{z}
C20:4 n-6	20.60 ± 0.67^{x}	28.86 ± 0.39^{y}	25.71 ± 0.21^{z}	22.43 ± 0.55^{w}
C22:4 n-6	0.68 ± 0.03^{x}	0.83 ± 0.03^{xy}	0.61 ± 0.02^{xz}	0.81 ± 0.14^{x}
C22:5 n-6	2.64 ± 0.17^{x}	3.06 ± 0.25^{xz}	4.88 ± 0.36^{y}	3.69 ± 0.25^{z}
C22:5 n-3	0.30 ± 0.02^{x}	0.27 ± 0.03^{x}	0.13 ± 0.01^{y}	0.26 ± 0.04^{x}
C22:6 n-3	4.22 ± 0.05^{x}	3.79 ± 0.29^{xz}	5.99 ± 0.27^{y}	4.55 ± 0.19^{xw}

[a]All values are means ± s.e., n=4/dietary group. Values in a row without a common letter (^{x,y,z}) differ significantly, $P < 0.05$, as determined by ANOVA in conjunction with LSD post-hoc analysis. Ob: Obese, Ob-Pirox: Piroxicam supplemented Obese, Ln: Lean, Ln-Pirox: Piroxicam supplemented Lean.

Table B 2: Percent fatty acid composition of total triglycerides in liver[a]

	Ob	Ob-Pirox	Ln	Ln-Pirox
C14:0	1.32 ± 0.06^{x}	1.46 ± 0.03^{x}	0.97 ± 0.13^{y}	0.86 ± 0.07^{y}
C16:0	34.97 ± 0.32^{x}	33.11 ± 0.83^{x}	35.59 ± 1.31^{x}	35.00 ± 1.23^{x}
C16:1 n-7	7.64 ± 0.82^{x}	8.49 ± 0.33^{x}	1.92 ± 0.36^{y}	1.69 ± 0.13^{y}
C18:0	2.92 ± 0.23^{x}	3.17 ± 0.21^{x}	5.36 ± 0.34^{y}	3.27 ± 0.42^{x}
C18:1 n-9	34.93 ± 1.13^{x}	38.20 ± 1.29^{x}	23.57 ± 2.15^{y}	27.26 ± 0.84^{y}
C18:1 n-7	3.59 ± 0.21^{x}	4.14 ± 0.11^{z}	1.70 ± 0.13^{y}	1.94 ± 0.05^{y}
C18:2 n-6	4.31 ± 0.20^{x}	3.65 ± 0.34^{x}	16.00 ± 1.69^{y}	22.33 ± 2.20^{z}
C18:3 n-6	0.23 ± 0.02^{x}	0.25 ± 0.03^{x}	0.23 ± 0.03^{x}	0.75 ± 0.07^{z}
C18:3 n-3	0.03 ± 0.00^{x}	0.02 ± 0.00^{x}	0.09 ± 0.02^{y}	0.12 ± 0.03^{y}
C20:2 n-6	0.04 ± 0.00^{x}	0.06 ± 0.00^{x}	0.11 ± 0.03^{x}	0.11 ± 0.05^{x}
C20:3 n-6	0.02 ± 0.00^{x}	0.02 ± 0.00^{x}	0.12 ± 0.01^{x}	0.13 ± 0.08^{x}
C20:4 n-6	0.28 ± 0.02^{x}	0.40 ± 0.07^{y}	1.06 ± 0.17^{z}	1.72 ± 0.18^{w}
C22:4 n-6	0.10 ± 0.00^{x}	0.03 ± 0.02^{x}	0.32 ± 0.07^{xy}	0.42 ± 0.20^{y}
C22:5 n-6	4.43 ± 0.44^{x}	2.36 ± 0.09^{y}	5.36 ± 1.19^{x}	1.39 ± 0.27^{y}
C22:5 n-3	0.02 ± 0.00^{x}	0.00 ± 0.00^{x}	0.03 ± 0.01^{x}	0.03 ± 0.02^{x}
C22:6 n-3	0.04 ± 0.00^{x}	0.04 ± 0.01^{x}	0.07 ± 0.01^{x}	0.07 ± 0.04^{x}

[a]All values are means ± s.e., n=4/dietary group. Values in a row without a common letter (^{x,y,z}) differ significantly, $P < 0.05$, as determined by ANOVA in conjunction with LSD post-hoc analysis. Ob: Obese, Ob-Pirox: Piroxicam supplemented Obese, Ln: Lean, Ln-Pirox: Piroxicam supplemented Lean.

Table B 3: Fatty acid concentration (mg/gm) of total triglycerides in liver

	Ob	Ob-Pirox	Ln	Ln-Pirox
C14:0	2.57	3.50	0.10	0.29
C16:0	68.14	79.73	3.49	11.93
C16:1 n-7	15.01	20.52	0.21	0.57
C18:0	5.67	7.59	0.53	1.08
C18:1 n-9	68.30	91.63	2.44	9.37
C18:1 n-7	7.06	9.96	0.17	0.67
C18:2 n-6	8.42	8.86	1.60	7.87
C18:3 n-6	0.44	0.60	0.02	0.26
C18:3 n-3	0.05	0.04	0.01	0.04
C20:2 n-6	0.08	0.13	0.01	0.04
C20:3 n-6	0.05	0.05	0.01	0.05
C20:4 n-6	0.54	0.98	0.09	0.60
C22:4 n-6	0.20	0.17	0.03	0.16
C22:5 n-6	8.48	5.65	0.45	0.43
C22:5 n-3	0.03	0.01	0.02	0.00
C22:6 n-3	0.07	0.06	0.01	0.04

Appendix C

Figures

Figure C 1: Coomassie stain of 10% gel showing equal loading and adequate separation of protein.

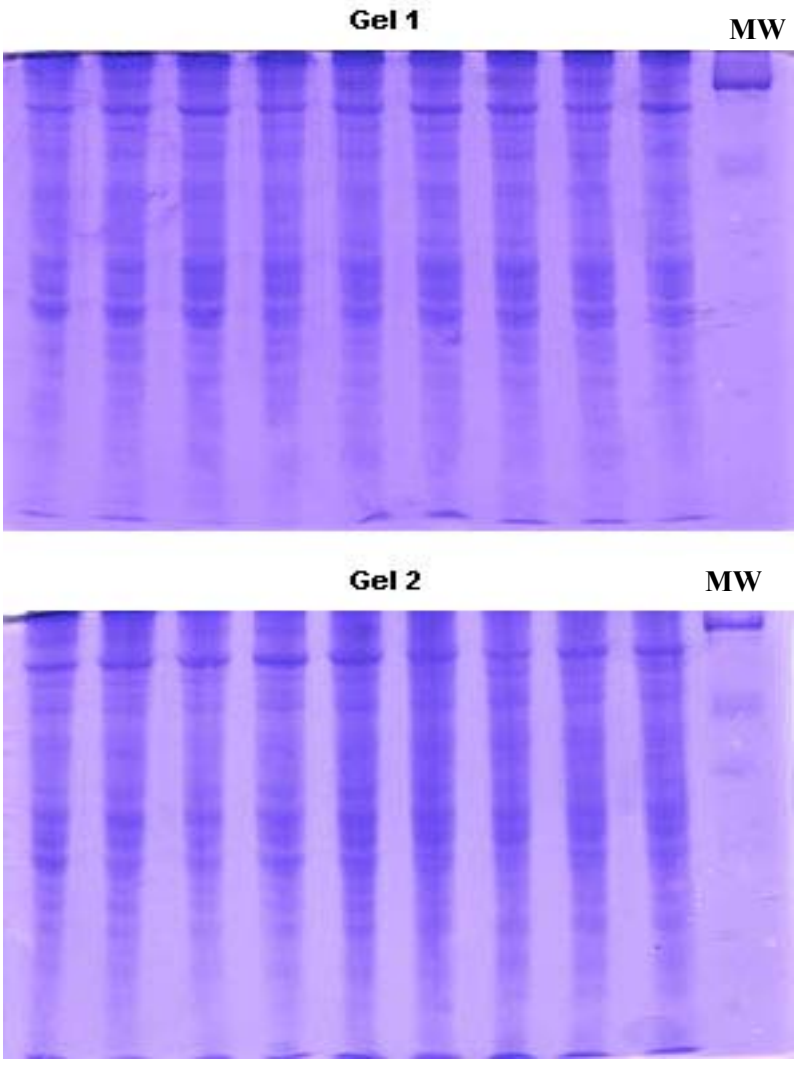

Figure C 2: Western blot analysis of IR-β protein expression from liver homogenates of Zucker rats. Equal amounts of 50 µg of liver proteins were separated by 8% SDS-PAGE gel and transferred onto PVDF membranes. Following incubation with primary antibodies at a final dilution of 1:1000 and corresponding HRP-conjugated secondary antibodies at a final dilution of 1:5000, the blots were developed on X-ray film using ECL Plus substrate. (A) Representative western blots of IKK-β, IR-β and β-actin using 50 µg of liver proteins of Zucker obese (Ob) and lean rats with or without piroxicam treatment. (B) Bar graphs representing quantified levels of IKK-β and IR-β proteins after the densitometric values of equal amount loaded two western blots was corrected for gel-to-gel variability using equal amount of liver homogenate as a positive control in each blot. All values are means ± s.e., n=4/dietary group. Bars without a common letter ($^{x, y, z}$) differ significantly, $p<0.05$, as determined by ANOVA in conjunction with LSD post-hoc analysis. Ob: Obese, Ob-Pirox: Piroxicam supplemented Obese, Ln: Lean, Ln-Pirox: Piroxicam supplemented Lean.

A

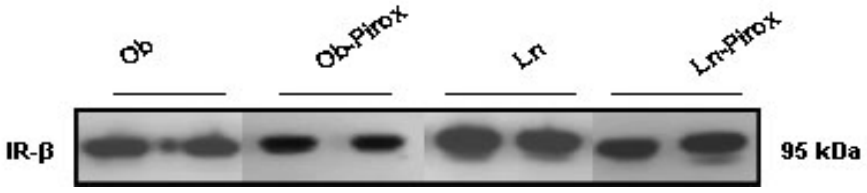
Ob
Ob-Pirox
Ln
Ln-Pirox
IR-β
95 kDa

B

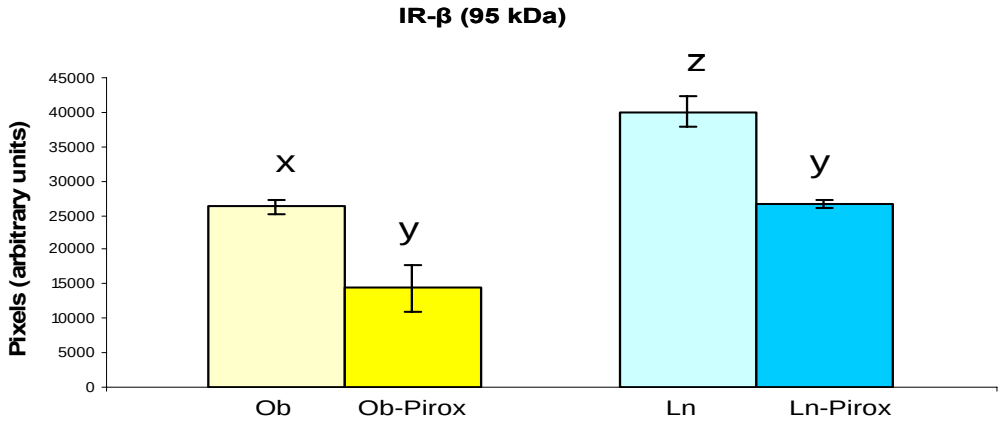
IR-β (95 kDa)
Pixels (arbitrary units)
45000
40000
35000
30000
25000
20000
15000
10000
5000
0
x
y
z
y
Ob
Ob-Pirox
Ln
Ln-Pirox

Figure C 3: Detection of sphingomyelinase in the liver homogenates of Zucker rats using the Amplex Red reagent-based assay. The sphingomyelinase assay was performed at pH 7.4 and pH 5.0 to determine the neutral and acidic sphingomyelinase activity, respectively. The assay was carried out by following the continuous sphingomyelinase assay protocol for neutral and two-step assay protocol for acidic according to the manufacturer's instruction. Briefly, 50 μg of equal amount of liver protein was used in order to detect the sphingomyelinase activity. Moreover, the stimulated (with sphingomyelin) as well as basal (without sphingomyelin) level of neutral and acidic sphingomyelinase was measured. The assay was based on the enzymatic hydrolysis of sphingomyelin to ceramide and phosphorylcholine, then hydrolyzing phosphorylcholine to choline and finally oxidizing choline to betaine and H_2O_2. Thus, H_2O_2 in the presence of horseradish peroxidase reacts with the Amplex Red reagent to generate highly fluorescent resorufin. The bar graph represents the activity of neutral and acidic sphingomyelinase with or without the addition of sphingomyelin measured in the liver homogenates of obese, lean, piroxicam treated obese and piroxicam treated lean rats. All values are means ± s.e., n=4/dietary group. Bars without a common letter ($^{x, y, z}$) or ($^{a, b, c}$) differ significantly, $p<0.05$, as determined by ANOVA in conjunction with LSD post-hoc analysis. Ob: Obese, Ob-Pirox: Piroxicam supplemented Obese, Ln: Lean, Ln-Pirox: Piroxicam supplemented Lean.

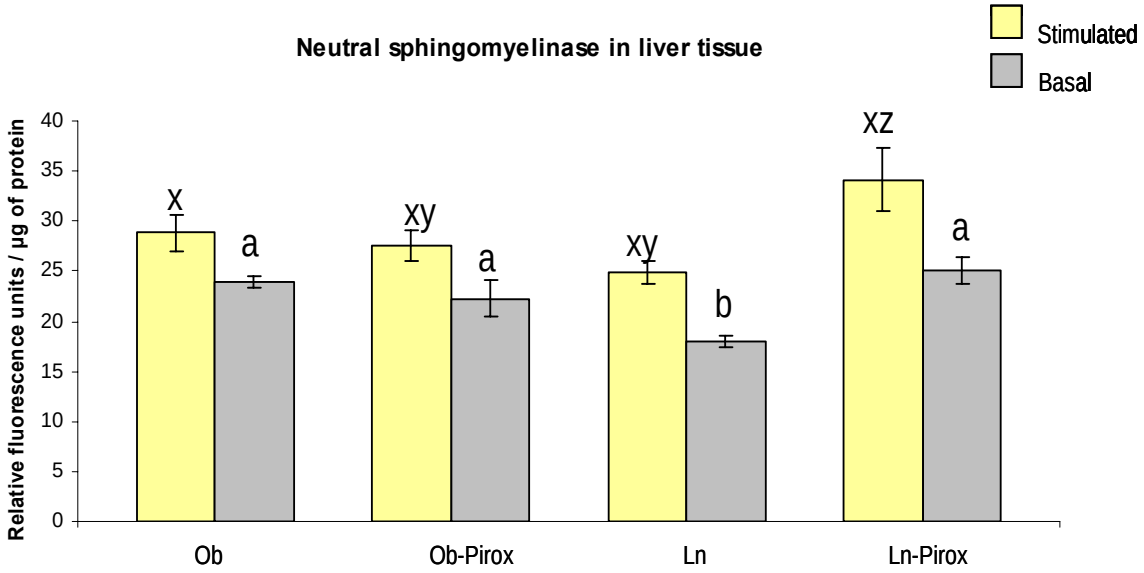
Neutral sphingomyelinase in liver tissue
Stimulated
Basal
Relative fluorescence units / µg of protein
40
35
30
25
20
15
10
5
0
x
a
xy
a
xy
b
xz
a
Ob
Ob-Pirox
Ln
Ln-Pirox

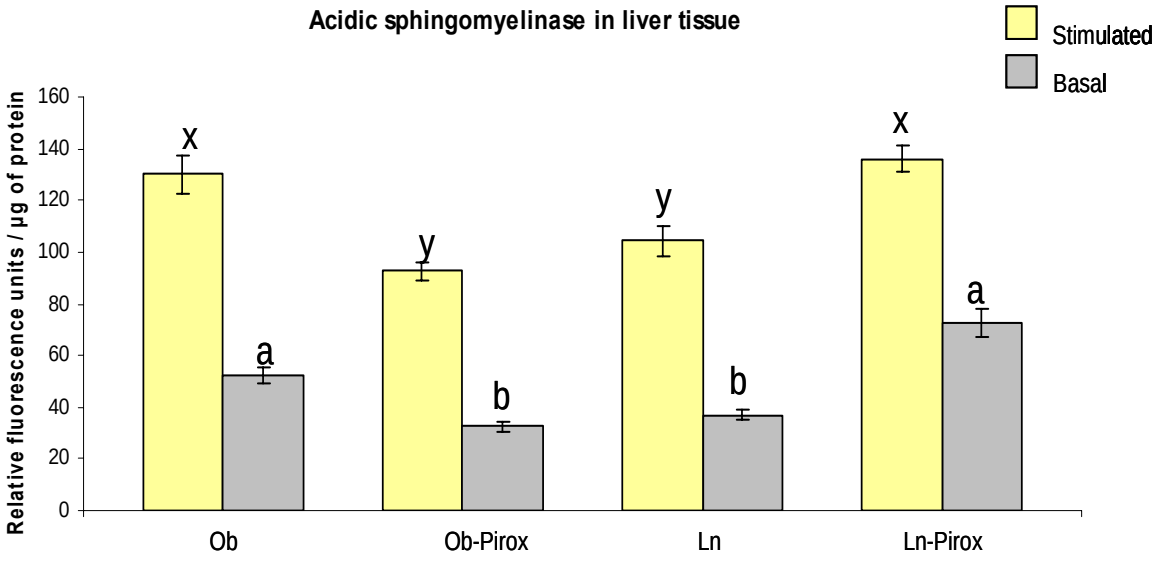
Acidic sphingomyelinase in liver tissue
Stimulated
Basal
Relative fluorescence units / µg of protein
160
140
120
100
80
60
40
20
0
x
a
y
b
y
b
x
a
Ob
Ob-Pirox
Ln
Ln-Pirox

Figure C 4: Western blot picture of caveolin-1 in lipid raft fractions of Zucker rat livers. Lipid rafts from rat livers were isolated after discontinuous sucrose gradient ultracentrifugation. After ultracentrifugation, the sucrose gradient was fractionated from top to bottom. Equal volumes of 3 μL raft fraction proteins were separated on 12% SDS-PAGE gel and immunoblotted with rabbit anti-caveolin-1 and rabbit anti-flotillin-1 raft marker proteins. The primary antibodies were added at a final dilution of 1:1000; the secondary antibodies were added at a final dilution of 1:5000 and the blots were developed on X-ray film using ECL Plus substrate. Western blot of caveolin-1 from all four trials using 3 μL from lipid raft fractions 5, 6, 7 of Zucker obese (Ob) and lean rats with or without piroxicam treatment. Ob: Obese, Ob-Pirox: Piroxicam supplemented Obese, Ln: Lean, Ln-Pirox: Piroxicam supplemented Lean.

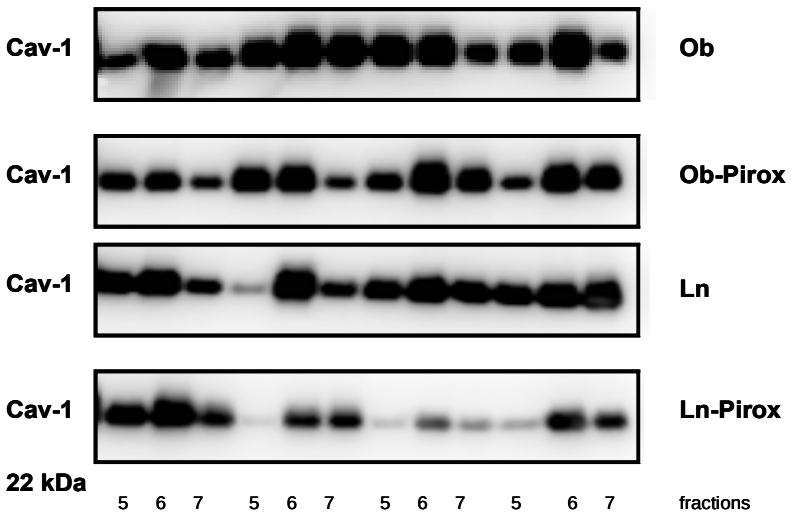
Cav-1
Ob
Cav-1
Ob-Pirox
Cav-1
Ln
Cav-1
Ln-Pirox
22 kDa
5 6 7 5 6 7 5 6 7 5 6 7
fractions

Figure C 5: Quantified levels of caveolin-1 and flotillin-1 from lipid raft fractions of Zucker rat livers. Bar graphs representing (A) the average densitometric values of fractions 5, 6, 7 and (B) the summation of fractions 5, 6, 7 from four independent experiments using 3 μL from lipid raft fractions of Zucker obese (Ob) and lean rats with or without piroxicam treatment. The gel-to-gel variability between four different blots was corrected by using equal amounts of liver homogenate as a positive control in each blot. Ob: Obese, Ob-Pirox: Piroxicam supplemented Obese, Ln: Lean, Ln-Pirox: Piroxicam supplemented Lean

A

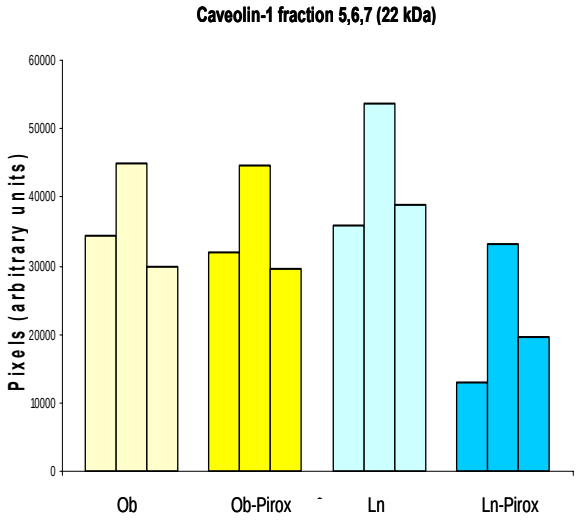
Caveolin-1 fraction 5,6,7 (22 kDa)
Pixels (arbitrary units)
60000
50000
40000
30000
20000
10000
0
Ob
Ob-Pirox
Ln
Ln-Pirox

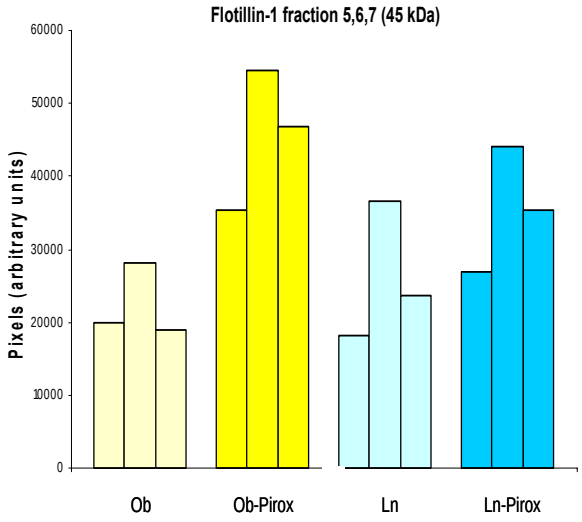
Flotillin-1 fraction 5,6,7 (45 kDa)
Pixels (arbitrary units)
60000
50000
40000
30000
20000
10000
0
Ob
Ob-Pirox
Ln
Ln-Pirox

B

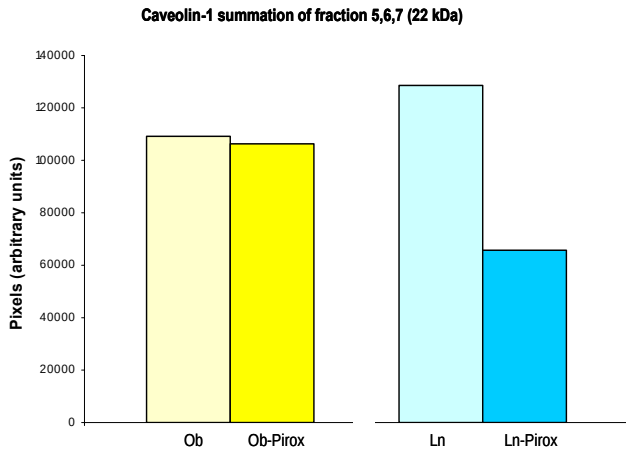
Caveolin-1 summation of fraction 5,6,7 (22 kDa)
Pixels (arbitrary units)
140000
120000
100000
80000
60000
40000
20000
0
Ob
Ob-Pirox
Ln
Ln-Pirox

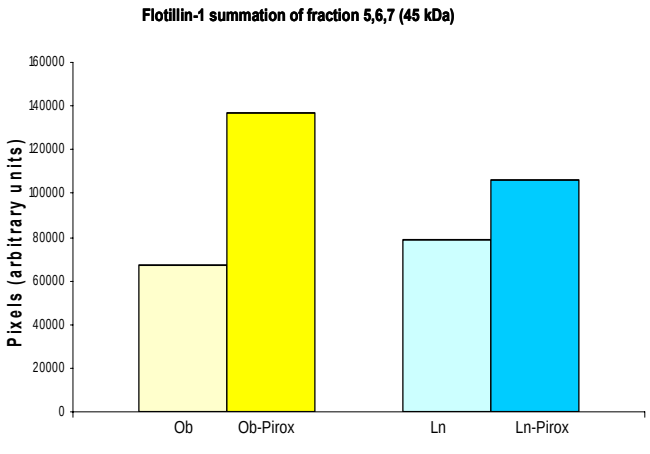
Flotillin-1 summation of fraction 5,6,7 (45 kDa)
Pixels (arbitrary units)
160000
140000
120000
100000
80000
60000
40000
20000
0
Ob
Ob-Pirox
Ln
Ln-Pirox

Figure C 6: Quantified levels of COX-2 from lipid raft fractions of Zucker rat livers. Bar graphs representing (A) the average densitometric values of fractions 5, 6, 7 and (B) the summation of fractions 5, 6, 7 from four independent experiments using 6 μL from lipid raft fractions of Zucker obese (Ob) and lean rats with or without piroxicam treatment. The gel-to-gel variability between the four different blots was corrected by using equal amounts of liver homogenate as a positive control in each blot. Ob: Obese, Ob-Pirox: Piroxicam supplemented Obese, Ln: Lean, Ln-Pirox: Piroxicam supplemented Lean

A

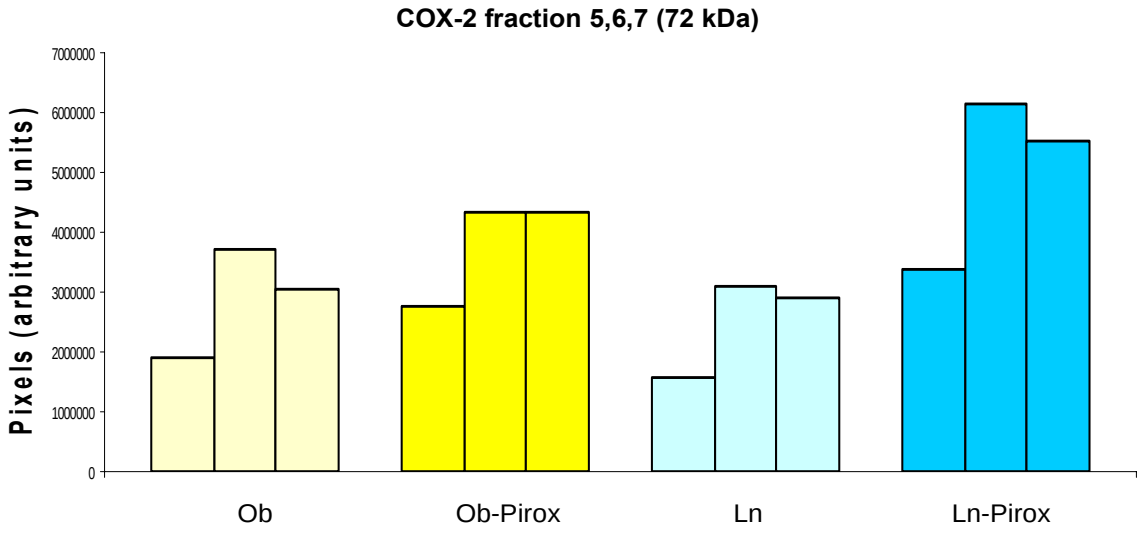
COX-2 fraction 5,6,7 (72 kDa)
Pixels (arbitrary units)
7000000
6000000
5000000
4000000
3000000
2000000
1000000
0
Ob
Ob-Pirox
Ln
Ln-Pirox

B

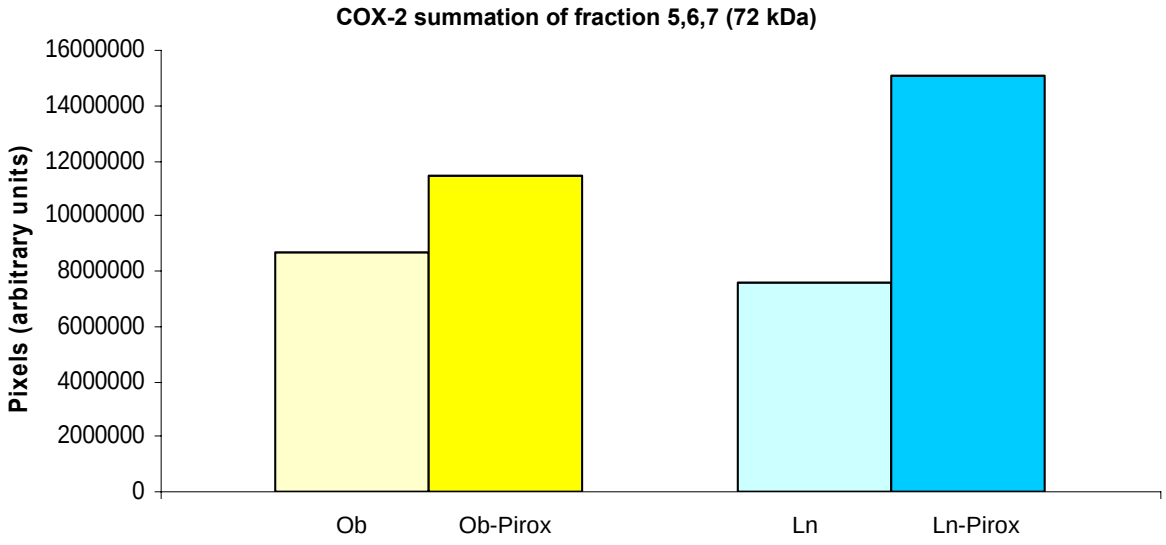
COX-2 summation of fraction 5,6,7 (72 kDa)
Pixels (arbitrary units)
16000000
14000000
12000000
10000000
8000000
6000000
4000000
2000000
0
Ob
Ob-Pirox
Ln
Ln-Pirox

Figure C 7: Quantified levels of TNF-RI and TNF-RII from lipid raft fractions of Zucker rat livers. Bar graphs representing (A) the average densitometric values of fractions 5, 6, 7 and (B) the summation of fractions 5, 6, 7 from four independent experiments using 6 μL from lipid raft fractions of Zucker obese (Ob) and lean rats with or without piroxicam treatment. The gel-to-gel variability between the four different blots was corrected by using equal amounts of liver homogenate as a positive control in each blot. Ob: Obese, Ob-Pirox: Piroxicam supplemented Obese, Ln: Lean, Ln-Pirox: Piroxicam supplemented Lean

A

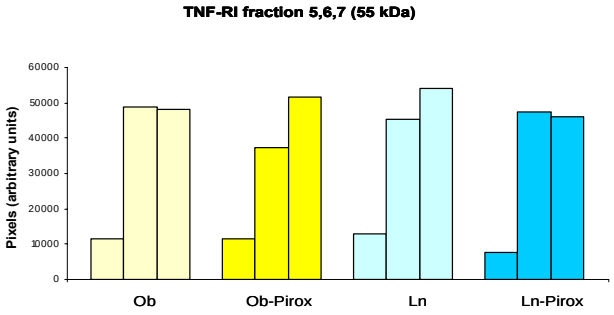
TNF-RI fraction 5,6,7 (55 kDa)
Pixels (arbitrary units)
60000
50000
40000
30000
20000
10000
0
Ob
Ob-Pirox
Ln
Ln-Pirox

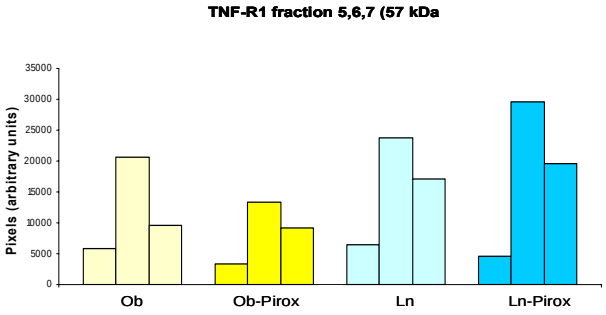
TNF-R1 fraction 5,6,7 (57 kDa
Pixels (arbitrary units)
35000
30000
25000
20000
15000
10000
5000
0
Ob
Ob-Pirox
Ln
Ln-Pirox

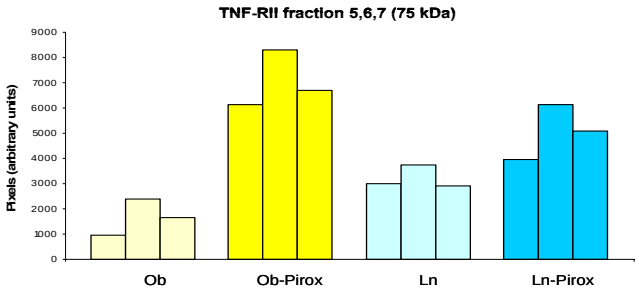
TNF-RII fraction 5,6,7 (75 kDa)
Pixels (arbitrary units)
9000
8000
7000
6000
5000
4000
3000
2000
1000
0
Ob
Ob-Pirox
Ln
Ln-Pirox

B

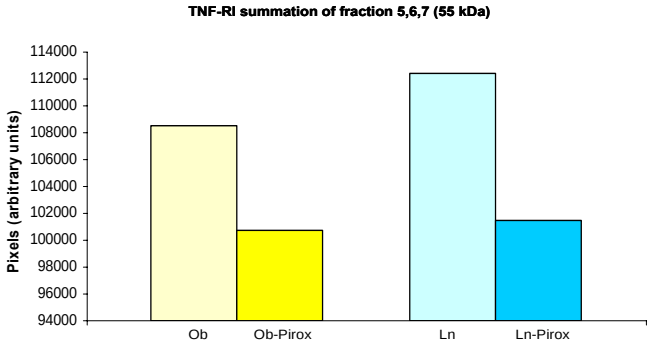
TNF-RI summation of fraction 5,6,7 (55 kDa)
Pixels (arbitrary units)
114000
112000
110000
108000
106000
104000
102000
100000
98000
96000
94000
Ob
Ob-Pirox
Ln
Ln-Pirox

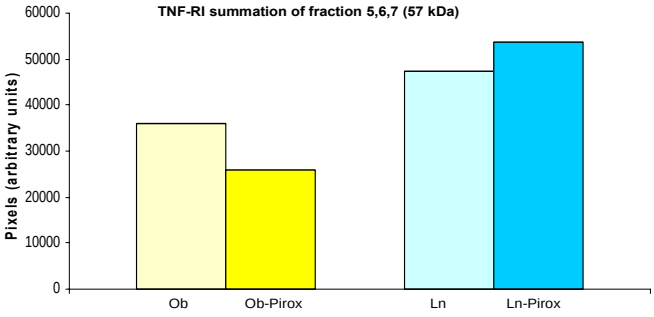
TNF-RI summation of fraction 5,6,7 (57 kDa)
Pixels (arbitrary units)
60000
50000
40000
30000
20000
10000
0
Ob
Ob-Pirox
Ln
Ln-Pirox

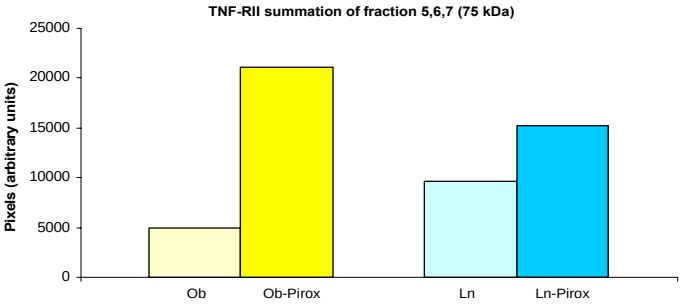
TNF-RII summation of fraction 5,6,7 (75 kDa)
Pixels (arbitrary units)
25000
20000
15000
10000
5000
0
Ob
Ob-Pirox
Ln
Ln-Pirox

Figure C 8: Detection of sphingomyelinase in the lipid raft fractions using the Amplex Red reagent-based assay. The sphingomyelinase assay was performed at pH 7.4 and pH 5.0 to determine the neutral and acidic sphingomyelinase activity, respectively, on lipid raft fractions extracted by sucrose density gradient ultracentrifugation from the liver of Zucker rats. The assay was carried out by following the continuous sphingomyelinase assay protocol for neutral and two-step assay protocol for acidic according to the manufacturer's instruction. In short, 20 μL of equal volume was used from each fraction of all four groups in order to detect the activity of sphingomyelinase. Moreover, the stimulated (with sphingomyelin) as well as basal (without sphingomyelin) level of neutral and acidic sphingomyelinase was measured. The assay was based on the enzymatic hydrolysis of sphingomyelin to ceramide and phosphorylcholine, then hydrolyzing phosphorylcholine to choline and finally oxidizing choline to betaine and H_2O_2. Thus, H_2O_2 in the presence of horseradish peroxidase reacts with the Amplex Red reagent to generate highly fluorescent resorufin. (A) Quantified levels of stimulated and basal levels of neutral sphingomyelinase in fraction 6 expressed on per μg of protein is presented in this graph. (B) Quantified levels of stimulated and basal levels of acidic sphingomyelinase in fraction 6 expressed on per μg of protein is presented in this graph. All values are means ± s.e., n=4/dietary group. Bars without a common letter ($^{x, y, z}$) or ($^{a, b, c}$) differ significantly, $p<0.05$, as determined by ANOVA in conjunction with LSD post-hoc analysis. Ob: Obese, Ob-Pirox: Piroxicam supplemented Obese, Ln: Lean, Ln-Pirox: Piroxicam supplemented lean.

A

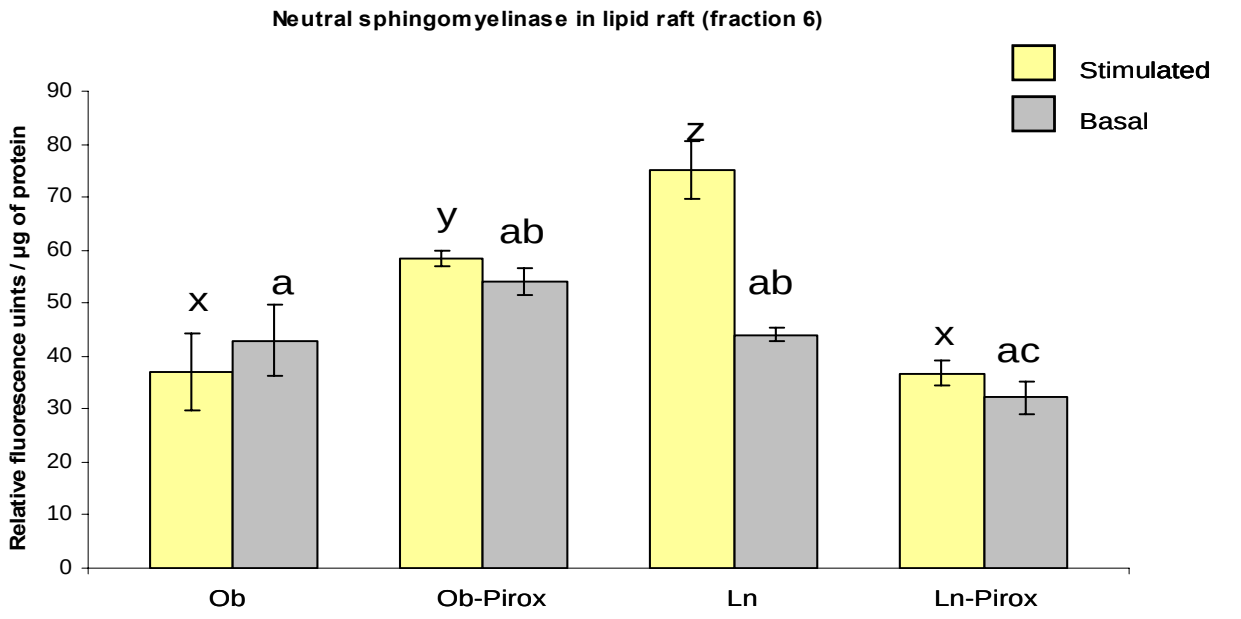
Neutral sphingomyelinase in lipid raft (fraction 6)
Stimulated
Basal
Relative fluorescence uints / µg of protein
90
80
70
60
50
40
30
20
10
0
x
a
y
ab
z
ab
x
ac
Ob
Ob-Pirox
Ln
Ln-Pirox

B

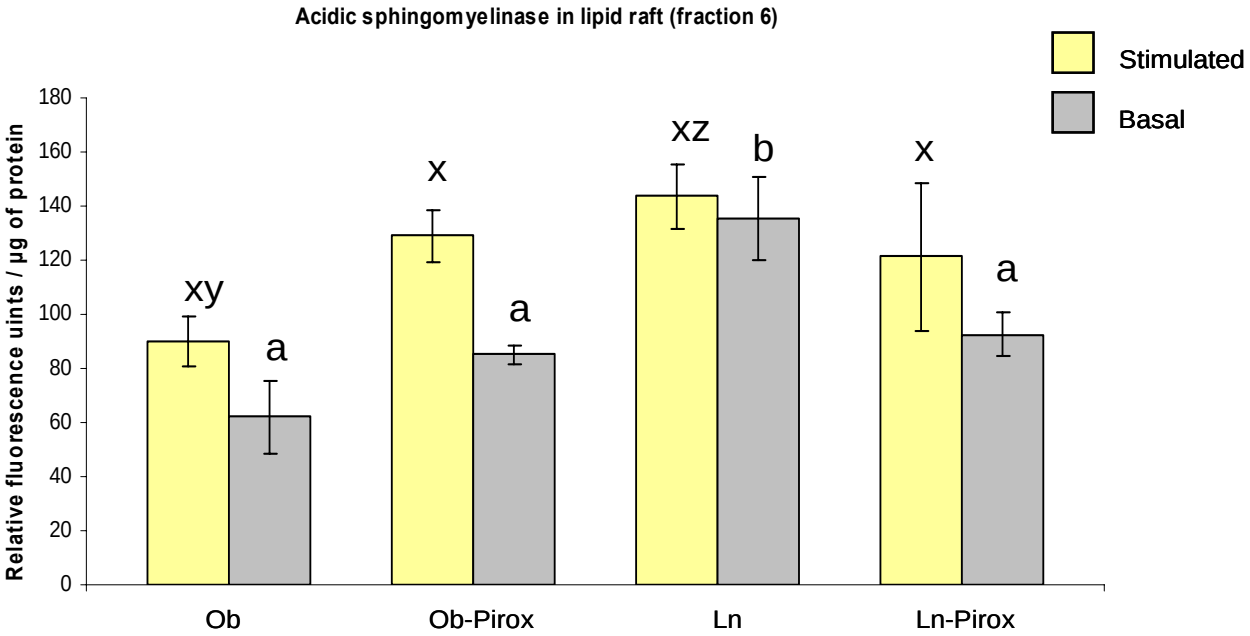
Acidic sphingomyelinase in lipid raft (fraction 6)
Stimulated
Basal
Relative fluorescence uints / µg of protein
180
160
140
120
100
80
60
40
20
0
xy
a
x
a
xz
b
x
a
Ob
Ob-Pirox
Ln
Ln-Pirox

Bibliography

Alonso M. A., Millán J. 2001. The role of lipid rafts in signalling and membrane trafficking in T lymphocytes. *J Cell Sci.*114(Pt 22): 3957-65

Adams L.A., Angulo P., Lindor K.D. 2005. Nonalcoholic fatty liver disease. *CMAJ.* 172(7): 899-905.

Adams L.A., Angulo P. 2006. Treatment of non-alcoholic fatty liver disease. *Postgrad Med J.* 82(967): 315-22.

Ashkenazi A., Dixit V.M. 1998. Death Receptors: signalling and modulation. *Science.* 287:1305–18.

Babitt J., Trigatti B., Rigotti A., Smart E.J., Anderson R.G., Xu S., Krieger M. 1997. Murine SR-BI, a high density lipoprotein receptor that mediates selective lipid uptake, is N-glycosylated and fatty acylated and colocalizes with plasma membrane caveolae. *J Biol Chem.* 272(20): 13242-9.

Balbis A., Baquiran G., Mounier C., Posner B.I. 2004. Effect of insulin on caveolin-enriched membrane domains in rat liver. *J Biol Chem.* 279(38): 39348-57.

Baumann C.A., Ribon V., Kanzaki M., Thurmond D.C., Mora S., Shigematsu S., Bickel P.E., Pessin J.E., Saltiel A.R. 2000. CAP defines a second signalling pathway required for insulin-stimulated glucose transport. *Nature.* 407(6801):202-71.

Bender F.C., Reymond M.A., Bron C., Quest A.F. 2000. Caveolin-1 levels are down-regulated in human colon tumors, and ectopic expression of caveolin-1 in colon carcinoma cell lines reduces cell tumorigenicity. *Cancer Res.* 60(20): 5870-8.

Bessessen D.H., Kushner R.F. 2002. Evaluation and management of obesity, Hanley & Belfus Inc: Philadelphia, PA.

den Boer M., Voshol P.J., Kuipers F., Havekes L.M., Romijn J.A. 2004. Hepatic steatosis: a mediator of the metabolic syndrome. Lessons from animal models. *Arterioscler Thromb Vasc Biol.* 24(4): 644-9.

Bollinger C.R., Teichgräber V., Gulbins E. 2005. Ceramide-enriched membrane domains. *Biochim Biophys Acta.* 1746(3): 284-94.

Bonizzi G., Piette J., Schoonbroodt S., Greimers R., Harvard L., Merville M.P., Bours V. 1999. Reactive Oxygen Intermediate-Dependent NFκB Activation by Interleukin-1 Requires 5-Lipoxygenase or NADPH Oxidase Activity. *Molecular and Cellular Biology.* 19(3): 1950-1960.

Brown D.A., and London E. 1998. Functions of lipid rafts in biological membranes. *Annu Rev Cell Dev Biol* 14: 111–36.

Brown D., Waneck G.L. 1992. Glycosyl–phosphatidylinositol-anchored membrane proteins. *J Am Soc Nephrol.* 3(4): 895–906.

Browning J.D., Horton J.D. 2004. Molecular mediators of hepatic steatosis and liver injury. *J Clin Invest.* 114(2): 147-52.

Bykov I.L., Palmen M., Rainsford K.D., Lindros K.O. 2006. Chronic effects of celecoxib, and cyclooxygenase-2 inhibitor, cause enhanced alcohol-induced liver steatosis in rats. *Inflammopharmacology.* 14(1-2): 36-41.

Cao Y., Pearman A.T., Zimmerman G.A., McIntyre T.M., Prescott S.M. 2000. Intracellular unesterified arachidonic acid signals apoptosis. *PNAS.* 97(21): 11280-11285.

Cha S.H., Jung N.H., Kim B.R., Kim H.W., Kwak J.O. 2004. Evidence for cyclooxygenase-1 association with caveolin-1 and -2 in cultured human embryonic kidney (HEK 293) cells. *IUBMB Life.* 56(4): 221-7.

Chen D., Wang M.W. 2005. Development and application of rodent models for type 2 diabetes. *Diabetes Obes Metab.* 7(4): 307-17.

Cohen A.W., Razani B., Wang X.B., Combs T.P., Williams T.M., Scherer P.E., Lisanti M.P. 2003. Caveolin-1-deficient mice show insulin resistance and defective insulin receptor protein expression in adipose tissue. *Am J Physiol Cell Physiol.* 285(1): C222-35.

Cohen A.W., Hnasko R., Schubert W., Lisanti M.P. 2004. Role of caveolae and caveolins in health and disease. *Physiol Rev.* 84(4): 1341–79.

Corpet D.E., Pierre F. 2003. Point: From animal models to prevention of colon cancer. Systematic review of chemoprevention in min mice and choice of the model system. *Cancer Epidemiol Biomarkers Prev.* 12(5): 391-400.

Cuvillier O., Pirianov G., Kleuser B., Vanek P.G., Coso O.A., Gutkind S., Spiegel S. 1996. Suppression of ceramide-mediated programmed cell death by sphingosine-1-phosphate. *Nature.* 381(6585): 800-3.

Day C.P., James O.F. 1998. Steatohepatitis: a tale of two "hits"? *Gastroenterology.* 114(4): 842-5.

Delmas D., Rebe C., Micheau O, Athias A., Gambert P., Grazide S., Laurent G, Latruffe N., Solary E. 2004. Redistribution of CD95, DR4 and DR5 in rafts accounts for the synergistic toxicity of resveratrol and death receptor ligands in colon carcinoma cells. *Oncogene.* 23(55): 8979-86.

Dey A., Maric C., Kaesemeyer W.H., Zaharis C.Z., Stewart J., Pollock J.S., Imig J.D. 2004. Rofecoxib decreases renal injury in obese Zucker rats. *Clin Sci (Lond).* 107(6): 561-70.

Dobrowsky R.T. 2000. Sphingolipid signalling domains floating on rafts or buried in caves? *Cell Signal.* 12(2): 81-90.

Dykstra M., Cherukuri A., Sohn H.W., Tzeng S.J., Pierce S.K. 2003. Location is everything: lipid rafts and immune cell signaling. *Annu Rev Immunol*. 21: 457-81.

Entingh-Pearsall A., Kahn C.R. 2004. Differential roles of the insulin and insulin-like growth factor-I (IGF-I) receptors in response to insulin and IGF-I. *J Biol Chem.* 279(36): 38016-24.

Engelman J.A., Zhang X.L., Galbiati F., Volonte D., Sotgia F., Pestell R.G., Minetti C., Scherer P.E., Okamoto T., Lisanti M.P. 1998. Molecular genetics of the caveolin gene family: implications for human cancers, diabetes, Alzheimer disease and molecular dystrophy. *Am J Hum Genet*. 63(6): 1578-87.

Fine S.W., Lisanti M.P., Galbiati F., Li M. 2001. Elevated expression of caveolin-1 in adenocarcinoma of the colon. *Am J Clin Pathol.* 115(5): 719-724.

Formiguera X., Canton A. 2004. Obesity: epidemiology and clinical aspects. *Best Pract Res Clin Gastroenterol.* 18(6): 1125-46.

Folch J., Lees M., Sloane Stanley G.H. 1957. A simple method for the isolation and purification of total lipids from animal tissues. *J Biol Chem.* 226(1): 497-509.

Fontaine V., Mohand-Said S., Hanoteau N., Fuchs C., Pfizenmaier K., Eisel U. 2002 Neurodegenerative and neuroprotective effects of tumor necrosis factor (TNF) in retinal ischemia: opposite roles of TNF receptor 1 and TNF receptor 2. *J. Neurosci.* 22(7):RC216.

Gebreselassie D., Bowen W.D. 2004. Sigma-2 receptors are specifically localized to lipid rafts in rat liver membranes. *Eur J Pharmacol.* 493(1-3):19-28.

Grassme H., Jekle A., Riehle A., Schwarz H., Berger J., Sandhoff K., Kolesnick R., Gulbins E. 2001. CD95-signaling via ceramide-rich membrane rafts. *J. Biol. Chem.* 276(23): 20589–20596.

Green J.E., Hudson T. 2005. The promise of genetically engineered mice for cancer prevention studies. *Nat Rev Cancer.* 5(3): 184-98.

Gulbins E., Li P.L. 2006. Physiological and pathophysiological aspects of ceramide. *Am J Physiol Regul Integr Comp Physiol.* 290(1): R11-26.

Hayden M.S., Ghosh S. 2006. Good cop, bad cop: the different faces of NF-kappaB. *Cell Death Differ*. 13(5): 759-72.

Heslin M.J., Hawkins A., Boedefeld W., Arnoletti J.P., Frolov A., Soong R., Urist M.M., Bland K.I. 2005. Tumor-associated down-regulation of 15-Lipoxygenase-1 is reversed by celecoxib in colorectal cancer. *Ann Surg.* 241(6): 941-947.

Hofmann C., Lorenz K., Braithwaite S.S., Colca J.R., Palazuk B.J., Hotamisligil G.S., Spiegelman B.M. 1994. Altered gene expression for tumor necrosis factor-alpha and its receptors during drug and dietary modulation of insulin resistance. *Endocrinology.* 134(1):264-70.

Hotamisligil G.S., Shargill N.S., Spiegelman B.M. 1993. Adipose expression of tumor necrosis factor-alpha: direct role in obesity-linked insulin resistance. *Science.* 259(5091):87-91.

Jalving M., Koornstra J.J., de Jong S., de Vries EGE., Kleibeuker. 2005. Review Article: the potential of combinational regimen with non-steroidal anti-inflammatory drugs in the chemoprevention of colorectal cancer. *Alimentary Pharmacology & Therapeutics.* 21(4): 321.

Kimura A., Mora S., Shigematsu S., Pessin J.E., Saltiel A.R. 2002. The insulin receptor catalyzes the tyrosine phosphorylation of caveolin-1. *J Biol Chem.* 277(33): 30153-8.

Ko Y.G., Lee J.S., Kang Y.S., Ahn J.H., Seo J.S. 1999. TNF-alpha-mediated apoptosis is initiated in caveolae-like domains. *J Immunol.* 162(12): 7217-23.

Kolesnick R.N., Goni F.M., Alonso A. 2000. Compartmentalization of ceramide signaling: physical foundations and biological effects. *J. Cell. Physiol.* 184(3): 285–300.

Kwak J.O., Lee W.K., Kim H.W., Jung S.M., Oh K.J., Jung S.Y., Huh Y.H., Cha S.H. 2006. Evidence for cyclooxygenase-2 association with caveolin-3 in primary cultured rat chondrocytes. *J Korean Med Sci.* 21(1): 100-6.

Legler D.F., Micheau O., Doucey M.A., Tschopp J., Bron C. 2003. Recruitment of TNF receptor 1 to lipid rafts is essential for TNFalpha-mediated NF-kappaB activation. *Immunity.* 18: 655–664.

Levi M.S., Borne R.F., Williamson J.S. 2001. A review of cancer chemopreventive agents. *Curr Med Chem.* 8(11): 1349-62.

Li S., Okamoto T., Chun M., Sargiacomo M., Casanova J.E., Hansen S.H., Nishimoto I., Lisanti M.P. 1995. Evidence for a regulated interaction between heterotrimeric G proteins and caveolin. *J Biol Chem.* 270(26): 15693–701.

Lin H.Z., Yang S.Q., Zeldin G., Diehl A.M. 1998. Chronic ethanol consumption induces the production of tumor necrosis factor-alpha and related cytokines in liver and adipose tissue. *Alcohol Clin Exp Res.* 22(5 Suppl): 231S-237S.

Liou J.Y., Deng W.G., Gilroy D.W., Shyue S.K., 2001. Wu K.K. Colocalization and interaction of cyclooxygenase-2 with caveolin-1 in human fibroblasts. *J Biol Chem.* 276(37): 34975-82.

Lotocki G., Alonso O.F., Dietrich W.D., Keane R.W. 2004. Tumor necrosis factor receptor 1 and its signaling intermediates are recruited to lipid rafts in the traumatized brain. *J Neurosci.* 24(49): 11010-6.

Maguy A., Hebert T.E., Nattel S. 2006. Involvement of lipid rafts and caveolae in cardiac ion channel function. *Cardiovasc Res.* 69(4): 798-807.

Malhi H., Gores G.J., Lemasters J.J. 2006. Apoptosis and necrosis in the liver: a tale of two deaths? *Hepatology*. 43(2 Suppl 1): S31-44.

Meric J.B., Rottey S., Olaussen K., Soria J.C., Khayat D., Rixe O., Spano J.P. 2006. Cyclooxygenase-2 as a target for anticancer drug development. *Crit Rev Oncol Hematol.* 59: 51-64.

Micheau O. and Tschopp J. 2003. Induction of TNF Receptor I-Mediated Apoptosis via Two Sequential Signaling Complexes. *Cell*. 114:181-90.

Miyaji M., Jin Z.X., Yamaoka S., Amakawa R, Fukuhara S., Sato S.B., Kobayashi T., Domae N., Mimori T., Bloom E.T., Okazaki T., Umehara H. 2005. Role of membrane sphingomyelin and ceramide in platform formation for Fas-mediated apoptosis. *J Exp Med.* 202(2): 249-59.

Moore K.L., Dalley A.F. 1999. Clinically Oriented Anatomy 4th Edition. Lippincott, Williams and Wilkins. pp: 249-251.

Morrison W.R., Smith L.M. 1964. Preparation of fatty acid methyl esters and dimethylacetals from lipids with boron fluoride-methanol. *J.Lipid Res*. 5: 600-8.

Mueller H., Kassack M.U., Wiese M. 2004. Comparison of the usefulness of the MTT, ATP, and calcein assays to predict the potency of cytotoxic agents in various human cancer cell lines. *J Biomol Screen*. 9(6): 506-15.

Ness G.C., Kohlruss N., Gertz K.R. 2003. Association of the low-density lipoprotein receptor with caveolae in hamster and rat liver. *Biochem Biophys Res Commun.* 303(1): 177-81.

Patlolla J.M., Swamy M.V., Raju J., Rao C.V. 2004. Overexpression of caveolin-1 in experimental colon adenocarcinomas and human colon cancer cell line. *Oncol Rep.* 11(5): 957-63.

Pike L.J. 2004. Lipid rafts: heterogeneity on the high seas. *Biochem J.* 378(Pt 2): 281-92.

Podar K., Anderson K.C. 2006. Caveolin-1 as a potential new therapeutic target in multiple myeloma. *Cancer Lett.* 233(1): 10-5.

Osawa Y., Banno Y., Nagaki M., Brenner D.A., Naiki T., Nozawa Y., Nakashima S., Moriwaki H. 2001. TNF-alpha-induced sphingosine 1-phosphate inhibits apoptosis through a phosphatidylinositol 3-kinase/Akt pathway in human hepatocytes. *J Immunol.* 167(1): 173-80.

Quest A.F., Leyton L., Parraga M. 2004. Caveolins, caveolae, and lipid rafts in cellular transport, signaling, and disease. *Biochem Cell Biol.* 82(1): 129-44.

Raju J., Bird R.P. 2006. Alleviation of hepatic steatosis accompanied by modulation of plasma and liver TNF-alpha levels by Trigonella foenum graecum (fenugreek) seeds in Zucker obese (fa/fa) rats. *Int J Obes (Lond).* 1-10.

Raman M., Allard J. 2006. Non alcoholic fatty liver disease: A clinical approach and review. *Can J Gastroenterol.* 20(5):345-9.

Reddy B.S., Maruyama H., Kelloff G. 1987. Dose-related inhibition of colon carcinogenesis by dietary piroxicam, a nonsteroidal antiinflammatory drug, during different stages of rat colon tumor development. *Cancer Res.* 47(20): 5340-6.

Remacle-Bonnet M., Garrouste F., Baillat G., Andre F., Marvaldi J., Pommier G. 2005. Membrane rafts segregate pro- from anti-apoptotic insulin-like growth factor-I receptor signaling in colon carcinoma cells stimulated by members of the tumor necrosis factor superfamily. *Am J Pathol.* 167(3): 761-73.

Rotolo J.A., Zhang J., Donepudi M., Lee H., Fuks Z., Kolesnick R. 2005. Caspase-dependent and independent activation of acid sphingomyelinase signaling. *J Biol Chem.* 280(28): 26425-34.

Saltiel A. R., Pessin J. E. 2002. Insulin signaling pathways in time and space. *Trends Cell Biol.* 12(2): 65-71.

Saltiel A.R., Kahn C.R. 2001. Insulin signalling and the regulation of glucose and lipid metabolism. *Nature*. 414(6865): 799-806.

Samad F., Uysal K.T., Wiesbrock S.M., Pandey M., Hotamisligil G.S., Loskutoff D.J. 1999. Tumor necrosis factor a is a key component in the obesity-linked elevation of plasminogen activator inhibitor 1. *Proc. Natl. Acad. Sci. USA.* 96:6902–7.

Scheel-Toellner D., Wang K., Assi L.K., Webb P.R., Craddock R.M., Salmon M., Lord J.M. 2004. Clustering of death receptors in lipid rafts initiates neutrophil spontaneous apoptosis. *Biochem Soc Trans.* 32(Pt 5): 679-81.

Schutze S., Wiegmann K., Machleidt T., Kronke M. 1995. TNF-induced activation of NF-kappa B. *Immunobiology.* 193(2-4):193-203.

Sherman K.E., Jones C. 1992. Hepatotoxicity associated with piroxicam use. *Gastroenterology.* 103(1): 354-5.

Siebler J., Galle P.R. 2006. Treatment of nonalcoholic fatty liver disease. *World J Gastroenterol.* 12(14): 2161-7.

Silverthorn D.U., Ober W.C., Garrison C.W., Silverthorn A.C. 1998. Human Physiology: An Integrated Approach. Prentice Hall, New Jersey, USA. pp: 685-790.

Simons K., Ehehalt R. 2002. Cholesterol, lipid rafts, and disease. *J. Clin. Invest.* 110(5): 597-603.

Simons K., Toomre D. 2000. Lipid rafts and signal transduction. *Nat Rev Mol Cell Biol*. 1(1): 31-9.

Smart E.J., Graf G.A., McNiven M.A., Sessa W.C., Engelman J.A., Scherer P.E., Okamoto T., Lisanti M.P. 1999. Caveolins, liquid-ordered domains, and signal transduction. *Mol Cell Biol.* 19(11): 7289–304.

Teoh N.C., Farrell G.C. 2003. Hepatotoxicity associated with non-steroidal

anti-inflammatory drugs. *Clin Liver Dis.* 7(2): 401-13.

Varfolomeev E.E. and Ashkenazi A. 2004. Tumor necrosis factor: an apoptosis juNKie? *Cell*. 116: 491–497.

Watson R.T., Shigematsu S., Chiang S.H., Mora S., Kanzaki M., Macara I.G., Saltiel A.R., Pessin J.E. 2001. Lipid raft microdomain compartmentalization of TC10 is required for insulin signaling and GLUT4 translocation. *J Cell Biol.* 154(4): 829-40.

Yang G., Troung L.D., Timme T.L., Ren C., Wheeler T.M., Park S.H., Nasu Y., Bangma C.H., Kattan M.W., Scardino P.T., Thompson T.C. 1998. Elevated expression of caveolin is associated with prostate and breast cancer. *Clin Cancer Res.* 4: 1873-1880.

Yang S.Q., Lin H.Z., Lane M.D., Clemens M., Diehl A.M. 1997. Obesity increases sensitivity to endotoxin liver injury: implications for the pathogenesis of steatohepatitis. *Proc Natl Acad Sci U S A.* 94(6): 2557-62.

Yang Z., Costanzo M., Golde D.W., Kolesnick R.N. 1993. Tumor necrosis factor activation of the sphingomyelin pathway signals nuclear factor kappa B translocation in intact HL-60 cells. *J Biol Chem*. 268(27):20520-3.

Yin M., Wheeler M.D., Kono H., Bradford B.U., Gallucci R.M., Luster M.I., Thurman R.G. 1999. Essential role of tumor necrosis factor alpha in alcohol-induced liver injury in mice. *Gastroenterology.* 117(4): 942-52.

Yuan M., Konstantopoulos N., Lee J., Hansen L., Li Z.W., Karin M., Shoelson S.E. 2001. Reversal of obesity- and diet-induced insulin resistance with salicylates or targeted disruption of Ikkbeta. *Science.* 293(5535): 1673-7.

Zucker L.M., Zucker T.F. 1961. Fatty, a new mutation in the rat. *J Hered* 51-52: 275-278.